

A DNA APTAMER TRANSDUCER DESIGNED TOWARD RAPID BIOSENSOR
DEVELOPMENT: A NOVEL APPROACH TO MODULAR BIOSENSING
PLATFORMS

by

Timothy Z Hachigian



A dissertation

submitted in partial fulfillment

of the requirements for the degree of

Doctor of Philosophy in Material Science and Engineering

Boise State University

August 2023

© 2023

Timothy Z Hachigian

ALL RIGHTS RESERVED

BOISE STATE UNIVERSITY GRADUATE COLLEGE

DEFENSE COMMITTEE AND FINAL READING APPROVALS

of the dissertation submitted by

Timothy Zavdiel Hachigian

Dissertation Title: A DNA Aptamer Transducer Designed Toward Rapid Biosensor Development: A Novel Approach to Modular Biosensing Platforms

Date of Final Oral Examination: 13 April 2023

The following individuals read and discussed the dissertation submitted by student Timothy Zavdiel Hachigian, and they evaluated the student's presentation and response to questions during the final oral examination. They found that the student passed the final oral examination.

Jeunghoon Lee, Ph.D. Chair, Supervisory Committee

Elton Graugnard, Ph.D. Member, Supervisory Committee

Lisa Warner, Ph.D. Member, Supervisory Committee

Eric Hayden, Ph.D. Member, Supervisory Committee

The final reading approval of the dissertation was granted by Jeunghoon Lee, Ph.D., Chair of the Supervisory Committee. The dissertation was approved by the Graduate College.

DEDICATION

I dedicate this work to two special people who have been instrumental in shaping my journey. Firstly, my lovely wife, Jessie, who has provided unwavering support throughout my graduate studies by staying by my side. I couldn't have made it this far without her. And secondly, my grandfather Alexander, who introduced me to the fascinating world of science and technology at a young age. He challenged me to think outside the box and made learning enjoyable. Thank you both for being a constant source of encouragement and inspiration.

ACKNOWLEDGMENTS

I would like to firstly acknowledge Dr. Jeunghoon Lee, who was my principle investigator in this work. He played an instrumental role in coaching my research activities and has cultivated my growth both as a professional scientist and a writer. Without him, I doubt I could have completed this work. Thank you, Dr. Lee, for the time and energy you have poured into my research journey.

I would like to acknowledge each member of my Ph.D. supervisory committee, who have overseen my dissertation work: Bhaskar Chittoori, Ph.D., Jeunghoon Lee, Elton Graugnard, Ph.D., Ph.D., Lisa Warner, Ph.D., and Eric Hayden, Ph.D. Thank you for your time and engagement with my Ph.D. process and for your continual support.

Next, I would like to acknowledge my colleagues in the Nanoscale Materials and Device Group. Namely, Natalya Hallstrom Ph.D., the W.M. Keck lab manager who supported all of my laboratory efforts and was always available for help when needed. Also, Drew Lysne for his friendship as a colleague studying DNA reaction networks and his support of my research goals.

Finally, I would like to acknowledge the faculty of the Micron School of Material Science and Engineering department at Boise State University who have excelled in fostering a culture of growth and have led the way in putting Boise State University on the map as a premier research institution.

ABSTRACT

Aptamer-based biosensors have garnered significant interest due to their versatility in detecting a wide range of analytes across various applications. In this work, a customizable Aptamer Transducer (AT) was introduced as a non-enzymatic and modular duplexed aptamer biosensing platform. The design modularity was accomplished by separating the aptamer input domain from the output domain. The AT was demonstrated to be capable of fully transducing an adenosine signal into arbitrary DNA outputs using a structure-switching aptamer design. The AT design utilized strand displacement reactions via toehold mediated strand displacement with fluorescence based reporting for signal detection. Furthermore, the AT was incorporated with two catalytic amplification networks to further demonstrate its customizability. In a subsequent study, the kinetic behavior and performance of modified ATs were investigated, and a high-throughput approach was developed for modifying ATs toward improving sensitivity based on an aptamer complementary element selection method. Modular biosensing platforms based on duplexed aptamers are advantageous for rapid development of low-cost tests since sensing and output domains can be easily customized, and studies that aim to develop such platforms are beneficial for the future development of selective and sensitive assays.

TABLE OF CONTENTS

DEDICATION	iv
ACKNOWLEDGMENTS	v
ABSTRACT	vi
LIST OF TABLES	x
LIST OF FIGURES	xi
LIST OF ABBREVIATIONS	xv
CHAPTER ONE: INTRODUCTION AND BACKGROUND FOR APTAMERS AND DYNAMIC DNA NANOTECHNOLOGY	1
1.1 Introduction.....	1
1.2 Background	5
1.2.1 DNA Structure and Dynamics	5
1.2.2 Aptamer Dynamics.....	8
1.2.3 DNA Strand Displacement	13
1.3 References.....	18
CHAPTER TWO: A CUSTOMIZABLE APTAMER TRANSDUCER NETWORK DESIGNED FOR FEED FORWARD COUPLING	24
2.3 Results and Discussion	28
2.3.2 Integration of AT with unique Reporters	29
2.3.3 AT + Entropy-Driven Catalytic Amplification.....	38
2.3.4 AT + 3-Arm Catalytic Amplification.....	42

2.5	Experimental.....	46
2.5.1	DNA Preparation.....	46
2.5.2	DNA Purification.....	47
2.5.3	Kinetics Experiments.....	47
2.6	References	49
CHAPTER 3: TARGETED SELECTION OF APTAMER COMPLEMENTARY ELEMENTS TOWARD RAPID SCREENING OF APTAMER TRANSDUCERS.....		54
3.1	Abstract	54
3.2	Introduction	55
3.3	Methods.....	58
3.3.1	DNA Preparation.....	58
3.3.2	DNA Purification.....	59
3.3.4	Kinetics Experiments.....	59
3.3.5	Kinetics Model Fitting.....	60
3.4	Results and Discussion.....	60
3.4.1	ACE Selection for τ' Integration.....	60
3.5	Conclusions	77
3.6	References	79
CHAPTER 4: FUTURE WORK AND FINAL REMARKS FOR THE APTAMER TRANSDUCER PLATFORM		83
4.1	Introduction.....	83
4.2	Future Work	84
4.2.1	Discussion of Biomolecular Insights for Adenosine Binding AT ...	84
4.2.2	AT Kinetics Model Refinement	86

4.2.3	Market Analysis of AT Sensors.....	87
4.2.4	AT Redesign: Incorporating other Aptamers	88
4.2.5	Multiplexing ATs.....	91
4.2.6	Signal Processing with Multiplexed ATs.....	96
4.3	Final Remarks	99
4.4	References.....	101
APPENDIX A.....		108
APPENDIX B		117

LIST OF TABLES

Table A1: Kinetics traces for each fuel concentration in excess of the AT concentration of 10 nM used for optimization of the AT-fuel reaction, reported with KR.	109
Table A2: Kinetics traces for each Na and Mg buffer salt concentration using 13 nM AT-fuel for 200 μ M 2 mM adenosine and a DNA initiated AT using ZR. The signal of the AT was especially sensitive to Mg concentration and therefore a high Mg buffer (25 mM Mg 0 mM Na 1xTE) concentration was used for all further experiments.	111
Table A3. Strand sequences for the four AT reaction networks including the AT strands (Output and Backbone), Fuel and the corresponding direct reporters for each AT. The substrates used for catalytic amplification for ZN and KN are also shown.....	113
Table A4. NUPACK was used to verify most probable secondary structures for ATs at 25 $^{\circ}$ C for both ATs and AT-Fuels. Equilibrium bonding probability remained constant for AT aptamer regions on each AT variant.	115
Table S1. Nupack predicted secondary structures for the AT Complex, AT Fuel, and resulting Waste 1 Complex. Raw kinetics traces for each AT system used fit with our kinetics model.....	120
Table S2. Strand sequences for AT reaction networks including the AT strands (Output and Backbone), Fuel and the reporter used to test all networks are shown. Note: Common Output strands in both 5' and 3' directions were bound to backbone single strands to develop each AT while modifications to each Backbone and Fuel strand were used to change the ACEs tested.	126

LIST OF FIGURES

- Figure 1.1 : Watson-crick base pairs (blue box) showing hybridized A•T and G•C pairs and the formation of a double helix structure with several stacked base pairs between bonded 3'-5' reversed single-strands. Hoogsteen base pairs (orange box) showing several alternate bonds which can form between purine bases. A G-tetrad with stabilizing M⁺ ion is shown (bottom right corner) and makes up the stacked bases in a G-quadruplexes shown under the non-double helix secondary structures where the DNA phosphate backbone distinguishes G-quadruplex types anti-parallel, hybrid, or parallel. An i-motif secondary structure which uses Hoogsteen base pairs is also shown.³³7
- Figure 1.2: (A) Compares the kinetic pathways for both conformational selection and induced fit mechanisms. For conformational selection, the substrate conforms to a state ready to accepted the target and then proceeds with binding, K_d^{Apt} is the binding affinity. Induced fit proceeds by fitting the target into the substrate as an intermediate and then transitions to the bound state, K_{Fit} is the affinity to form the intermediate state. (B) Conformational selection versus induced fit mechanisms applied to a duplexed aptamer. The Oligo represents a short aptamer complementary element (ACE) that prevents aptamer-ligand binding until it becomes dehybridized. (C) Occupancy of a single-site aptamer f compared to the ligand concentration $[T]$. The dissociation constant K_d , binding affinity, is defined at the concentration $[T]$ when there is 50% occupancy of the aptamer binding sites. Sigmoid binding curves for K_d 10, 100, and 1000 nM aptamers are shown.^{39,40} 10
- Figure 1.3: Intuitive energy landscape showing the free energy change during each strand displacement step. A 6 nt toehold provides a net lowering of the free energy before and after displacement due to the 6 additional base pairs formed during the reaction.⁴² 15
- Figure 2.1: (A) Reaction schematics of the AT binding to adenosine, releasing ssDNA output, and reacting with a reporter complex. The structure switching aptamer input region is shown in the blue box and the ssDNA output region is shown in the brown box. (B) Fluorescence intensity normalized by the maximum intensity of the 2 mM adenosine trace shows the kinetic behavior of the AT reacting with a ZR reporter as initiated by 20 μ M – 2 mM adenosine, using 13 nM protected fuel, over 300 minutes. Calculated 2σ of the leakage trace (green dash) and the leakage moving

average (red line) are also shown. (C) Initial rates of the AT reacting with ZR and KR reporters using both 13 nM and 300 nM AT fuel (10 nM AT complex, 20 nM Reporter) in 1×TE 25 mM Mg²⁺ (D) Initial rates of the AT reacting with ZR and KR using low concentrations of adenosine 2-20 μM compared to the AT leakage rate. Initial rates above 2σ of the leak are considered detected. 31

Figure 2.2: (A) Reaction schematic for AT coupled linear amplification network, AT was redesigned to incorporate 4, 5 domains from 5'-3' ends. (B) Fluorescence intensities of the AT reacted with ZRm (AT+ZRm) compared to AT reacted with ZN (AT+ZN) from 2-20 μM adenosine for 24 hrs (1xTE 25 mM Mg²⁺) (C) Comparison of leak subtracted differential intensities at 24 hours showing amplification fold for each adenosine concentration from 2-2000 μM..... 37

Figure 2.3: (A) Reaction schematic for AT coupled 3-arm amplification network, AT was redesigned to incorporate 1, c, a domains from 5'-3' ends. Note: the AT μ domain has been moved to preserve 5'-3' of the amplifier RN (B) Fluorescence intensities of the AT reacted with KRm (AT+KRm) compared to AT reacted with KN (AT+KN) from 2-20 μM adenosine for 24 hrs (1xTE 25 mM Mg²⁺) (C) Comparison of leak subtracted differential intensities at 24 hours showing amplification fold for each adenosine concentration from 2-2000 μM..... 41

Figure 3.1 (A) AT reaction schematic, the adenosine AT first reacts with 2 adenosine molecules for structure-switching and then a fuel reacts with the available toehold releasing the output O1. O1 reacts further with a reporter complex. Alterations to the AT (B) τ' length (C) τ' start-site and (D) τ' single-mismatch were used to test the behavior of the AT structure-switching mechanism. (E) Selected ATs from the ACE-scan data are listed based on their τ' alterations. Both 5' and 3' versions of Selected ATs 1-12 were tested giving a total of 24 ATs compared to the control AT, the original AT from our previous work..... 61

Figure 3.2: Both k₁ and K_{d,eff} are shown for Selected 5' ATs 1-12 in the 5' direction, which were estimated by fitting the 20 μM, 200 μM and 2 mM reaction traces. The selected ACEs are grouped by τ' length, τ' start-site domain, and τ' single mismatch shown as the for comparison of reaction rate and equilibrium constants. The values below the AT sample numbers represent the length of τ', position of start-site mismatch for τ' start-site domain, and the position of the single mismatch from the τ'-β₁' interface. (Note: AT 6 has 8 nt long while ATs 7-12 are 12 nt long. Also, ATs 11 and 12 have 2 and 3 nt long start-site mismatch, respectively) 66

Figure 3.3: Both k₁ and K_{d,eff} are shown for Selected 3' ATs 1-12 in the 5' direction which were estimated by fitting the 20 μM, 200 μM and 2 mM reaction

traces. The selected ACEs are grouped by τ' length, τ' start-site domain, and τ' single mismatch for comparison of reaction rate and equilibrium constants. Note that missing data points for specific concentrations did not produce any distinguishable signal above system noise. The values below the AT sample numbers represent the length of τ' , position of start-site mismatch for τ' start-site domain, and the position of the single mismatch from the τ' - β_1' interface. (Note: AT 6 has 8 nt long while ATs 7-12 are 12 nt long. Also, ATs 11 and 12 have 2 and 3 nt long start-site mismatch, respectively).....70

Figure 3.4: (A) A Pearson Correlation (R) (blue) between the ACE-Scan data results and the AT relative performance $k_1/K_{d,eff}$ for each tested adenosine concentration showing a strong correlation between different adenosine concentrations and a moderate correlation between ACE-scan and AT data. Roughly 34-50% ACE-Scan prediction corresponded to relative performance. P-values (orange) are also shown which indicate statistical significance for the data population analyzed. (B) Direct comparison of relative performance $k_1/K_{d,eff}$ for ATs tested versus ACE-scan $k_{off,diff}$ where ACE-scan predicted response increases from left to right (red). 5' ATs were normalized to AT 12 while 3' ATs were normalized to AT 6. ACE- scan $k_{off,diff}$ with low or negative data corresponded well with 3' ATs that had low signal. 8 nt length ATs overperformed compared to $k_{off,diff}$75

Figure 4.1: A concurrent mode for two multiplexed ATs designed to simultaneously sense adenosine and thrombin in a single solution each utilizing their own unique output domains to trigger two separate FRET reporters with different fluorescence emission wavelengths. Fluorescence measurements in scan mode are predicted to reveal two emission peaks separated by the fluorophores' maximum emission intensities, $\Delta\lambda$92

Figure 4.2: A consecutive mode for two multiplexed ATs designed to sense adenosine and thrombin in a single solution reacting at a set time interval Δt . At time t_1 fuel F1 is added to solution, reacting until near completion, providing a response due to the presence of thrombin. At time t_2 fuel F2 is added causing the reaction to continue, with a response due to the presence of adenosine, until output strands are O1 and O2 are depleted. The fluorescence intensity plot is predicted to be a single stair-stepped kinetics trace with a response for each step consistent with the aptamer sensing and strand displacement of each individual AT.95

Figure 4.3: (A) Multiplexed ATs reacted in a consecutive format where the a and b domains from each AT are fed-forward into an amplification reaction network. The transduction step in this format can be represented by a logical OR operation since either AT reaction will produce an output signal prior to amplification. (B) Multiplexed ATs reacted in a concurrent

format where output domains are unique fed into a logical AND gate displacement network with or without (+/-) the presence of an Amplification reaction network. (C) Logical AND gate operation based on work by Zhang and Seelig.⁵⁶ 98

Figure A1: AT reacted with 13 nM to 700 nM AT-fuel using 20, 200, and 2000 μ M adenosine. Fluorescence intensities were measured after 300 minutes. 300 nM fuel was selected for excess fuel experiments since it had much greater intensity for 20 μ M adenosine and lower leak compared to 500 nM. Data is shown here without error bars intentionally as it was not triplicated and only used as a rapid approximation for the optimal AT fuel concentration. 110

Figure A2. AT-ZR reacted with 2 mM Cytidine, Uridine, and Adenosine using 300 nM AT-fuel. Fluorescence intensities were measured after 24 hrs and subtracted by the AT network leakage measured at 24 hrs. The Adenosine intensity was 9.56x and 7.93x greater than the Cytidine and Uridine intensities respectively showing that the AT is selective to Adenosine.. 112

LIST OF ABBREVIATIONS

A	Adenine
ACE	Aptamer Complementary Element
ARN	Aptamer Reaction Network
AT	Aptamer Transducer
C	Cytosine
DNA	Deoxyribonucleic Acid
dsDNA	Double Stranded DNA
FRET	Fluorescence Resonance Energy Transfer
G	Guanine
HG	Hoogsteen Base Pair
HIV-RT	Human Immunodeficiency Virus Reverse Transcriptase
HPLC	High Performance Liquid Chromatography
IABkFQ	Iowa Black Quencher
IDT	Integrated DNA Technologies
IEL	Intuitive Energy Landscape
IgE	Immunoglobulin E
KN	Kotani's Network
KR	Kotani's Reporter
NUPACK	Nucleic Acid Package
PAGE	Polyacrylamide Gel Electrophoresis

PCR	Polymerase Chain Reaction
PMMA	Polymethyl Methacrylate
RNA	Ribonucleic Acid
SELEX	Systematic Evolution of Ligands by Exponential Enrichment
ssDNA	Single Stranded DNA
T	Thymine
TAE Buffer	Tris-Acetic Acid-EDTA Buffer
TBA	Thrombin Binding Aptamer
TE Buffer	Tris-EDTA Buffer
TET Dye	Tetrachlorofluorescein Dye
WC	Watson-Crick Base Pair
ZN	Zhang's Network
ZR	Zhang's Reporter

CHAPTER ONE: INTRODUCTION AND BACKGROUND FOR APTAMERS AND DYNAMIC DNA NANOTECHNOLOGY

1.1 Introduction

Sensing technologies have played a fundamental role in the development of our modern society by providing more precise measurements of known physical phenomenon. As our understanding of the physical phenomenon has increased, so too has our ability to manipulate the physical properties of matter at smaller and smaller dimensions. Our ability to detect and resolve physical structures at the nanometer length scale using various detection methods, such as transmission electron microscopy, atomic force microscopy, and scanning tunneling electron microscopy, are all examples of technological advancements made in part due to advances in sensing technologies. In terms of biological sensors, there are opportunities to improve the recognition of specific compounds and detect analytes at increasingly lower concentrations for biomedical, biotechnological, and environmental applications. Aptamers used in sensors that utilize deoxyribose nucleic acid (DNA) as a material for the detection of small molecules or macromolecules is a particular area of interest due to the programmability of DNA, since DNA can be programmed to conform to a wide range of possible structural motifs at the nanoscale.^{1,2} Based on the inherent structural diversity of DNA, many different aptamers have been discovered that target a variety of analytes, which have been previously hard to detect since they often require specialized expertise or sophisticated equipment.^{1,3}

More specifically, aptamers are oligonucleotides whose tertiary structures are capable of binding to target molecules with high affinity.²⁻⁶ Aptamers can bind to either macromolecules or small molecules with a binding strength that is proportional to the number of interactions between the target molecule and an aptamer's binding region. The net increase in entropy due to aptamer ligand binding is overcome by the enthalpic gain due to the interaction between DNA and ligand making it thermodynamically stable. In the case of macromolecules, such as a protein, the aptamer will conform in some way to the surface of the targeted macromolecule, and for small molecules, the DNA typically conforms to create a binding pocket capable of accepting the targeted small molecule.^{2,7} In both cases, van der Waals bonding, hydrogen bonding, and π orbital stacking all contribute to the binding affinity of a given aptamer-ligand pair.⁸ In addition, aptamers may possess multiple binding sites each with their own specific affinity, and these sites may or may not behave cooperatively.^{3,6,8} The sensitivity of aptamers greatly depends on the strength of the interactions between the aptamer and its respective target; and therefore, identification of aptamers with an increased binding affinity towards a single target is imperative in future biosensor development.^{2,6,7,9}

Identification of aptamers that bind a specific target is conducted through a process known as Systematic Evolution of Ligands by Exponential Enrichment (SELEX).^{1,4,10,11} SELEX relies on a combinatorial approach wherein a large library of DNA or RNA strands, differing in sequence, are added to a solution containing a target. Then sequences with the best binding strength are removed with the target after binding. The highest affinity sequences are then isolated and replicated using polymerase chain reaction (PCR). The enriched library, after PCR, is then reintroduced to the target and the

cycle is repeated until the library contains only candidate sequences with the highest binding strength. After many rounds of SELEX, a candidate aptamer toward a specific target can be identified from the enriched pool and its selectivity toward the target can be measured.^{4,7,10,11} Once aptamer stands have been identified they can be used to design biosensors or advanced therapeutics.²⁻⁹

Aptamer-based biosensors have been developed in a variety of formats and can be classified into two main categories, surface-immobilized sensors, and solution-based sensors.^{5,9,12-17} Surface immobilized sensors rely on the conformational changes induced by aptamer-ligand binding to produce a net change in either fluorescence at the surface or a change in conductivity of the surface, usually by bringing an electron-donating label closer to a conductive surface through aptamer ligand binding, in the case of electrochemical sensing.^{10,18-20} On the other hand, solution-based sensors are typically fluorometric or colorimetric sensors that rely on either direct aptamer labeling using fluorophores and quenchers or the use of a separate Fluorescence Resonance Energy Transfer (FRET) based reporting DNA/RNA complex, which functions through a series of toehold mediated strand displacement reaction steps.^{9,12,13,17,18,21} For colorimetric sensors, gold nanoparticle aggregation is often used to create a color change in solution with the use of aptamers as linkers or to initiate aggregation.^{3,22,23} One advantage of designing FRET-based biosensors is their ability to incorporate signal processing methods using DNA strand displacement cascades for logic operations, amplification, and/or multiplexing.^{12,13,23-26} Complex DNA strand displacement networks, that incorporate multiple aptamers, which can process, amplify, and detect a variety of targets in a single solution simultaneously, could provide a significant platform to develop

advanced multiplexed biosensors.^{20,26–28} The simultaneous detection of multiple disease biomarkers toward a single illness is an application for such multiplexed DNA-based biosensors among many others. Additionally, if multiplexed biosensing networks can be developed in a modular and customizable format, newly discovered aptamers can be easily incorporated into existing biosensor designs thus allowing for the rapid development of new or improved biosensors.^{10,20,27}

Our previous research has focused on the development of a modular and flexible format for aptamer strand displacement systems.⁴⁹ Toward this goal, we have developed an aptamer transducer that has been able to sense adenosine in solution down to 2 μM when combined with a feed-forward network for amplification of DNA output strands. For comparison, the intrinsic K_d of the adenosine aptamer is 6 μM where K_d denotes the concentration where 50% of aptamers in solution are bound to a ligand. Concentrations under K_d become harder to detect since the aptamer binding exponentially decreases under this limit. Additionally, our aptamer transducer design was shown to easily incorporate multiple output signals by accommodating different DNA sequences that are released after aptamer ligand binding and a series of toehold mediate strand displacement steps. By integrating our design with two feed-forward amplification networks, we demonstrated that the aptamer transducer can flexibly translate an adenosine signal into an arbitrary output sequence thus allowing the design to target a wide variety of signal processing networks.^{25,29} In the next phase of our research, we aimed to further optimize our aptamer transducer framework by studying the role of the aptamer input domains to greater depth. The aptamer complementary element (ACE) domain in our aptamer transducer provided the necessary bases for both the structure-switching mechanism of

the aptamer transducer and acts as a toehold in further strand displacement reaction steps. By screening ACE domains with different lengths and binding positions along the aptamer domain, we explored the kinetics of the aptamer transducer and studied the process of structure-switching caused by aptamer-ligand binding. Finally, in the last chapter we suggest future research for our aptamer transducer platform, which would integrate multiple aptamers into its design to develop a multiplexed single solution biosensor. Also, by incorporating intermediate feed-forward networks and strand displacement cascades for signal processing into the biosensing platform, further logic operations and signal amplification processes could be achieved.

1.2 Background

1.2.1 DNA Structure and Dynamics

Before understanding the behavior of our aptamer transducer, it is important to define the basic building blocks upon which DNA-based biosensors are developed. Hence, one must understand the structure and dynamics of DNA, which is a molecule responsible for encoding living organisms and a useful self-assembly material that can be utilized to construct nanomachines engineered toward a variety of applications.^{9,10,15,20,25,27,30-32} A single-stranded DNA molecule is constructed from a backbone of alternating deoxyribose sugar and phosphate groups, attached to each of these sugars is either a purine base, adenine or guanine, or a pyrimidine base, cytosine or thymine. For single strands, a chain of deoxyribose and purine or pyrimidine bases, nucleotides, are linked by phosphates and can extend for millions of bases within the genome or as little as 100 or fewer bases for synthetically prepared DNA oligonucleotides.^{31,32} The formation of double-stranded DNA, also known as

“hybridization”, occurs when two single strands of DNA with complementary bases, guanine with cytosine and adenine with thymine, form a network of hydrogen bonds with Watson-Crick base pairing; resulting in the well-known double helix structure, as shown in Figure 1.^{31,32} It is important to note that G•C pairs are more thermodynamically stable since three hydrogen bonds are formed within this base pair as compared with A•T pairs, which only has two hydrogen bonds.^{25,31–34} A double strand is considered fully complementary when two adjacent single strands have bases that are completely complementary and there are not any available bases for further base pairing.^{31,32,34} Further, two complementary single strands typically undergo Watson-crick base pairing, as shown in Figure 1, in an antiparallel configuration, where 5’ to 3’ terminal ends of each strand are oriented in opposite directions, where the terminal ends of a single strand are defined by a 5’ end that terminates with a phosphate group and a 3’ end that terminates with a sugar.^{31,32} In addition to fully complementary strands, partially complementary single strands can lead to a variety of DNA that secondary structures that can include hairpin loops, internal loops, bulges, branching loops, junctions, helices, and unstructured single strands, all of which can arise from different configurations of single or double stranded DNA strands forming a complex.^{29,32,34–37}

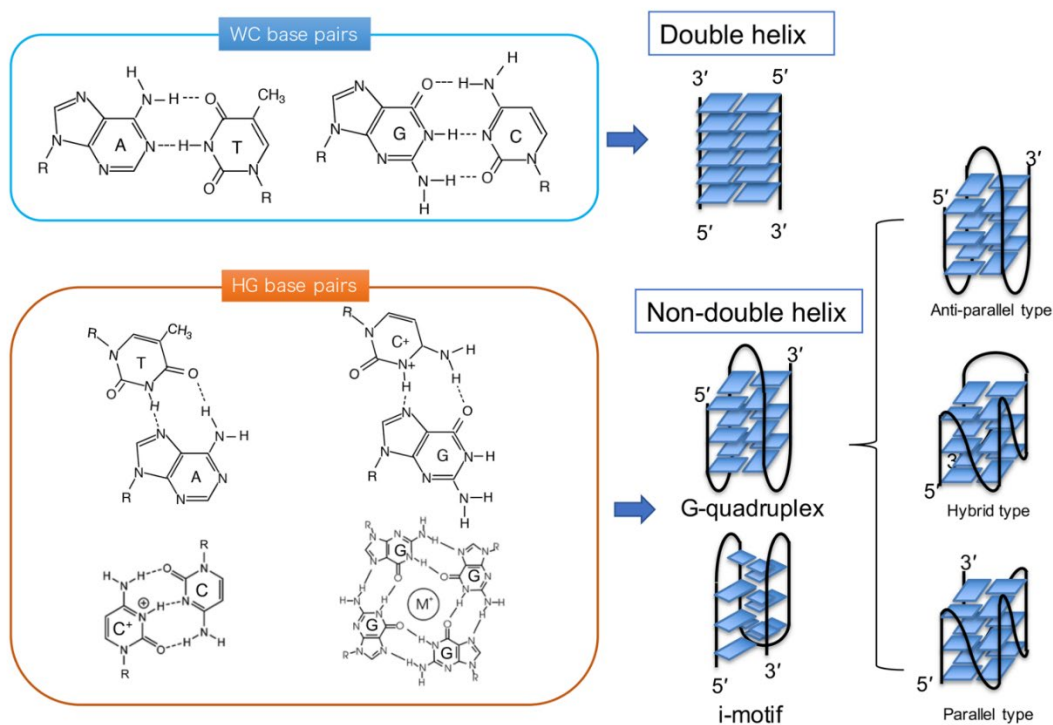


Figure 1.1 : Watson-crick base pairs (blue box) showing hybridized A•T and G•C pairs and the formation of a double helix structure with several stacked base pairs between bonded 3'-5' reversed single-strands. Hoogsteen base pairs (orange box) showing several alternate bonds which can form between purine bases. A G-tetrad with stabilizing M⁺ ion is shown (bottom right corner) and makes up the stacked bases in a G-quadruplexes shown under the non-double helix secondary structures where the DNA phosphate backbone distinguishes G-quadruplex types anti-parallel, hybrid, or parallel. An i-motif secondary structure which uses Hoogsteen base pairs is also shown.³³

DNA secondary structure formation can be controlled by alterations in conditions of the system such as temperature, pH, solvent, and presence of counter-ions in solution.^{31,32} Typically, DNA strands are solvated in aqueous conditions, however, many secondary structures are not able to form without the presence of a counter ion to screen the negative charges caused by the DNA phosphate backbone.^{31,32} Secondary structure formation is aided by adding Na⁺ or Mg²⁺ to solution for charge screening, and in particular for Mg²⁺ or other ions with a 2+ charge, there is an even greater effect that is observed that is caused by counter ions acting as a bridge between two complementary

domains.³⁸ Temperature is another important factor to consider for secondary structure formation since secondary structures dehybridize or “melt” upon reaching a high enough temperature. In other words, when heat energy is added to the system, base pairs begin to dehybridize until all complementary domains are unpaired, which occurs when the binding energy between complementary domains has been overcome.^{31,32} Thermal cycling and annealing of DNA structures has become an important processing step for controlling the outcome of secondary structure formation, since unintended secondary structures can be melted at high temperature and cooled slowly to hybridize into alternate DNA complexes.^{31,32} Secondary structure formation can also occur with non-canonical base pairing where DNA bases form hydrogen bond in a different orientation or scheme compared to the standard Watson-Crick base pairing. Hoogsteen base pairing (Figure 1) is one example of non-canonical base pairing in which the nitrogen on the purine base bonds to the C6 amino group of an opposing base.³³ Hoogsteen base pairing is of particular importance for the formation of secondary structures within many of the known aptamers, since many aptamers rely on the formation of G-quadruplex structures, Figure 1, where guanine rich strands form tetrads, where Hoogsteen base pairing occurs between the adjacent guanines.^{4,7,27,33} G-quadruplex structures are often observed in ligand binding pockets of aptamers and create a structural and chemical environment well-suited for specific interactions with a target molecule.⁷

1.2.2 Aptamer Dynamics

Aptamer folding kinetics and the dynamics of aptamer ligand binding have been a major topic of study in the field. There have been two proposed kinetic pathways for aptamer-ligand binding: conformational selection or induced fit binding, as illustrated by

Figure 1A.^{7,39} Conformational selection assumes that the aptamer exists in many different thermodynamically accessible conformations, that are in equilibrium; including a small population that is in the “ligand binding competent” conformation. Presence of the ligand shifts the equilibrium to the bound state. Inducted fit binding occurs when the ligand physically interacts with the binding site, inducing the conformation into the bound state. Recently, studies have suggested that the mechanism for most aptamer-ligand binding is due to the induced fit mechanism as seen in Figure 2B and that additional counter ions in solution act to lower the activation energy required for aptamer-ligand conformation and binding.^{7,39} Regardless of the mechanism responsible for binding, aptamer-ligand binding is generally considered to be a weak interaction and therefore bound complexes are not stable indefinitely, hence aptamer-ligand binding occurs for only a specified lifetime, which depends on the strength of the interaction.^{39,40}

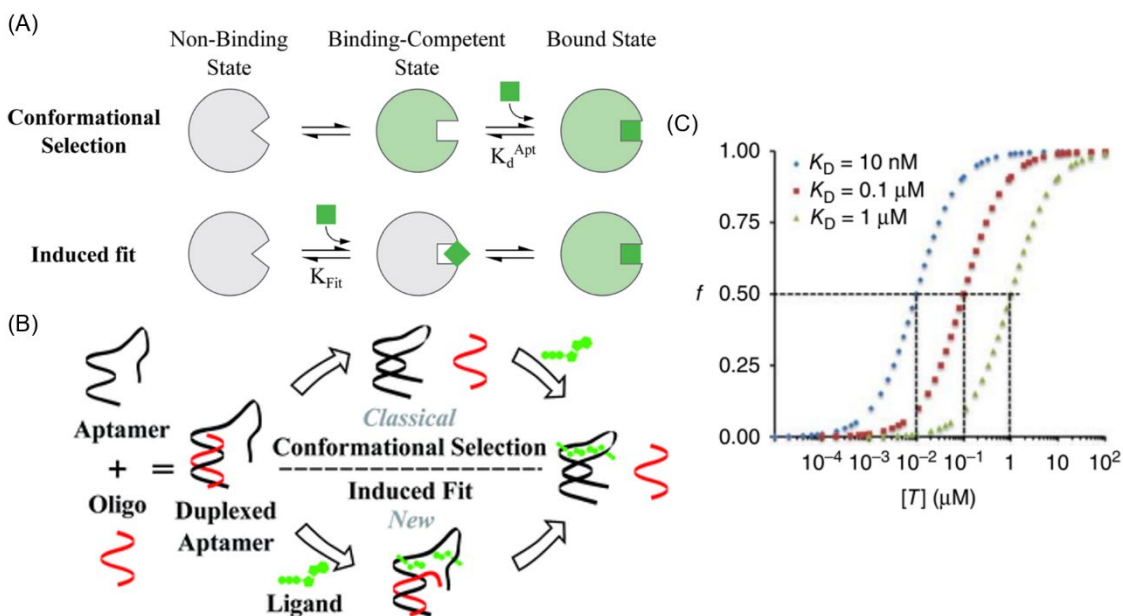
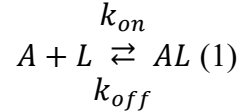


Figure 1.2: (A) Compares the kinetic pathways for both conformational selection and induced fit mechanisms. For conformational selection, the substrate conforms to a state ready to accepted the target and then proceeds with binding, K_d^{Apt} is the binding affinity. Induced fit proceeds by fitting the target into the substrate as an intermediate and then transitions to the bound state, K_{Fit} is the affinity to form the intermediate state. (B) Conformational selection versus induced fit mechanisms applied to a duplexed aptamer. The Oligo represents a short aptamer complementary element (ACE) that prevents aptamer-ligand binding until it becomes dehybridized. (C) Occupancy of a single-site aptamer f compared to the ligand concentration $[T]$. The dissociation constant K_d , binding affinity, is defined at the concentration $[T]$ when there is 50% occupancy of the aptamer binding sites. Sigmoid binding curves for K_d 10, 100, and 1000 nM aptamers are shown.^{39,40}

Due to the inherent reversibility and transient behavior of aptamer-ligand binding which can occur within nanoseconds to minutes depending on binding strength, aptamer ligand-binding is best modeled as an equilibrium reaction, where the k_{on} and k_{off} are the on and off rates of the aptamer respectively and which follows the general relationship⁴⁰:



$$k_{on}[A][L] = k_{off}[AL] \quad (2)$$

The ratio of k_{off}/k_{on} is defined as the aptamer dissociation constant (K_d) and is a generally useful metric for comparing the binding strength of aptamers, where the inverse of K_d is the association constant (K_a).⁴⁰

$$K_d = \frac{1}{K_a} = \frac{k_{off}}{k_{on}} = \frac{[A][L]}{[AL]} \quad (3)$$

Using the relationship given in (3), the aptamer concentration $[A]$ can be alternatively calculated using $[A]_t$, the total aptamer in the system, by subtracting the bound aptamer $[AL]$, assuming $[A]_t$ remains constant throughout.⁴⁰

$$K_d = \frac{([A]_t - [AL])[L]}{[AL]} \quad (4)$$

Rearrangement to find the ratio of bound aptamer $[AL]$ to total aptamer $[A]_t$ defines f , the fraction of occupied binding sites reflective of a Langmuir isotherm (Figure 2C) with respect to $[L]$ and K_d where K_d is defined by the ligand concentration $[L]$ at 50% occupancy, $f=0.5$.⁴⁰

$$f = \frac{[AL]}{[A]_t} = \frac{1}{\frac{K_d}{[L]} + 1} \quad (5)$$

At the half maximum ligand concentration, K_d concentration, 50% of the aptamer ligand binding sites in solution are occupied at any given moment in time.⁴⁰ In general, when the K_d is higher the k_{off} rate is much greater than the k_{on} rate and therefore the aptamer ligand binding interaction is considered to be a relatively weak interaction and is reflective of the aptamer ligand binding affinity.⁴⁰ Many studies aim to improve the overall performance, lower the K_d , of specific aptamers toward their targets by sequence

alterations, binding site mutations, and base pair mismatches.^{3,6,26,40,41} In some cases, aptamers undergo further rounds of selection using SELEX to find sequences that possess an even greater binding affinity, a lower K_d .⁴¹ Further, many aptamer biosensors rely on the hybridization of a short complementary sequence, usually between 2-12 base pairs, to the aptamer somewhere along its binding domain, which are referred to as aptamer complementary elements (ACE).^{2,7,39} An ACE is dehybridized upon aptamer ligand binding as the aptamer conforms to accept an incoming ligand, allowing the ACE to become available for further DNA reactions. Sensors that rely on an ACE in this way are considered “structure-switching aptamer biosensors”.^{2,7,9,39} Structure-switching biosensors offer a reliable means of easily detecting the conformational changes occurring in an aptamer-ligand binding provided one can select an adequate ACE that will readily dissociate during the binding interaction. With the presence of a hybridized ACE, the dissociation constant K_d of the aptamer is raised, now considered as effective K_d ($K_{d,eff}$), due to the activation energy penalty incurred by having hybridized bases that must be displaced for ligand-binding to occur.^{2,7,9,39} Selecting an ACE of appropriate length and position within the aptamer sequence that yields a $K_{d,eff}$ near that of the original aptamer K_d provides the highest sensitivity and therefore biosensors that utilize the structure-switching mechanism should be designed to use an optimal ACE. Careful selection of the ACE is also an important consideration for downstream reactions that will utilize the sequence for functioning, especially when considering the ACE sequence as a toehold for strand displacement reactions. The ACE must be selected to avoid crosstalk interactions with other strands that may be present.

1.2.3 DNA Strand Displacement

Incorporation of applicable DNA reaction networks that utilize toehold-mediated strand displacement allows for the development of nucleic acid circuits within aptamer biosensors that possess diverse functionality such as logic operations, signal amplification, or signaling, and do not require the use of enzymes or other constituents other than DNA for function.^{12,13,17,30} The process of toehold-mediated strand displacement occurs when an incumbent strand fully displaces a signal strand that is hybridized to a backbone forming a substrate complex, the backbone possesses a toehold sequence to promote initiation of the displacement process.⁴² An intuitive energy landscape (IEL), as shown in Figure 3, is useful for visualizing the steps required for strand displacement and provides useful representation of the energy barriers present within the entire process.⁴² First, the incumbent strand must overcome an energy barrier associated with binding to the toehold, called toehold initiation, where one or more bases hybridize with a complementary sequence on the exposed substrate. Toehold initiation is the rate limiting step for strand displacement since a high energy barrier is associated with the incumbent strand being positioned and oriented properly for toehold binding to occur or, in other words, initial hybridization of the toehold reduces entropy in the system and therefore incurs a significant energy penalty.⁴² In the next step, all of the bases present in the toehold hybridize, lowering the net free energy due to enthalpic gains.⁴² Finally, a series of displacement steps, called propagation or branch migration, occur by a random walk process where bases on the substrate are replaced by complementary bases along the incumbent strand, and are replaced one base at a time.⁴² This first step in branch migration requires the dehybridization of a signal base, which raises the free energy, and

then proceeds with the replacement of a complementary incumbent base, which again lowers the free energy producing a sawtooth pattern seen in the IEL.⁴² The branch migration process continues until either the incumbent strand fully displaces the signal strand or the toehold domains of the backbone and incumbent spontaneously dehybridize.⁴² Since spontaneous dissociation of the toehold can occur, it is best to select a toehold with greater than 3 bases and consider incorporating a high G•C content for greater stability.⁴² Strand displacement can occur by both 3-way branch migration where a single strand replaces another single strand on a substrate or by 4-way branch migration where two double strands swap complementary strands. 4-way branch migration is considered the kinetically slower process since it requires the dissociation and hybridization of two bases per strand displacement step compared to 3-way branch migration, which only requires one.²⁵

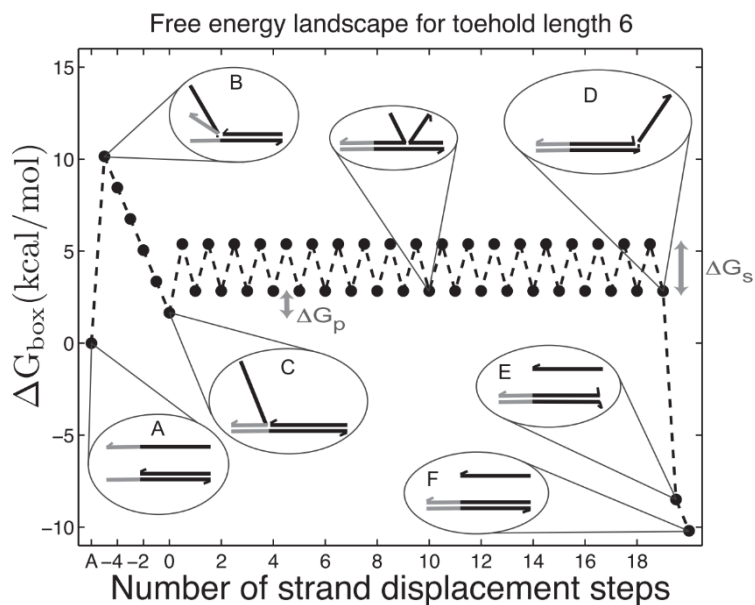


Figure 1:3: Intuitive energy landscape showing the free energy change during each strand displacement step. A 6 nt toehold provides a net lowering of the free energy before and after displacement due to the 6 additional base pairs formed during the reaction.⁴²

Ideally, strand displacement would always occur through the intended reaction pathway. However, DNA reaction networks that utilize strand displacement possess the potential to react in an unintended way causing what is known as network leakage.^{25,36} Leakage in a strand displacement reaction typically occurs at the terminal end of the substrate opposite to toehold where an incumbent strand or complex binds and displaces the backbone strand prematurely.^{25,36} This can lead to an increase in signal even without the presence of an incumbent reacting in the intended pathway, starting with the initiation of the toehold domain.^{25,36} Another potential vulnerability for leakage are nick sites where there is a break in the DNA sequence on a substrate.^{25,36} Many have hypothesized the main cause of leakage to be due to breathing of the DNA double helix, where bases

become transiently unpaired only to hybridize once again.^{25,36} If breathing were the main cause it would mean that incumbent strands could initiate a toehold anywhere along the substrate, but particularly at the ends where there is little steric hindrance to block the incumbent strand. Many strategies have been developed to help mitigate network leakage; including base pair mismatches, G•C clamps, availability-driven design, interfering strands, double-long domain and triple long domain designs.^{25,36,43} Regardless of network leakage, which can cause some error, DNA strand displacement has provided a reliable means to develop DNA reaction networks with useful functionality.

DNA strand displacement is a powerful tool for developing dynamic DNA nanotechnology, where DNA structures can be manipulated at the nanoscale.^{25,34,44} Yurke et al. first demonstrated this nanotechnological advancement through the development of nanotweezers that were able to open and close on-demand through a strand displacement process.⁴⁴ Further studies have expanded the field of strand displacement to develop sensors, sequence transducers, signal amplifiers, logic gates, and even perform basic computations.^{17,25,29,45–48} In particular, strand displacement networks, which that perform signal amplification, are important for developing aptamer biosensors, since they can amplify weak signals and effectively raise the sensitivity of the network.^{25,29} A logical next step in the development of aptamer-based sensors is the incorporation of DNA strand displacement systems to perform various signal processing and recognition steps. One of the simplest of these aptamer biosensing approaches involves developing a fluorescence-based reporting system that can provide a net increase in the fluorescence of a solution when the ACE acts as an incumbent to separate a dye and quencher labeled FRET reporter complex.^{12,13,17} Other systems have utilized strand displacement for

functionality in a variety of formats to develop aptamer biosensors including surface-based sensors, electrochemical sensors, and colorimetric sensors that use gold nano particles to provide a color change.^{2,3,5,7,12,13,15-17,19,22} Strand displacement cascades, which incorporate many substrates with both consecutive and concurrent reaction steps, can be used to develop multiplexed reaction networks providing that many targets could be simultaneously detected by aptamers in solution.^{10,20} Multiplexed aptamer reaction networks offer promising applications for the detection of multiple disease biomarkers simultaneously in solution.^{10,27,40} While many different motifs for aptamer-based sensors utilizing strand displacement reactions have been explored, there are still many nuances yet to be discovered, and the future applicability of these devices is yet to be fully realized.

In the chapters that follow, we introduce the aptamer transducer (AT) platform using the adenosine binding DNA aptamer, a promising aptamer-based sensor that integrates strand displacement reactions for signal processing. The next chapter discusses and introduces the AT platform for the first time and demonstrates that it can produce a customizable output signal capable of being an input to further signal processing using strand displacement reaction networks. Chapter 3 explores the AT to further depth and provides a deeper understanding of the structure-switching mechanism and provides a selection process for determining ACEs that improve AT sensitivity. In the final chapter, we conclude this work by providing a path forward for continued research with the AT and discuss future goals and challenges of the field.⁴⁹

1.3 References

- (1) Luo, Y. Functional Nucleic Acid Biosensors for Small Molecules. In *Functional Nucleic Acid Based Biosensors for Food Safety Detection*; Luo, Y., Ed.; Springer Singapore: Singapore, 2018; pp 249–306. https://doi.org/10.1007/978-981-10-8219-1_10.
- (2) Munzar, J. D.; Ng, A.; Juncker, D. Duplexed Aptamers: History, Design, Theory, and Application to Biosensing. *Chem. Soc. Rev.* **2019**, *48* (5), 1390–1419. <https://doi.org/10.1039/c8cs00880a>.
- (3) Armstrong, R. E.; Strouse, G. F. Rationally Manipulating Aptamer Binding Affinities in a Stem-Loop Molecular Beacon. *Bioconjug. Chem.* **2014**, *25* (10), 1769–1776. <https://doi.org/10.1021/bc500286r>.
- (4) Huizenga, D. E.; Szostak, J. W. A DNA Aptamer That Binds Adenosine and ATP. *Biochemistry* **1995**, *34* (2), 656–665. <https://doi.org/10.1021/bi00002a033>.
- (5) Monserud, J. H.; Macri, K. M.; Schwartz, D. K. Toehold-Mediated Displacement of an Adenosine-Binding Aptamer from a DNA Duplex by Its Ligand. *Angew. Chem. Int. Ed.* **2016**, *55* (44), 13710–13713. <https://doi.org/10.1002/anie.201603458>.
- (6) Zhang, Z.; Oni, O.; Liu, J. New Insights into a Classic Aptamer: Binding Sites, Cooperativity and More Sensitive Adenosine Detection. *Nucleic Acids Res.* **2017**, *45* (13), 7593–7601. <https://doi.org/10.1093/nar/gkx517>.
- (7) Munzar, J. D.; Ng, A.; Juncker, D. Comprehensive Profiling of the Ligand Binding Landscapes of Duplexed Aptamer Families Reveals Widespread Induced Fit. *Nat. Commun.* **2018**, *9* (1), 343. <https://doi.org/10.1038/s41467-017-02556-3>.
- (8) Plach, M.; Schubert, T. Biophysical Characterization of Aptamer-Target Interactions. *Aptamers Biotechnol.* **2019**, 1–15.
- (9) Nutiu, R.; Li, Y. Structure-Switching Signaling Aptamers: Transducing Molecular Recognition into Fluorescence Signaling. *Chem. - Eur. J.* **2004**, *10* (8), 1868–1876. <https://doi.org/10.1002/chem.200305470>.

- (10) Shaban, S. M.; Kim, D.-H. Recent Advances in Aptamer Sensors. *Sensors* **2021**, *21* (3). <https://doi.org/10.3390/s21030979>.
- (11) Tuerk, C.; Gold, L. Systematic Evolution of Ligands by Exponential Enrichment: RNA Ligands to Bacteriophage T4 DNA Polymerase. *Science* **1990**, *249* (4968), 505–510.
- (12) Cheng, S.; Zheng, B.; Wang, M.; Zhao, Q.; Lam, M. H.; Ge, X. Determination of Adenosine Triphosphate by a Target Inhibited Catalytic Cycle Based on a Strand Displacement Reaction. *Anal. Lett.* **2014**, *47* (3), 478–491. <https://doi.org/10.1080/00032719.2013.841179>.
- (13) Cheng, S.; Zheng, B.; Wang, M.; Ge, X.; Lam, M. H. A Target-Triggered Strand Displacement Reaction Cycle: The Design and Application in Adenosine Triphosphate Sensing. *Anal. Biochem.* **2014**, *446* (1), 69–75. <https://doi.org/10.1016/j.ab.2013.10.021>.
- (14) Carrasquilla, C.; Li, Y.; Brennan, J. D. Surface Immobilization of Structure-Switching DNA Aptamers on Macroporous Sol-Gel-Derived Films for Solid-Phase Biosensing Applications. *Anal. Chem.* **2011**, *83* (3), 957–965. <https://doi.org/10.1021/ac102679r>.
- (15) Meng, H.-M.; Liu, H.; Kuai, H.; Peng, R.; Mo, L.; Zhang, X.-B. Aptamer-Integrated DNA Nanostructures for Biosensing, Bioimaging and Cancer Therapy. *Chem. Soc. Rev.* **2016**, *45* (9), 2583–2602. <https://doi.org/10.1039/C5CS00645G>.
- (16) Shlyahovsky, B.; Li, D.; Weizmann, Y.; Nowarski, R.; Kotler, M.; Willner, I. Spotlighting of Cocaine by an Autonomous Aptamer-Based Machine. *J. Am. Chem. Soc.* **2007**, *129* (13), 3814–3815. <https://doi.org/10.1021/ja069291n>.
- (17) Zhu, J.; Zhang, L.; Zhou, Z.; Dong, S.; Wang, E. Aptamer-Based Sensing Platform Using Three-Way DNA Junction-Driven Strand Displacement and Its Application in DNA Logic Circuit. *Anal. Chem.* **2014**, *86* (1), 312–316. <https://doi.org/10.1021/ac403235y>.

- (18) Fu, B.; CAo, J.; Wang, L.; Jiang, W. A Novel Enzyme-Free and Label-Free Fluorescence Aptasensor for Amplified Detection of Adenosine. *Biosens. Bioelectron.* **2013**, *44* (1), 52–56. <https://doi.org/10.1016/j.bios.2012.12.059>.
- (19) Xiao, Y.; Piorek, B. D.; Plaxco, K. W.; Heeger, A. J. A Reagentless Signal-on Architecture for Electronic, Aptamer-Based Sensors via Target-Induced Strand Displacement. *J. Am. Chem. Soc.* **2005**, *127* (51), 17990–17991. <https://doi.org/10.1021/ja056555h>.
- (20) Yu, H.; Alkhamis, O.; Canoura, J.; Liu, Y.; Xiao, Y. Advances and Challenges in Small-Molecule DNA Aptamer Isolation, Characterization, and Sensor Development. *Angew. Chem. Int. Ed.* **2021**, *60* (31), 16800–16823. <https://doi.org/10.1002/anie.202008663>.
- (21) Meng, C.; Dai, Z.; Guo, W.; Chu, Y.; Chen, G. Selective and Sensitive Fluorescence Aptamer Biosensors of Adenosine Triphosphate. *Nanomater. Nanotechnol.* **2016**, *6*, 33. <https://doi.org/10.5772/63985>.
- (22) Lee, J.; Jeon, C. H.; Ahn, S. J.; Ha, T. H. Highly Stable Colorimetric Aptamer Sensors for Detection of Ochratoxin A through Optimizing the Sequence with the Covalent Conjugation of Hemin. *The Analyst* **2014**, *139* (7), 1622–1627. <https://doi.org/10.1039/c3an01639k>.
- (23) Ravan, H. Implementing a Two-Layer Feed-Forward Catalytic DNA Circuit for Enzyme-Free and Colorimetric Detection of Nucleic Acids. *Anal. Chim. Acta* **2016**, *910*, 68–74. <https://doi.org/10.1016/j.aca.2016.01.013>.
- (24) Jung, C.; Ellington, A. D. Diagnostic Applications of Nucleic Acid Circuits. *Acc. Chem. Res.* **2014**, *47* (6), 1825–1835. <https://doi.org/10.1021/ar500059c>.
- (25) Kotani, S.; Hughes, W. L. Multi-Arm Junctions for Dynamic DNA Nanotechnology. *J. Am. Chem. Soc.* **2017**, *139* (18), 6363–6368. <https://doi.org/10.1021/jacs.7b00530>.
- (26) Li, B.; Ellington, A. D.; Chen, X. Rational, Modular Adaptation of Enzyme-Free DNA Circuits to Multiple Detection Methods. *Nucleic Acids Res.* **2011**, *39* (16), e110. <https://doi.org/10.1093/nar/gkr504>.

- (27) Seok Kim, Y.; Ahmad Raston, N. H.; Bock Gu, M. Aptamer-Based Nanobiosensors. *30th Anniv. Issue* **2016**, *76*, 2–19. <https://doi.org/10.1016/j.bios.2015.06.040>.
- (28) Hoang Trung Chau, T.; Hoang Anh Mai, D.; Ngoc Pham, D.; Thi Quynh Le, H.; Yeol Lee, E. Developments of Riboswitches and Toehold Switches for Molecular Detection—Biosensing and Molecular Diagnostics. *Int. J. Mol. Sci.* **2020**, *21* (9). <https://doi.org/10.3390/ijms21093192>.
- (29) Zhang, D. Y.; Turberfield, A. J.; Yurke, B.; Winfree, E. Engineering Entropy-Driven Reactions and Networks Catalyzed by DNA. *Science* **2007**, *318* (5853), 1121–1125. <https://doi.org/10.1126/science.1148532>.
- (30) Dai, Y.; Furst, A.; Liu, C. C. Strand Displacement Strategies for Biosensor Applications. *Trends Biotechnol.* **2019**, *37* (12), 1367–1382.
- (31) Fan, C. 1974-. *DNA Nanotechnology : From Structure to Function*; Springer: Berlin ;, 2013. <https://doi.org/10.1007/978-3-642-36077-0>.
- (32) Jin, J.-Il.; Grote, J. G. 1955-. *Materials Science of DNA*; CRC Press/Taylor & Francis: Boca Raton, FL, 2012.
- (33) Takahashi, S.; Sugimoto, N. Watson–Crick versus Hoogsteen Base Pairs: Chemical Strategy to Encode and Express Genetic Information in Life. *Acc. Chem. Res.* **2021**, *54* (9), 2110–2120. <https://doi.org/10.1021/acs.accounts.0c00734>.
- (34) Zhang, D. Y.; Seelig, G. Dynamic DNA Nanotechnology Using Strand-Displacement Reactions. *Nat. Chem.* **2011**, *3* (2), 103–113. <https://doi.org/10.1038/nchem.957>.
- (35) Zadeh, J. N.; Steenberg, C. D.; Bois, J. S.; Wolfe, B. R.; Pierce, M. B.; Khan, A. R.; Dirks, R. M.; Pierce, N. A. NUPACK: Analysis and Design of Nucleic Acid Systems. *J. Comput. Chem.* **2011**, *32* (1), 170–173. <https://doi.org/10.1002/jcc.21596>.
- (36) Lysne, D.; Jones, K.; Stosius, A.; Hachigian, T.; Lee, J.; Graugnard, E. Availability-Driven Design of Hairpin Fuels and Small Interfering Strands for

- Leakage Reduction in Autocatalytic Networks. *J. Phys. Chem. B* **2020**, *124* (16), 3326–3335. <https://doi.org/10.1021/acs.jpccb.0c01229>.
- (37) Bochman ML; Paeschke K; Zakian VA. DNA Secondary Structures: Stability and Function of G-Quadruplex Structures. *Nat. Rev. Genet.* **2012**, *13* (11), 770–780. <https://doi.org/10.1038/nrg3296>.
- (38) Guérout, M.; Boittin, O.; Mauffret, O.; Etchebest, C.; Hartmann, B. Mg²⁺ in the Major Groove Modulates B-DNA Structure and Dynamics. *PLOS ONE* **2012**, *7* (7), e41704. <https://doi.org/10.1371/journal.pone.0041704>.
- (39) Munzar, J. D.; Ng, A.; Corrado, M.; Juncker, D. Complementary Oligonucleotides Regulate Induced Fit Ligand Binding in Duplexed Aptamers. *Chem. Sci.* **2017**, *8* (3), 2251–2256. <https://doi.org/10.1039/C6SC03993F>.
- (40) Dong, Y. *Aptamers for Analytical Applications : Affinity Acquisition and Method Design*; Wiley-VCH: Weinheim, Germany, 2018.
- (41) Gao, S.; Zheng, X.; Jiao, B.; Wang, L. Post-SELEX Optimization of Aptamers. *Anal. Bioanal. Chem.* **2016**, *408* (17), 4567–4573. <https://doi.org/10.1007/s00216-016-9556-2>.
- (42) Srinivas, N.; Ouldrige, T. E.; Sulc, P.; Schaeffer, J. M.; Yurke, B.; AA, L.; JP, D.; Winfree, E. On the Biophysics and Kinetics of Toehold-Mediated DNA Strand Displacement. *Nucleic Acids Res.* **2013**, *41* (22), 10641–10658. <https://doi.org/10.1093/nar/gkt801>.
- (43) Wang, B.; Thachuk, C.; Ellington, A. D.; Winfree, E.; Soloveichik, D. Effective Design Principles for Leakless Strand Displacement Systems. *Proc. Natl. Acad. Sci. U. S. A.* **2018**, *115* (52), E12182–E12191. <https://doi.org/10.1073/pnas.1806859115>.
- (44) Yurke, B.; Turberfield, A. J.; Mills, A. P.; Simmel, F. C.; Neumann, J. L. A DNA-Fuelled Molecular Machine Made of DNA. *Nature* **2000**, *406* (6796), 605–608. <https://doi.org/10.1038/35020524>.
- (45) Seelig, G.; Soloveichik, D.; Zhang, D. Y.; Winfree, E. Enzyme-Free Nucleic Acid Logic Circuits. *Science* **2006**, *314* (5805), 1585–1588.

- (46) Song, T.; Garg, S.; Mokhtar, R.; Bui, H.; Reif, J. Analog Computation by DNA Strand Displacement Circuits. *ACS Synth. Biol.* **2016**, *5* (8), 898–912. <https://doi.org/10.1021/acssynbio.6b00144>.
- (47) Li, W.; Yang, Y.; Yan, H.; Liu, Y. Three-Input Majority Logic Gate and Multiple Input Logic Circuit Based on DNA Strand Displacement. *Nano Lett.* **2013**, *13* (6), 2980–2988. <https://doi.org/10.1021/nl4016107>.
- (48) Qian, L.; Winfree, E. A Simple DNA Gate Motif for Synthesizing Large-Scale Circuits. *J. R. Soc. Interface* **2011**, *8* (62), 1281–1297. <https://doi.org/10.1098/rsif.2010.0729>.
- (49) Hachigian, T.; Lysne, D.; Graugnard, E.; Lee, J. Customizable Aptamer Transducer Network Designed for Feed-Forward Coupling. *ACS Omega* **2021**, *6* (41), 26888–26896. <https://doi.org/10.1021/acsomega.1c03146>.

CHAPTER TWO: A CUSTOMIZABLE APTAMER TRANSDUCER NETWORK
DESIGNED FOR FEED FORWARD COUPLING

This chapter was published by the American Chemical Society in the journal *ACS Omega* and should be referenced appropriately as below.

“Hachigian, Tim, et al. "Customizable Aptamer Transducer Network Designed for Feed-Forward Coupling." *ACS Omega*, 6 (41): 26888-26896. Copyright 2021 American Chemical Society.”

*Boise State University, Micron School of Materials Science and Engineering,
1910 University Dr., Boise, Idaho 83725, United States*

Reproduced by permission of the American Chemical Society.

2.1 Abstract

Solution based biosensors that utilize aptamers have been engineered in a variety of formats to detect a range of analytes for both medical and environmental applications. However, since aptamers have fixed base sequences, incorporation of aptamers into DNA strand displacement networks for feed-forward signal amplification and processing requires significant redesign of downstream DNA reaction networks. We designed a novel aptamer transduction network that releases customizable output domains, which can then be used to initiate downstream strand displacement reaction networks without any sequence redesign of the downstream reaction networks. In our aptamer transducer, aptamer input domains are independent of output domains within the same DNA complex and are reacted with a fuel strand after aptamer-ligand binding. Aptamer transducers were designed to react with two fluorescence dye-labeled reporter complexes to show the customizability of the output domains, as well as being used as feed-forward inputs to

two previously studied catalytic reaction networks, which can be used as amplifiers. Through our study we show both successful customizability and feed-forward capability of our aptamer transducers.

2.2 Introduction

Aptamers are single stranded nucleic acid sequences that bind selectively to a target ligand with high affinity. Identification of aptamers occurs through systematic evolution of ligands by exponential enrichment (SELEX), which has identified several hundred sequences to date.¹⁻⁶ A duplexed aptamer is formed by hybridizing an aptamer with a short complementary sequence known as an aptamer complementary element.^{7,8} Duplexed aptamers that release an aptamer complementary element upon biomolecular interaction with the sensing target have been used as sensing elements in novel aptamer biosensors.^{1,2} Biosensors utilizing such duplexed aptamers have been developed in a variety of formats, including solution FRET, surface FRET, solution fluorescence, surface fluorescence, electrochemistry, nucleic acid circuits, colorimetry, and nanoparticle FRET.^{3,5-22} While these approaches all offer biosensing capability, biosensors that incorporate nucleic acid circuits in particular, offer unique advantages because of their natural compatibility with DNA reaction networks capable of signal processing, signal amplification, and logic operations.^{23,24} Aptamer Reaction Networks (ARNs) are DNA reaction networks that incorporate an aptamer as an element to trigger a nucleic acid circuit. The usefulness of an ARN lies in its ability to transduce a biomolecular input of target analytes into a nucleic acid signal.^{18,25,26} When integrated with simple and inexpensive detection technologies, ARNs could one day become a potential replacement for assays that require more intensive labor or expensive

equipment.²⁶ Investigation of more sensitive and well-designed ARN circuit components is critical for the development of sensing technologies for medical diagnostic and environmental applications.

Because an ARN produces a DNA output, it is capable of triggering further logic operations and signal amplification by downstream DNA reaction networks through feed-forward signaling.²⁷ This feed-forward capability has made reaction networks a noted area of interest in aptamer biosensing.^{1,13,15,18,28} For example, Cheng et al. demonstrated the coupling of the adenosine aptamer into a feed-forward catalytic reaction network employing both target inhibited and target triggered approaches to amplify the detection of adenosine.^{15,28} Furthermore, they utilized the aptamer strand or its complement to trigger a catalytic cycle in their network design. In this example, however, the ARN produced an output that is dependent on the aptamer sequence.^{15,28} As a result, these networks require significant sequence redesign of downstream DNA reaction networks for their intended function. Zhu et al., for example, developed an aptamer transduction unit based on a three-way junction that could translate a target-inhibited aptamer signal into an arbitrary output. The network's feed-forward capability, however, was not demonstrated.²¹ Other approaches toward developing a universal aptamer biosensor lack a transduction step and operate as labeled molecular beacons or as simple direct colorimetric devices.^{7,13,16,17,19,25}

While feed-forward functionality has been considered by some groups,^{1,13,15,18,28} the community has focused more on modifications to increase the sensitivity of ARNs. Since aptamer biosensors are generally limited by the inherent aptamer-ligand binding affinity (K_d), approaches for designing more sensitive detectors depend on modifying an

aptamer strand because its effective binding affinity ($K_{d,eff}$) can be improved with targeted alterations to its base sequence, including hybridization of complementary elements.^{1–3,7–14,14–23,25,26,28–34} For example, many studies have aimed to optimize the adenosine aptamer effective binding affinity ($K_{d,eff}$) by manipulating the location of the aptamer sequence in their biosensor designs or by direct aptamer sequence alterations such as truncation and mutation.^{25,35} These studies have shown that even greater binding affinities can be achieved for many of the known aptamers using such modifications. Screening of novel aptamers through SELEX is another route for identifying selective aptamer sequences that yield greater sensitivities toward the same target.³¹ As novel and more sensitive aptamers are developed and discovered, general approaches for incorporating them into modular ARNs will be critical for the creation of biosensors with improved functionalities and performances.

While many studies have dealt with increasing aptamer sensitivity, relatively few studies have attempted to incorporate such aptamers into two-layer feed-forward networks.^{13,28} A feed-forward DNA reaction network is composed of multiple consecutive reaction networks in which the output of the first network functions as the input for the subsequent network. Using feed-forward functionality allows for greater modularity between reaction networks, since different reaction networks can be chained together to achieve multi-functionality. For example, an ARN can be first used for biosensing and then can be chained to a catalytic network for signal amplification. Using an ARN in a feed-forward network presents a unique challenge since the output of an ARN is dependent on the base sequence of the aptamer, which in turn requires a redesign of a subsequent network. Therefore, there is significant motivation to design ARNs that

can transduce a molecular signal from the target into multiple DNA outputs without the need for significant domain level redesigns of downstream networks.

In this work, we introduce an *Aptamer Transducer (AT)* as a non-enzymatic, modular, and customizable ARN that can be implemented in two-layer feed-forward reaction networks. Using the well-known Huizenga & Szostak adenosine aptamer, we have designed and tested a practical biosensing platform that can fully transduce an adenosine signal into arbitrary DNA outputs based on a structure-switching aptamer design, where the AT's output domain is not dependent on the sequence of the adenosine aptamer.³⁰ This design modularity was accomplished by separating the aptamer input domain from the output domain, which is sequestered in a hairpin region of the AT complex. Incorporating an additional fuel strand into the AT design allows for the release of the output strand upon successful toehold mediated DNA strand displacement. Two dye and quencher labeled reporter complexes, differing in sequence, were used to show that the AT can successfully output differing signals. To further demonstrate the ATs customizability, we incorporated the AT with two catalytic amplification networks – an entropy-driven catalytic network developed by Zhang et al.²³ and a 3-arm catalytic amplification network developed by Kotani et al.²⁴

2.3 Results and Discussion

As illustrated in Figure 1A, two critical regions for the functionality of AT are the aptamer input region (blue box) and the DNA Output region (brown box). The 6-nt long aptamer complement domain τ' is duplexed to the aptamer input domain (α), forming the structure-switching element of the sensor. Upon aptamer-ligand binding, the τ' domain dehybridizes from the aptamer to act as a toehold for an invading fuel strand. DNA strand

displacement is initiated once the τ' domain of the AT and τ domain of the fuel hybridize, initiating 3-way branch migration to replace β_1 of the output strand. DNA strand displacement continues with 4-way branch migration through the μ domain. Finally, the 3-way branch migration through the β_2 domain releases the output signal from the backbone of the AT, which makes available λ and μ domains as a ssDNA signal for downstream reactions. The μ' was added to the fuel strand to suppress the cross-talk between μ domain of the fuel and μ' domain of the reporter complex.

Overall, the AT is analogous to an AND gate that requires both the ligand and the fuel as inputs to transduce a ligand signal into a ssDNA output. Using a fuel strand in the design allowed us to keep the aptamer and output sequences independent in the AT complex. Additionally, the reaction benefits from using a fuel, since the AT reaction becomes more irreversible. Once fuel has reacted with the substrate, it is much less likely for the original AT to reform, and therefore any output domains that are released remain available for downstream reactions. Since the λ and μ domains are independent of the aptamer sequence, their domain level sequences can be customized toward any desired output. To support this claim, multiple reporter probes and ATs differing in output sequences have been designed and tested using the same aptamer input region.

2.3.2 Integration of AT with unique Reporters

The adenosine binding DNA aptamer was chosen as the α domain, since it has been a well-studied aptamer in previous ARNs, providing a good basis for comparing sensitivity.^{16,18,21,22,26,31,32} The reaction of the AT, as illustrated in Figure 1A, proceeds with the binding of adenosine with the α domain, which has been shown to have two possible binding sites, freeing the τ' toehold.^{16,18,21,22,26,31,32} Next, the fuel strand releases

the output strand producing a waste 1 complex and frees λ and μ domains. These output domains can initiate other downstream reaction networks or reporters. Since λ and μ domains are independent of the α domain, they can be custom-designed to suit the input required for subsequent DNA reaction networks. To test the customizability of λ and μ domains, the AT was first integrated with duplexed dye-quencher reporters.

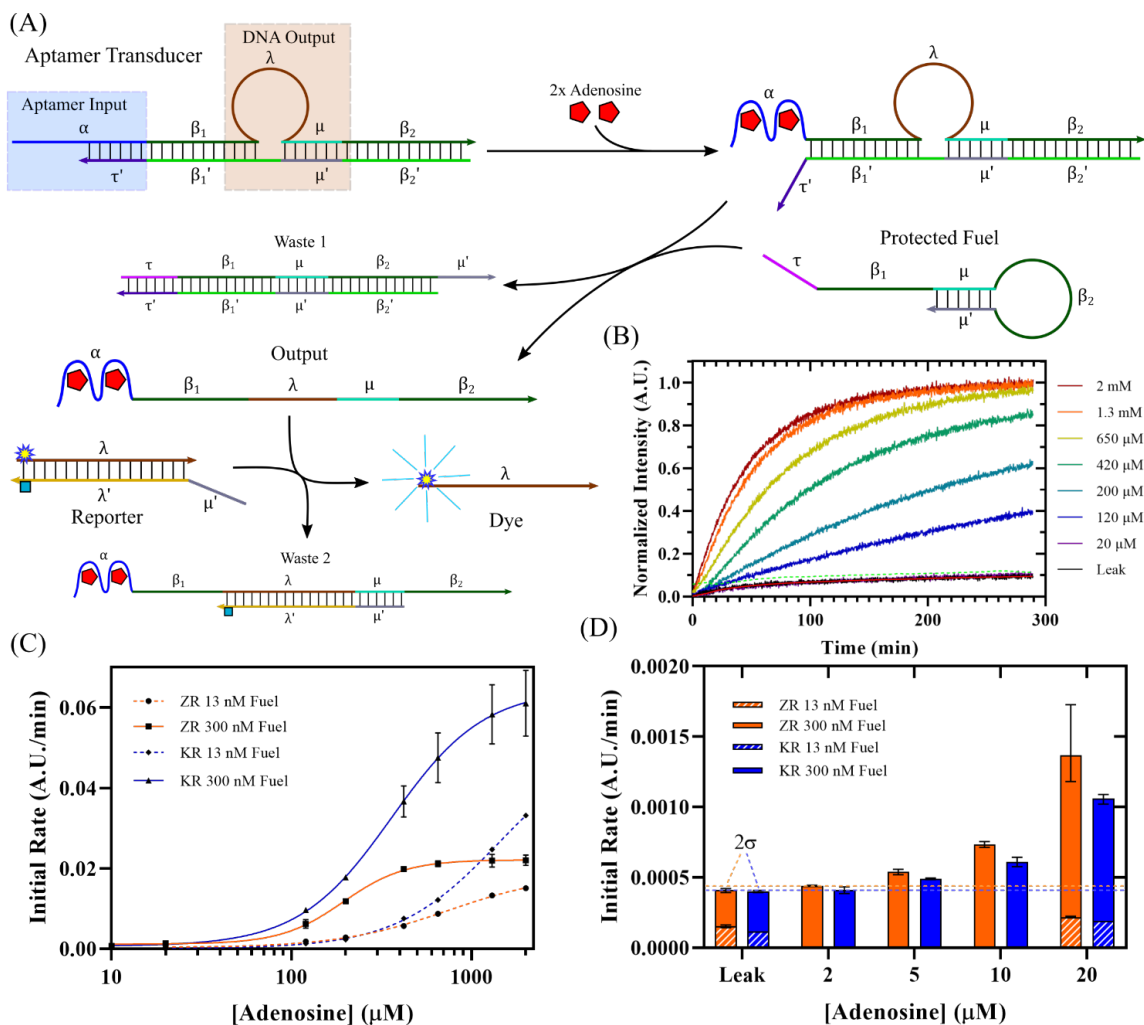


Figure 2.1: (A) Reaction schematics of the AT binding to adenosine, releasing ssDNA output, and reacting with a reporter complex. The structure switching aptamer input region is shown in the blue box and the ssDNA output region is shown in the brown box. (B) Fluorescence intensity normalized by the maximum intensity of the 2 mM adenosine trace shows the kinetic behavior of the AT reacting with a ZR reporter as initiated by 20 μM – 2 mM adenosine, using 13 nM protected fuel, over 300 minutes. Calculated 2σ of the leakage trace (green dash) and the leakage moving average (red line) are also shown. (C) Initial rates of the AT reacting with ZR and KR reporters using both 13 nM and 300 nM AT fuel (10 nM AT complex, 20 nM Reporter) in $1\times\text{TE}$ 25 mM Mg^{2+} (D) Initial rates of the AT reacting with ZR and KR using low concentrations of adenosine 2-20 μM compared to the AT leakage rate. Initial rates above 2σ of the leak are considered detected.

Two distinct TET/Iowa Black labeled reporters, whose sequences were derived from two amplification networks reported by Zhang et al. (ZR) and Kotani et al. (KR), were used to track the concentration of the output signal strand and overall reaction kinetics.^{23,24} These two reporters were chosen because they have previously been shown as reliable reporters for their respective amplification reaction networks. Upon dehybridization of the reporter by the output strand, the dye and the quencher are separated, reducing the fluorescence quenching and increasing the TET dye's fluorescence signal that can be continuously monitored. In addition, two unique reporter complexes were used to validate the modularity of the AT output domains. By showing that the AT can accommodate two unique reporter sequences selected from previous network designs, we validate that the AT can output arbitrary DNA sequences through redesign of only two domains and demonstrate the AT's universal signal transduction capability. In addition to modularity, initial testing with simple reporters allowed us to characterize fundamental AT network performance metrics such as reaction rates, network leakage, and detection sensitivity without convoluting the system with additional reaction steps. The AT's ability to accommodate customized outputs is further supported by showing that different output domain lengths can be incorporated, since a universal transduction platform should not be constrained by output domain lengths or specific DNA sequences.

ZR and KR were mixed with their respective AT and were triggered by adenosine concentrations ranging from 2 μ M to 2 mM. The limit of detection for adenosine sensing was determined by calculating the second standard deviation (2σ) of the leakage kinetic trace in each system, which describes the system's overall reaction without the presence

of adenosine. Any signal that exceeds 2σ was considered sensed with 95% confidence limits above the system noise.^{28,36} Representative kinetic traces for the AT reacting with the ZR is shown in Figure 1B. Over 300 minutes, the ATs integrated with ZR and KR were able to resolve varying adenosine concentrations. Initial reaction rates were determined by linearly fitting fluorescence intensity versus time traces for each adenosine concentration, within the first 30 minutes, using ATs reacted with ZR and KR and two fuel concentrations (13 nM and 300 nM, Figure 1C and 1D), the slope that represent the initial reaction rates were used as a metric to compare reaction kinetics for each system. At adenosine concentrations above 120 μM , KR reacts more quickly than ZR because of its longer toehold (μ' domain) and greater GC content, which is 7 nt for ZR with 28% GC content and 10 nt for KR with 50% GC content. A higher initial reaction rate for KR is expected since longer toeholds with greater GC content provide favorable energetics for initial toehold binding and a greater barrier to spontaneous toehold dissociation.^{30,37} At low adenosine concentrations (20 μM and below, Figure 1D) ZR showed slightly faster reaction rates although both systems were not able to detect 2 μM adenosine because their rates approached the leakage reaction rate. Since the overall rate was limited by the generation of output signal at low adenosine concentrations, the impact of reaction rates between KR and ZR, due to their different toehold lengths, is significantly reduced. In fact, the reaction rates of AT with ZR are slightly faster than AT with KR due to fewer strand displacement steps involved in the 4-way branch migration reaction through μ and μ' domains which takes place during the reaction between AT and the fuel, affecting the overall reaction rate at 20 μM adenosine and lower. Overall, these results indicate that a longer μ domain with higher GC content (28% versus 50%) greatly accelerates the

reaction rate of the AT for higher ligand concentrations, but the rates at lower ligand concentrations take a slight reduction.

As shown in Figure 1C, the initial reaction rates exhibited a sigmoidal relationship as a function of adenosine concentration. Such behavior is typical of substrate ligand binding, which originates from the inherent equilibrium reaction between adenosine molecules and the α domain of the AT.^{8,28} For other studies involving direct aptamer measurement, the aptamer binding affinity (K_d), which depends on aptamer-ligand binding strength and steady-state equilibrium, is determined by the sigmoid half-maximum concentration.^{8,28} Since aptamer binding is generally a weak interaction, initial rates quickly decay when the ligand concentration is below the K_d .^{8,28} The K_d of the adenosine aptamer sequence used in this work was previously found to be 6 μ M, which is near the concentration range found to initiate reaction of the AT and fuel, strongly indicates that the AT and adenosine interaction is the main cause for varied initial reaction rates.^{8,28} A maximum reaction rate is reached when all the ATs are bound in steady-state equilibrium to adenosine. Only ATs that are transiently bound to adenosine are available for strand displacement with the fuel, and the population of such ATs increase exponentially with higher adenosine concentrations. Conversely, reactions at lower adenosine concentrations proceed more slowly since fuel strands encounter ATs bound to adenosine molecules at a reduced rate. In the case of the AT reaction in the presence of a reporter, the sigmoidal relation caused by aptamer ligand binding is convoluted by two additional strand displacement steps, and therefore the aptamer binding affinity (K_d) or effective binding affinity ($K_{d,eff}$) cannot be directly determined. Instead, we define H_{max} as the ligand concentration at half-maximum for initial reaction

rate of the AT and use it to compare the performances of AT-reporter reactions. H_{\max} should theoretically approach the inherent $K_{d,eff}$ of the aptamer input region ($\alpha + \tau'$) when the reaction between the aptamer and the ligand is the rate determining step. We initially tested a range of fuel concentrations from 13 nM – 500 nM, which showed diminishing reaction rate increase above 300 nM [See Supporting Information S1. Optimization of AT-Fuel Concentration Fuel Optimization]. In addition, we optimized the AT reaction conditions with varying buffer salt conditions and performed a selectivity test with two other purine nucleosides – cytidine and uridine - to demonstrate its selectivity [See Supporting Information S2 and S3]. Based on these initial data, we chose to test the AT kinetics with fuel concentrations at 13 nM, which is near the AT concentration of 10 nM, and 300 nM at which the reaction rates leveled off. We observed that the initial reaction rate increased considerably when the fuel concentration increased from 13 nM to 300 nM, which led to the decrease of H_{\max} by a factor of around 4 (4.2 for ZR and 3.9 for KR). The faster reactions can be attributed to the decreased reaction time between the fuel strands and activated ATs, which is significant because the overall reaction rate, hence the detection limit, could be increased without higher adenosine concentration.

One potential downside of increasing the fuel concentration is an increase in the AT reaction network leakage, which is defined as the unintentional reaction of ATs with the fuel without the presence of an input (adenosine).³⁸ In the case of the AT network, leakage occurs when fuel strands displace the output strand by breathing or fraying of several domains (β_1 , β_2 , and μ) that leads to branch migration.³⁸ Such leakage diminishes the sensitivity of the AT device because it is more difficult to differentiate the initial reaction rates at lower adenosine concentrations from the leakage. Although increasing

the fuel concentration from 13 to 300 nM nearly doubles the leakage rate, the initial reaction rate at 20 μM adenosine increased by 5-6 times. Moreover, initial reaction rates at lower adenosine concentrations (10 μM and less) were only measurable with 300 nM fuel concentrations since signals at the low concentrations were not detectable when the fuel concentration was 13 nM.

As expected, our results show that the AT reaction is rate limited by two primary factors - (1) the equilibrium reaction rate of the adenosine with the AT and (2) the AT-fuel reaction rate when the fuel concentration is similar to the concentration of AT. The second factor can be mitigated by using excess fuel strands as discussed above. Overall, our ATs were able to successfully accommodate two customized outputs with a limit of detection around 5 μM of adenosine. Therefore, the AT platform demonstrated both the modularity and customizability required for incorporation into feed-forward reaction networks. In the next section we demonstrate that the AT can be customized to act as inputs to two amplification reaction networks.

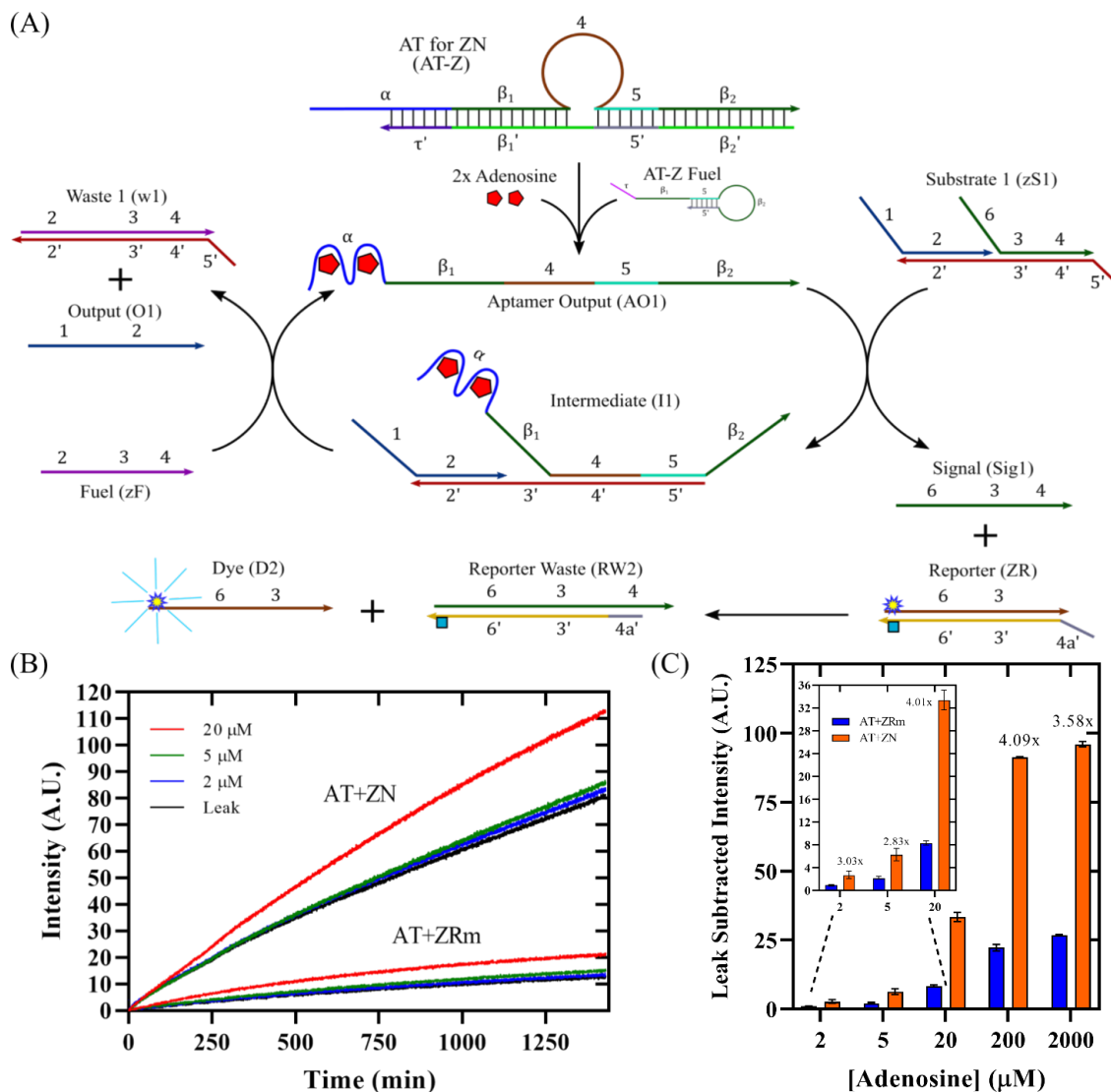


Figure 2.2: (A) Reaction schematic for AT coupled linear amplification network, AT was redesigned to incorporate 4, 5 domains from 5'-3' ends. (B) Fluorescence intensities of the AT reacted with ZRm (AT+ZRm) compared to AT reacted with ZN (AT+ZN) from 2-20 μM adenosine for 24 hrs ($1 \times \text{TE } 25 \text{ mM Mg}^{2+}$) (C) Comparison of leak subtracted differential intensities at 24 hours showing amplification fold for each adenosine concentration from 2-2000 μM .

2.3.3 AT + Entropy-Driven Catalytic Amplification

In order to further validate the modularity of the AT, we redesigned the output strands to initiate DNA reaction networks capable of signal amplification, which is essential for improving signal recognition and the limit of detection.^{18,23,24} Catalytic reaction networks, which recycle catalyst strands, are commonly used for non-enzymatic DNA amplification.^{23,24} We chose the entropy-driven catalytic network developed by Zhang et al. (ZN) and 3-arm junction catalytic network developed by Kotani et al. (KN) to test such modularity of the AT.^{23,24} By demonstrating the AT's feed-forward capability with at least two published reaction networks, the applicability of the ATs to a variety of novel DNA reaction networks could be better evaluated.

As shown in Figure 2A, the integration of AT with ZN (AT-ZN) was accomplished while preserving the original sequences of ZN and by incorporating the initiator sequence into **4** and **5** domains of the aptamer output strand (AO1). Our approach is in contrast to other aptamer amplification networks that modify sequences of the ZN.^{18,31} In order to use ZN without such sequence redesign, the λ and μ domains from the original AT design (Figure 1A) were replaced with **4** and **5** domains of the ZN while keeping other original domains of AT the same. The catalytic network is initiated when the aptamer output strand (AO1) is used as the catalyst binding to the **5'** domain toehold on the ZN substrate (zS1). Upon binding, the **3'** toehold domain of zS1 becomes available when the signal strand (Sig1) is released, allowing for toehold binding of the fuel strand of ZN (zF), which then leads to the release of the output strand (O1) and the aptamer output strand (AO1). The ZR then detects the signal strand (Sig1) and produces a fluorescence signal that can be measured to track the progress of the adenosine sensing

reaction. Multiple signal strands (Sig1) can be produced from regenerated aptamer output strand (AO1) and therefore the catalytic network amplifies the AT output signal.

To measure the signal amplification achieved by AT-ZN, a modified reporter (ZRm), whose sequence is presented in the Supporting Information (S4), was designed to directly detect AO1 produced from the reaction of AT-ZN with adenosine by targeting 4 and 5 domains. All amplification experiments were carried out in presence of 300 nM AT-Z fuel since it produced the optimal AT sensitivity in our initial kinetics investigation using ZR. A ratio of 5:1 ZN to AT was used so that the catalytic reaction did not limit the overall reaction rate. The coupled ZN-AT network was continuously monitored for 24 hours to detect adenosine signals (Figure 2B). Adenosine concentrations ranging from 2 μM -2000 μM were detected with the direct reporting method, though overall intensities remained low even after 24 hours. In comparison, the AT-ZN system showed a multifold increase of the leak-subtracted fluorescence intensity compared to the direct reporting method (Figure 2C).

Overall, the AT-ZN system resulted in successful amplification of the reporter fluorescence signal and an enhancement of the adenosine detection limit from 5 to 2 μM (Figure 2C). Compared to the direct reporting network using ZRm, the addition of an amplification network allows the reaction to continue generating signal after the AT has produced an output due to the presence of excess (5:1) ZN. Recycling of the AT output strands (AO1) continued the amplification reaction, leading to higher final fluorescence intensities compared with the direct reporting network that uses ZRm as the reporter. The 5:1 substrate to AT ratio allowed the system to amplify low adenosine concentrations by a factor of about 3-4 fold when compared to AT without an amplification network

(Figure 2C). While an adenosine signal was successfully amplified, leakage from the AT network was also amplified in the process. Thus, minimization of the AT network leakage is an important consideration in improving device performance, especially when coupled to an amplifier. Similarly, the catalytic network in use must not introduce extraneous leakage to avoid signal interference.

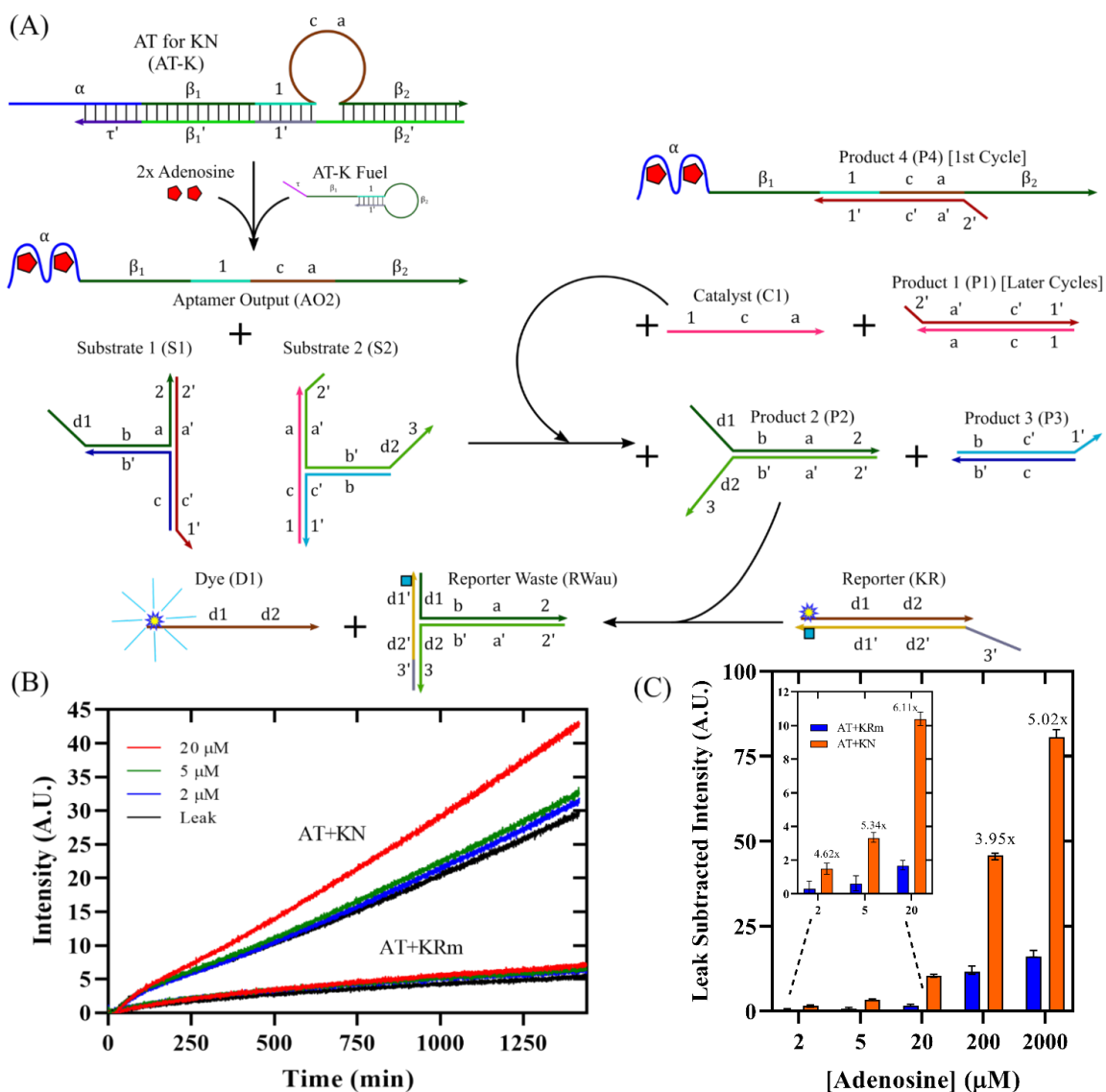


Figure 2.3: (A) Reaction schematic for AT coupled 3-arm amplification network, AT was redesigned to incorporate 1, c, a domains from 5'-3' ends. Note: the AT μ domain has been moved to preserve 5'-3' of the amplifier RN (B) Fluorescence intensities of the AT reacted with KRm (AT+KRm) compared to AT reacted with KN (AT+KN) from 2-20 μM adenosine for 24 hrs (1xTE 25 mM Mg^{2+}) (C) Comparison of leak subtracted differential intensities at 24 hours showing amplification fold for each adenosine concentration from 2-2000 μM .

2.3.4 AT + 3-Arm Catalytic Amplification

The second catalytic network by Kotani et al. (KN), which utilizes 3-arm substrates, was integrated with the AT to create AT-KN. One difference between AT-ZN and AT-KN is how the catalyst is recycled. AT-ZN reuses the Aptamer Output strand (AO1 in Figure 2A) for catalytic amplification, while KN outputs a new catalyst strand (C1) that acts as the catalyst for multiple cycles (Figure 3A). This difference in the design of AT-KN plays a role in improved amplification compared to ZN, since the initial AT output strands (AO1) contain extraneous domains that could add steric hindrance to the system. The KN has been shown to have a rate comparable to ZN having rate constants within an order of magnitude of each other.²⁴ Another important difference between KN and ZN is that KN was shown to reduce the rate of catalytic network leakage, which requires a slower 4-arm branch migration.²⁴ Reduction in the leakage of the amplifying network translates to improvements in network stability and lower detection limit of the AT network in principle.

Integrating the AT with the KN required slight modification of the AT network design since the location of the toehold domain (**1** domain) is on the 5' end of its input compared to ZN whose toehold domain (domain **5**) is on the 3' end of the input (Figure 3A). To accommodate such differences, the μ and μ' domains simply have been moved to the opposite side of the λ domain, which further validates the sequence modularity and customizability of the AT design since other known feed-forward networks may require 3' to 5' reversal for function. In addition to changing the location of the toehold (domain **1**), **c** and **a** domains were changed so that the probe strand could initiate the KN. The operation of AT-KN is initiated by the strand displacement between the aptamer output

strand (AO2) and Substrate 1 (S1) which form Product 4 (P4). The remainder of S1 then reacts with Substrate 2 (S2) to generate Product 2 (P2), Product 3 (P3), and a catalyst strand (C1). C1 strand then reacts with S1 and generate Product 1 (P1) thus initiating another cycle. Since the C1 strand is regenerated for each subsequent reaction cycle, the system continues to operate as long as the S1 and S2 strands are available. The P2 strand reacts with the reporter (KR) to generate fluorescence signals that can be continuously monitored.

Similar to AT-ZN system and the use of ZRm, a modified reporter (KRm), whose sequence is presented in the Supporting Information (S4), was designed to directly detect AO2 produced from the reaction of AT-ZN with adenosine by targeting **1**, **c**, and **a** domains. As with the AT-ZN system, AT-KN substrates (S1 and S2) were reacted at 5:1 substrate to AT with excess AT-K fuel at 300 nM. After reacting for 24 hours, the AT-KN was able to achieve a limit of detection of 2 μM , whereas the AT-KRm was able to detect only 20 μM . A net amplification of about 4-6 times was achieved by the KN system comparing the leak subtracted signals for AT-KRm and AT-KN (Figure 3C). Specifically, the fluorescence signal with 2 μM adenosine was amplified by around 4.6 times while there was little to detectable signal exhibited by the AT-KRm control. This result confirms that the KN can effectively boost even relatively weak adenosine signals into a detectable range. This may be partly due to the AT-KN's ability to produce a smaller and more reactive catalyst strand, as well as smaller leakage signal produced the KN.

The adenosine detection tests with the feed-forward network reactions (AT-ZN and AT-KN) clearly demonstrate both modularity and customizability of the AT to

effectively trigger downstream amplification networks. In both cases, redesigned AT outputs produced catalytic inputs to their targeted amplification reaction networks (ZN and KN) with minimal modification of the AT without any need for redesign of the original networks. One difference between the AT-ZN and AT-KN systems is the role of AT aptamer output strands (AO1 and AO2) in their respective amplification networks. AO1 acts as the catalyst for ZN for every catalytic cycle whereas AO2 is involved only in the initial catalytic cycle of KN, which contributes to greater amplification of AT-KN. These different operation mechanisms, however, are a function of the design of original network. ATs integrated with ZN components (AT-ZN and AT-ZRm) showed a greater initial reaction rate than AT-KN and AT-KRm (Figures 2B and 3B), which could be attributed to ZN and ZRm's shorter duplex domains (**4** and **4'**, 16 nts) of the substrate compared to such domains in KN and KRm (**a c** and **a' c'**, 45 nts). The AT-KN and AT-KRm branch migration domains were ~3 times longer, which contributed to their ~4 times smaller fluorescence intensity when compared with the AT-ZN and AT-ZRm systems.³⁹ Despite slower reaction triggered by AO2, the AT-KN showed ~ 52%, 89%, and 52% greater amplification compared to AT-ZN for low adenosine concentrations, 2 μ M, 5 μ M and 20 μ M respectively demonstrating that the KN is a more effective amplification network for our ATs due to its lower leakage rate and its smaller catalyst strand.

In comparison to published feed-forward adenosine detection network that also uses the entropy-driven catalytic network by Zhang et al. and has been shown to have a detection limit of 20 nM adenosine, the sensitivity and detection limits of our feed-forward AT networks requires further improvement and optimization.^{23,31} A thorough

investigation of network leakage mechanisms and design alterations to the AT could help improve the sensitivity of the adenosine sensor, especially when coupled to a catalytic network for amplification of the AT output. Regardless of these limitations, our feed-forward AT network is a more versatile platform based on its customizability that allows the sequence and domain designs for previously optimized catalytic amplification networks to be incorporated as demonstrated with ZN and KN. Future study of the AT should aim to test the modularity of the α input domain with different aptamers to understand its applicability to detect other analytes. Understanding the interaction between the τ' domain and other aptamer sequences poses a potential challenge since many structure-switching mechanisms are not yet well understood. Hence, a thorough study of the τ' domain's interactions with other aptamers and their respective secondary structures is vital for expanding the usefulness of the AT network. Additionally, rational design and testing of the τ' domain will provide a greater understanding of how decreasing the $K_{d,eff}$ of the AT might increase the downstream catalytic amplification and improve sensitivity. Multiplexed AT systems capable of detecting many ligands simultaneously with targeted and customizable AT networks could allow development of more sophisticated biosensing tools, as the understanding of aptamer structure-switching mechanisms by the community advances.

2.4 Conclusions

We demonstrated that the aptamer transducer network that contains independent aptamer sensing and downstream signal domains can function as a modular aptamer reaction network, which can produce customizable DNA outputs. Our aptamer transducer successfully detected adenosine and produced four different output strands that were

integrated into different reporting and amplification networks without any modifications to the downstream reaction networks. The limit of adenosine detection was limited by the $K_{d,eff}$ of the aptamer input domain. Integration of aptamer transducers with amplification networks resulted in multifold increase of fluorescence signals indicating successful downstream reactions and enhanced detection limits.

Overall, our aptamer transducer framework was successfully designed as a novel non-enzymatic modular aptamer sensor unit that can be incorporated into many other reaction networks for direct target detection. Our work with the aptamer transducer framework provides a good platform for the investigation of more general and modular aptamer reaction network systems that could lead to more sensitive and universal biosensing systems.

2.5 Experimental

2.5.1 DNA Preparation

DNA strands were purchased from Integrated DNA Technologies (IDT). [See Supporting Information S4. Strand Sequences for Aptamer Transducer and Catalytic Amplification Networks for a list of base sequences.] Prior to ordering, validation of the correct secondary structures was tested using NUPACK.⁴⁰ [See Supporting Information S5. NUPACK Secondary Structures of ATs] Dye- or quencher-labeled strands or those longer than 80 nucleotides (nt) were purified by high performance liquid chromatography (HPLC) by IDT. Dye strands were modified on the 5' end with Tetrachlorofluorescein (TET) and quencher strands were modified on the 3' end with Iowa Black Quencher (IABkFQ, IDT). Upon receiving, strands were re-suspended until they reached $\sim 100 \mu\text{M}$ in $1\times\text{TE}$ buffer (Sigma-Aldrich). AT, catalytic substrates, and reporter complexes were

stoichiometrically mixed in 1×TE buffer with 12.5 mM MgCl₂ (1×TE Mg²⁺). Prior to annealing and PAGE purification, samples were diluted to 20 μM in 1×TAE buffer. All dsDNA complexes were annealed at 90 °C for 5 minutes and then cooled to 20 °C at a rate of 5 °C per minute to room temperature.

2.5.2 DNA Purification

DNA strands were purified by PAGE gel electrophoresis prior to use. 1.5 mm thick 10 cm × 10 cm non-denatured 10% gels for PAGE (acrylamide:bis = 29:1) were prepared with 1×TAE buffer. A loading buffer was prepared by mixing a 50:50 solution containing ficcol and bromophenol blue. Previously annealed samples were mixed with loading buffer (4:1) prior to being loaded into gel wells in 25 μL increments.

Electrophoresis was carried out at 150 V, 100 mA, 20 W, for 2.5 hrs. Bands cut from each gel contained the purified complex which were eluted in ~ 500 μL 1×TE buffer with 25 mM MgCl₂. After 48 hours of elution, purified DNA complexes were transferred to new low binding Eppendorf Tubes.

2.5.3 Kinetics Experiments

Samples were vortexed and centrifuged before quantification using a NanoDrop One (Thermo Scientific) at 260 nm. Extinction coefficients, provide by IDT, were used to determine the DNA complex concentrations prior to mixing the reactants. Purified and diluted DNA samples were reacted in stoichiometric quantities. Reaction kinetics were measured with Varian or Agilent Cary Eclipse fluorometers using transparent disposable PMMA cuvettes (excitation λ=522 nm, emission λ=539 nm, 25 °C).

Acknowledgments

We thank members of the Boise State Nanoscale Materials and Device group for valuable assistance with this work. We also thank Boise State University Micron School of Materials Science & Engineering Department for supporting this work. This work was supported in part by grant no. 1706065 from the National Science Foundation.

Supporting Information

The Supporting information is available free of charge on the ACS Publications website.

Strand sequences, NUPACK secondary structures results, optimization of AT-Fuel concentrations, optimization of buffer salt concentrations, and selectivity of the AT targeting adenosine are provided.

Author Information

Tim Hachigian: timhachigian@u.boisestate.edu

Drew Lysne: drewlysne@u.boisestate.edu

Elton Graugnard: eltongraugnard@boisestate.edu

Jeunghoon Lee: jeunghoonlee@boisestate.edu

2.6 References

- (1) Ellington, A. D.; Szostak, J. W. In Vitro Selection of RNA Molecules That Bind Specific Ligands. *Nature* **1990**, *346* (6287), 818–822.
<https://doi.org/10.1038/346818a0>.
- (2) Huizenga, D. E.; Szostak, J. W. A DNA Aptamer That Binds Adenosine and ATP. *Biochemistry* **1995**, *34* (2), 656–665. <https://doi.org/10.1021/bi00002a033>.
- (3) Tuerk, C.; Gold, L. Systematic Evolution of Ligands by Exponential Enrichment: RNA Ligands to Bacteriophage T4 DNA Polymerase. *Science* **1990**, *249* (4968), 505–510. <https://doi.org/10.1126/science.2200121>.
- (4) Luo, Y. Functional Nucleic Acid Biosensors for Small Molecules. In *Functional Nucleic Acid Based Biosensors for Food Safety Detection*; Luo, Y., Ed.; Springer Singapore: Singapore, 2018; pp 249–306. https://doi.org/10.1007/978-981-10-8219-1_10.
- (5) Shaban, S. M.; Kim, D.-H. Recent Advances in Aptamer Sensors. *Sensors* **2021**, *21* (3). <https://doi.org/10.3390/s21030979>.
- (6) Yu, H.; Alkhamis, O.; Canoura, J.; Liu, Y.; Xiao, Y. Advances and Challenges in Small-Molecule DNA Aptamer Isolation, Characterization, and Sensor Development. *Angew. Chem. Int. Ed.* **2021**, *60* (31), 16800–16823.
<https://doi.org/10.1002/anie.202008663>.
- (7) Munzar JD; Ng A; Juncker D. Duplexed Aptamers: History, Design, Theory, and Application to Biosensing. *Chem. Soc. Rev.* **2019**, *48* (5), 1390–1419.
<https://doi.org/10.1039/c8cs00880a>.
- (8) Munzar, J. D.; Ng, A.; Juncker, D. Comprehensive Profiling of the Ligand Binding Landscapes of Duplexed Aptamer Families Reveals Widespread Induced Fit. *Nat. Commun.* **2018**, *9* (1), 343. <https://doi.org/10.1038/s41467-017-02556-3>.
- (9) Monserud, J. H.; Macri, K. M.; Schwartz, D. K. Toehold-Mediated Displacement of an Adenosine-Binding Aptamer from a DNA Duplex by Its Ligand. *Angew.*

- Chem. Int. Ed.* **2016**, *55* (44), 13710–13713.
<https://doi.org/10.1002/anie.201603458>.
- (10) Carrasquilla, C.; Li, Y.; Brennan, J. D. Surface Immobilization of Structure-Switching DNA Aptamers on Macroporous Sol-Gel-Derived Films for Solid-Phase Biosensing Applications. *Anal. Chem.* **2011**, *83* (3), 957–965.
<https://doi.org/10.1021/ac102679r>.
- (11) Nutiu, R.; Li, Y. Structure-Switching Signaling Aptamers: Transducing Molecular Recognition into Fluorescence Signaling. *Chem. - Eur. J.* **2004**, *10* (8), 1868–1876. <https://doi.org/10.1002/chem.200305470>.
- (12) Nutiu, R.; Li, Y. Structure-Switching Signaling Aptamers. *J. Am. Chem. Soc.* **2003**, *125* (16), 4771–4778. <https://doi.org/10.1021/ja028962o>.
- (13) Shlyahovsky, B.; Li, D.; Weizmann, Y.; Nowarski, R.; Kotler, M.; Willner, I. Spotlighting of Cocaine by an Autonomous Aptamer-Based Machine. *J. Am. Chem. Soc.* **2007**, *129* (13), 3814–3815. <https://doi.org/10.1021/ja069291n>.
- (14) Meng, C.; Dai, Z.; Guo, W.; Chu, Y.; Chen, G. Selective and Sensitive Fluorescence Aptamer Biosensors of Adenosine Triphosphate. *Nanomater. Nanotechnol.* **2016**, *6*, 33. <https://doi.org/10.5772/63985>.
- (15) Li, B.; Ellington, A. D.; Chen, X. Rational, Modular Adaptation of Enzyme-Free DNA Circuits to Multiple Detection Methods. *Nucleic Acids Res.* **2011**, *39* (16), e110. <https://doi.org/10.1093/nar/gkr504>.
- (16) Ravan, H. Implementing a Two-Layer Feed-Forward Catalytic DNA Circuit for Enzyme-Free and Colorimetric Detection of Nucleic Acids. *Anal. Chim. Acta* **2016**, *910*, 68–74. <https://doi.org/10.1016/j.aca.2016.01.013>.
- (17) Zhou, Z.; Du, Y.; Dong, S. Double-Strand DNA-Templated Formation of Copper Nanoparticles as Fluorescent Probe for Label-Free Aptamer Sensor. *Anal. Chem.* **2011**, *83* (13), 5122–5127. <https://doi.org/10.1021/ac200120g>.
- (18) Cheng, S.; Zheng, B.; Wang, M.; Zhao, Q.; Lam, M. H.; Ge, X. Determination of Adenosine Triphosphate by a Target Inhibited Catalytic Cycle Based on a Strand

- Displacement Reaction. *Anal. Lett.* **2014**, *47* (3), 478–491.
<https://doi.org/10.1080/00032719.2013.841179>.
- (19) Wang, J.; Munir, A.; Zhou, S. H. Au NPs-Aptamer Conjugates as a Powerful Competitive Reagent for Ultrasensitive Detection of Small Molecules by Surface Plasmon Resonance Spectroscopy. *Talanta TA - TT* - **2009**, *79* (1), 72–76.
<https://doi.org/10.1016/j.talanta.2009.03.003>.
- (20) Meng, H.-M.; Liu, H.; Kuai, H.; Peng, R.; Mo, L.; Zhang, X.-B. Aptamer-Integrated DNA Nanostructures for Biosensing, Bioimaging and Cancer Therapy. *Chem. Soc. Rev.* **2016**, *45* (9), 2583–2602. <https://doi.org/10.1039/C5CS00645G>.
- (21) Zhu, J.; Zhang, L.; Zhou, Z.; Dong, S.; Wang, E. Aptamer-Based Sensing Platform Using Three-Way DNA Junction-Driven Strand Displacement and Its Application in DNA Logic Circuit. *Anal. Chem.* **2014**, *86* (1), 312–316.
<https://doi.org/10.1021/ac403235y>.
- (22) Zheng, D.; Seferos, D. S.; Giljohann, D. A.; Patel, P. C.; Mirkin, C. A. Aptamer Nano-Flares for Molecular Detection in Living Cells. *Nano Lett.* **2009**, *9* (9), 3258–3261. <https://doi.org/10.1021/nl901517b>.
- (23) Zhang, D. Y.; Turberfield, A. J.; Yurke, B.; Winfree, E. Engineering Entropy-Driven Reactions and Networks Catalyzed by DNA. *Science* **2007**, *318* (5853), 1121–1125. <https://doi.org/10.1126/science.1148532>.
- (24) Kotani, S.; Hughes, W. L. Multi-Arm Junctions for Dynamic DNA Nanotechnology. *J. Am. Chem. Soc.* **2017**, *139* (18), 6363–6368.
<https://doi.org/10.1021/jacs.7b00530>.
- (25) Xiao, Y.; Piorek, B. D.; Plaxco, K. W.; Heeger, A. J. A Reagentless Signal-on Architecture for Electronic, Aptamer-Based Sensors via Target-Induced Strand Displacement. *J. Am. Chem. Soc.* **2005**, *127* (51), 17990–17991.
<https://doi.org/10.1021/ja056555h>.
- (26) Fu, B.; CAo, J.; Wang, L.; Jiang, W. A Novel Enzyme-Free and Label-Free Fluorescence Aptasensor for Amplified Detection of Adenosine. *Biosens. Bioelectron.* **2013**, *44* (1), 52–56. <https://doi.org/10.1016/j.bios.2012.12.059>.

- (27) Wang, K.; He, M.; Zhai, F.; Chen, R.; Yu, Y. A Label-Free and Enzyme-Free Ratiometric Fluorescence Biosensor for Sensitive Detection of Carcinoembryonic Antigen Based on Target-Aptamer Complex Recycling Amplification. *Sens. Actuators B Chem.* **2017**, *253*, 893–899. <https://doi.org/10.1016/j.snb.2017.07.047>.
- (28) Armstrong, R. E.; Strouse, G. F. Rationally Manipulating Aptamer Binding Affinities in a Stem-Loop Molecular Beacon. *Bioconjug. Chem.* **2014**, *25* (10), 1769–1776. <https://doi.org/10.1021/bc500286r>.
- (29) Jung, C.; Ellington, A. D. Diagnostic Applications of Nucleic Acid Circuits. *Acc. Chem. Res.* **2014**, *47* (6), 1825–1835. <https://doi.org/10.1021/ar500059c>.
- (30) Zhang, D. Y.; Seelig, G. Dynamic DNA Nanotechnology Using Strand-Displacement Reactions. *Nat. Chem.* **2011**, *3* (2), 103–113. <https://doi.org/10.1038/nchem.957>.
- (31) Cheng, S.; Zheng, B.; Wang, M.; Ge, X.; Lam, M. H. A Target-Triggered Strand Displacement Reaction Cycle: The Design and Application in Adenosine Triphosphate Sensing. *Anal. Biochem.* **2014**, *446* (1), 69–75. <https://doi.org/10.1016/j.ab.2013.10.021>.
- (32) Cho, E. J.; Yang, L.; Levy, M.; Ellington, A. D. Using a Deoxyribozyme Ligase and Rolling Circle Amplification to Detect a Non-Nucleic Acid Analyte, ATP. *J. Am. Chem. Soc.* **2005**, *127* (7), 2022–2023. <https://doi.org/10.1021/ja043490u>.
- (33) Liu, J.; Lu, Y. Non-Base Pairing DNA Provides a New Dimension for Controlling Aptamer-Linked Nanoparticles and Sensors. *J. Am. Chem. Soc.* **2007**, *129* (27), 8634–8643. <https://doi.org/10.1021/ja072075+>.
- (34) Zhang, Z.; Oni, O.; Liu, J. New Insights into a Classic Aptamer: Binding Sites, Cooperativity and More Sensitive Adenosine Detection. *Nucleic Acids Res.* **2017**, *45* (13), 7593–7601. <https://doi.org/10.1093/nar/gkx517>.
- (35) Nakamura, I.; Shi, A.-C.; Nutiu, R.; Yu, J.; Li, Y. Kinetics of Signaling-DNA-Aptamer-ATP Binding. *Phys. Rev. E Stat. Nonlin. Soft Matter Phys.* **2009**, *79* (3), 31906. <https://doi.org/10.1103/PhysRevE.79.031906>.

- (36) Lee, J.; Jeon, C. H.; Ahn, S. J.; Ha, T. H. Highly Stable Colorimetric Aptamer Sensors for Detection of Ochratoxin A through Optimizing the Sequence with the Covalent Conjugation of Hemin. *The Analyst* **2014**, *139* (7), 1622–1627. <https://doi.org/10.1039/c3an01639k>.
- (37) Dunn, K. E.; Trefzer, M. A.; Johnson, S.; Tyrrell, A. M. Investigating the Dynamics of Surface-Immobilized DNA Nanomachines. *Sci. Rep.* **2016**, *6*, 29581. <https://doi.org/10.1038/srep29581>.
- (38) Lysne, D.; Jones, K.; Stosius, A.; Hachigian, T.; Lee, J.; Graugnard, E. Availability-Driven Design of Hairpin Fuels and Small Interfering Strands for Leakage Reduction in Autocatalytic Networks. *J. Phys. Chem. B* **2020**, *124* (16), 3326–3335. <https://doi.org/10.1021/acs.jpcc.0c01229>.
- (39) Srinivas, N.; Ouldrige, T. E.; Sulc, P.; Schaeffer, J. M.; Yurke, B.; AA, L.; JP, D.; Winfree, E. On the Biophysics and Kinetics of Toehold-Mediated DNA Strand Displacement. *Nucleic Acids Res.* **2013**, *41* (22), 10641–10658. <https://doi.org/10.1093/nar/gkt801>.
- (40) Zadeh, J. N.; Steenberg, C. D.; Bois, J. S.; Wolfe, B. R.; Pierce, M. B.; Khan, A. R.; Dirks, R. M.; Pierce, N. A. NUPACK: Analysis and Design of Nucleic Acid Systems. *J. Comput. Chem.* **2011**, *32* (1), 170–173. <https://doi.org/10.1002/jcc.21596>.

CHAPTER 3: TARGETED SELECTION OF APTAMER COMPLEMENTARY
ELEMENTS TOWARD RAPID SCREENING OF APTAMER TRANSDUCERS

This chapter was published by the American Chemical Society in *The Journal of Physical Chemistry B* and should be referenced appropriately as below.

“Hachigian, Tim, et al. "Targeted Selection of Aptamer Complementary Elements Toward Rapid Screening of Aptamer Transducers." *ACS The Journal of Physical Chemistry B*, Copyright 2023 American Chemical Society.”

*Boise State University, Micron School of Materials Science and Engineering,
1910 University Dr., Boise, Idaho 83725, United States*

3.1 Abstract

Biosensing using aptamers has been a recent interest for their versatility in detecting many different analytes across a wide range of applications, including medical and environmental applications. In our last work, we introduced a customizable aptamer transducer (AT) which could successfully feed-forward many different output domains to target a variety of reporters and amplification reaction networks. In this paper, we explore the kinetic behavior and performance of novel ATs by modifying the aptamer complementary element (ACE) chosen based on a technique for exploring the ligand-binding landscape of duplexed aptamers. Using published data, we selected and constructed several modified ATs that contains ACEs with varying lengths, position of the start-sites, and of the positions of single-mismatches, whose kinetic responses were tracked with a simple fluorescence reporter. A kinetic model for ATs was derived and used to extract the strand-displacement reaction constant k_1 and the effective aptamer dissociation constant $K_{d,eff}$, allowing us to calculate a relative performance metric, $k_1/K_{d,eff}$. Comparing our results with the predictions based on the literature data, we

provide useful insight into the dynamics of the adenosine AT's duplexed aptamer domain and suggest a high-throughput approach for future ATs to be developed with improved sensitivity. The performance of our ATs showed moderate correlation to those predicted by the ACE-scan method. Here, we find that predicted performance based on our ACE selection method were moderately correlated to our ATs performance.

3.2 Introduction

Duplexed aptamer biosensors have been a major interest within dynamic DNA nanotechnology within recent years due to the potential for rapid development of sensing platforms that can be deployed to detect low levels of analytes in assays across many major fields including medical, environmental, hazard detection, and food safety applications.^{1-7,7-20} Several major benefits of aptamer biosensors include their ability to replace tests that require the use of sophisticated lab equipment or technical expertise and to be deployed as easily manufactured paper devices or microfluidic chips.^{16,18,19,21} Modular biosensing platforms based on duplexed aptamers are advantageous for the high-throughput synthesis of low-cost tests since sensing and output domains can be easily customized and remain independent of one another thus allowing for customization of relevant aptamers and output sequences depending on application.^{11,22-24} As new and more sensitive aptamers with lower dissociation constant K_d are discovered and engineered, biosensors based on a modular duplexed aptamer platform could outperform current sensing technologies and would be easily deployable in places where expensive equipment is not available.^{5,11,17,25-28} Therefore, studies that aim to develop novel modular platforms for rapid development of aptamer biosensors are beneficial for the future development of selective and sensitive assays.

In our previous work, we introduced the aptamer transducer (AT), a modular and customizable duplexed aptamer biosensing platform that accommodated customizable output domains. We demonstrated that the AT could signal differing fluorescence-based reporters, and we later showed the AT could produce output strands that can feed-forward input into catalytic DNA reaction networks for signal amplification.^{23,29,30} The Huizenga and Szostak adenosine binding DNA aptamer was used to show that the AT could transduce an adenosine signal into multiple output domains using a single duplexed aptamer domain that served as the aptamer complementary element (ACE). During structure-switching of the adenosine aptamer, the ACE is displaced by aptamer ligand, making it available to hybridize with invading strands by acting as the toehold to initiate a strand displacement cascade.^{9,17,23,25} The ACE selected for our original study was 6 nt-long and was held constant throughout the study to elucidate the effects of differing output domains.²³ While successful operation of the AT was demonstrated with the 6 nt-long ACE in the Control AT, it is possible that a more well optimized ACE exists to improve the sensitivity of the aptamer region leading to a better overall performance of ATs yet it is still unknown what kinetic processes dictate the behavior of the aptamer and τ' domain of an AT.

Studying the kinetic behavior of changing the τ' domain (Figure 1) within the original adenosine AT involves selection and testing of several possible ACEs that bind to different sub-domains of the 23 nt-long adenosine aptamer to maximize the effective dissociation constants, $K_{d,eff}$. Sampling many possible ACEs to optimize the τ' domain for enhanced sensitivity, lowering the $K_{d,eff}$, would prove to be a repetitive and slow task using conventional lab techniques. Moreover, Munzar et al. demonstrated a novel process

called ACE-Scan that utilizes a DNA microarray to test the sensitivity and kinetic behavior of many ACEs in parallel. The ACE-scan method works by hybridizing dye labeled aptamers to ACEs on functionalized on the microarray and measuring differences in fluorescence after a series of washing steps with or without the presence of a ligand. Aptamers that dehybridize from the microarray in the absence of a ligand reduce fluorescence where dehybridization of aptamers in the absence and presence of a ligand is quantified by k_{off} and k^*_{off} , respectively. The measured k_{off} and k^*_{off} were used to distinguish between aptamers operating via conformational selection from those operating via induced fit mechanisms.²⁵ The induced fit mechanism occurs when the ligand causes an aptamer to spontaneously reconfigure and bind to the ligand in the process, which is facilitated by the proximity of the ligand allowing the aptamer to overcome the energy barrier associated with reconfiguration.²⁵ On the other hand, conformational selection occurs when the aptamer reconfigures itself prior to binding to the ligand.²⁵ Munzar et al. tested several different aptamers, including the adenosine binding DNA aptamer, using the ACE-scan method and revealed that the induced fit mechanism is the most likely kinetic pathway for adenosine binding and identified several promising ACE candidates to improve the performance of biosensors that uses the duplexed aptamer.²⁵ Their study reported a wide range of adenosine aptamer binding ACEs' performances using k^*_{off} and k_{off} rates of aptamer single-strands leaving ACEs functionalized to a microarray surface. They studied ACE-aptamer complexes that possessed a variety of duplex lengths, duplex start sites along the aptamer binding domain, and single-nucleotide mismatches within the aptamer binding domain in order to change the rate of aptamer binding as compared to the control aptamer.²⁵ Results

determined by the Munzar et al. study facilitated rapid selection of promising ACEs, possessing a range of sensitivities measured by their k_{off}^* and k_{off} rates, allowing us to alter our τ' domain to observe varied kinetic behavior of altered ATs.

In this study, we aim to understand the underlying kinetics and biophysics of our adenosine AT, and more specifically to understand the structural and kinetic factors that influence the overall rate of reaction of the AT due to alterations in the τ' domain sequence. To accomplish this aim, we selected and tested a wide range of ACEs to replace the τ' domain adopted in our previous study which resulted in improvements to the sensitivity compared to our control AT. By improving our original AT using ACEs selected from the ACE-scan data, we devised an efficient method for both understanding the biophysics of ATs and for improving upon current ATs which do not require the redesign of a much larger pool of ATs. By demonstrating the effectiveness of this AT development process, we further suggest an avenue to rapidly develop biosensors in the future as well as provide an insight on the factors influencing the performance of ATs.

3.3 Methods

3.3.1 DNA Preparation

DNA strands were purchased from Integrated DNA Technologies (IDT). [See Supporting Information S3 Strand Sequences for Aptamer Transducers] Prior to ordering, validation of secondary structures was tested for all complexes using NUPACK.³⁴ [See Supporting Information S2 Aptamer Transducer Secondary Structures and Raw Kinetics Traces] Dye or quencher labeled strands were purified by high performance liquid chromatography (HPLC) by IDT. Dye strands were modified on the 5' end with Tetrachlorofluorescein (TET) and quencher strands were modified on the 3' end with

Iowa Black Quencher (IABkFQ, IDT). Upon receiving, strands were re-suspended until they reached $\sim 100 \mu\text{M}$ in $1\times\text{TE}$ buffer (Sigma-Aldrich). ATs and reporter complexes were stoichiometrically mixed in $1\times\text{TAE}$ buffer with 12.5 mM MgCl_2 . Samples were annealed at $90 \text{ }^\circ\text{C}$ for 5 minutes and then cooled to $20 \text{ }^\circ\text{C}$ at a rate of $5 \text{ }^\circ\text{C}$ per minute to room temperature before being purified by PAGE.

3.3.2 DNA Purification

All DNA complexes were purified by PAGE gel electrophoresis. 1.5 mm thick $10 \text{ cm} \times 10 \text{ cm}$ non-denatured 10% gels for PAGE (acrylamide:bis = 29:1) were prepared with $1\times\text{TAE}$ buffer. A 50:50 solution containing ficcol and bromophenol blue was used as loading buffer. Annealed samples were mixed with loading buffer (4:1) and loaded into PAGE gels in $25 \mu\text{L}$ increments. Electrophoresis was carried out at 150 V , 100 mA , 20 W , for 2.5 hrs. Bands cut from each gel contained the purified complex which were eluted in $\sim 500 \mu\text{L}$ $1\times\text{TE}$ buffer with 25 mM MgCl_2 . After 24 hours of elution, purified DNA complexes were kept in low binding Eppendorf Tubes prior to mixing for reaction kinetics measurement.

3.3.4 Kinetics Experiments

Samples were vortexed and centrifuged before their concentration was quantified by absorbance measurements on a NanoDrop One (Thermo Scientific) at 260 nm . Extinction coefficients, provide by IDT, were used to determine the DNA complex concentrations prior to mixing the reactants. Purified and diluted DNA samples were reacted in stoichiometric quantities. Reaction kinetics were measured with Varian or Agilent Cary Eclipse fluorometers using transparent disposable PMMA cuvettes (excitation $\lambda=522 \text{ nm}$, emission $\lambda=539 \text{ nm}$, $25 \text{ }^\circ\text{C}$).

3.3.5 Kinetics Model Fitting

The derived kinetics model was applied to the normalized and leak subtracted kinetics traces, normalized by the maximum fluorescence output obtained from a positive control experiment, for 20 μM , 200 μM and 2 mM adenosine. A least squares regression was applied to the traces via SciPy a Python3 package. [See Supporting Information S4 Python3 Code for AT Kinetics Fitting]

3.4 Results and Discussion

3.4.1 ACE Selection for τ ' Integration

To examine the kinetic properties of the adenosine AT, 21 adenosine ACEs with varying k_{off}^* and k_{off} rates were selected from a pool of 251 ACEs that were characterized by Munzar et al.²⁵ The selected ACEs differed in length, start-site domain, and single-mismatch location of the 21 selected, 12 of the ACEs were selected from the ACE-scan data in the 5' direction and 9 were selected in the 3' direction, which possessed identical design modifications in each direction. To ensure testing of same design factors in each direction (5' vs 3' directions), we included 3 ACEs, 12 nt-long ACEs having single-mismatches, that were not included the ACE-scan study. In total, 24 ACEs were tested and compared to our previously published original AT, which serves as the control, that

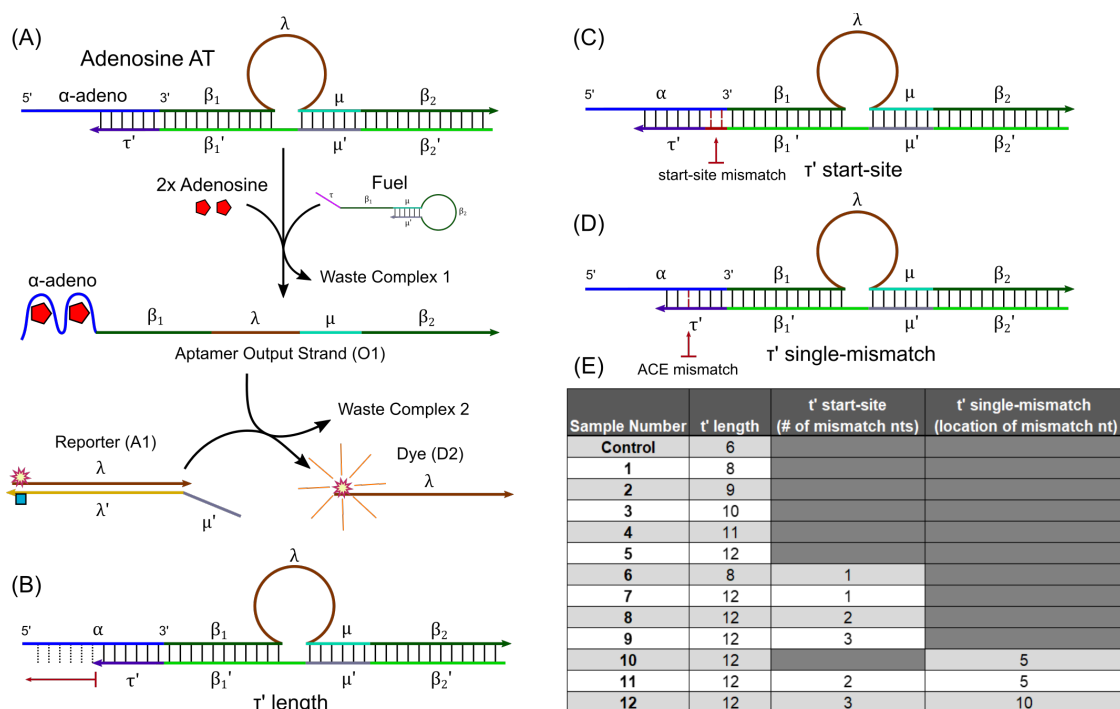


Figure 3.1 (A) AT reaction schematic, the adenosine AT first reacts with 2 adenosine molecules for structure-switching and then a fuel reacts with the available toehold releasing the output O1. O1 reacts further with a reporter complex. Alterations to the AT (B) τ' length (C) τ' start-site and (D) τ' single-mismatch were used to test the behavior of the AT structure-switching mechanism. (E) Selected ATs from the ACE-scan data are listed based on their τ' alterations. Both 5' and 3' versions of Selected ATs 1-12 were tested giving a total of 24 ATs compared to the control AT, the original AT from our previous work.

included an ACE with a 6 nt-long toehold and no additional alterations to start-site or single-mismatches. ACEs selected from this pool were incorporated as τ' domains in our AT design to act as both a structure-switching element for biosensing and a toehold to initiate strand displacement with the fuel strand. Each AT was tested and its kinetic trace was fitted with a simple kinetics model (derivation shown later in *AT Kinetics Model* section) to determine the effective dissociation constant $K_{d,eff}$ of the respective AT complex and to determine the strand displacement reaction rate constant k_1 for direct comparison. The relative performances of each AT quantified by k_1 and $K_{d,eff}$ were then

correlated to ACE-scan results for comparison to determine the effectiveness of our ACE selection process for ATs.²⁵

The AT reaction schematic (Figure 1A), which applies to all AT reactions in this study, illustrates two adenosines binding to the α domain activating the AT complex and subsequent dehybridization of the α aptamer domain from the ACE (τ' domain) making the toehold available for strand displacement with a fuel strand. The invading fuel strand then reacts with the activated AT complex undergoing a toehold-mediated strand displacement that releases the aptamer output single strand O1 and creates a waste complex. The released output strand O1 is then available to react with the reporter complex, since μ and λ domains are no longer sequestered, leading to an increase in the overall solution fluorescence by separating the dye from the quencher, creating a second waste complex at the same time. Here, FRET reporting is used to track the overall reaction of the adenosine ATs, where $K_{d,eff}$ and k_l can be extracted from their kinetic traces.

We chose ACEs that are 8-12 nts long to alter the τ' domain length in comparison to the control (6 nts long) as shown by ACEs 1-5 (Figure 1E), since the ACE-scan study demonstrated that the length of the ACEs affected structure-switching significantly, evidenced by their differences between k_{off} and k^*_{off} rates. Figure 1B schematically shows how τ' with different lengths were incorporated into the altered AT design, where longer τ' domains extend further into aptamer from either the 5' or 3' directions and hybridize with additional bases. Extension of the τ' domain was anticipated to affect the AT reactivity by several competing factors including stabilization of the ACE-aptamer duplex due to increased hybridization, a net decrease in the rate of

structure-switching due to more bonds to dehybridize in the structure-switching process, and only a slight increase in the rate of toehold binding of the fuel to the τ' toehold due to a greater number of available bases for toehold initiation after structure-switching since rates marginally increase beyond 6-7 nts for the toehold.³¹ In addition, we expect a net reduction in the rate of leakage, which happens when the fuel strand reacts with the AT without the presence of adenosine, due to a decrease in the probability of spontaneous structure-switching events since the number of hybridized bases in the ACE was increased. Overall, it would generally be expected that increasing the length of τ' would decrease the sensitivity of the AT device since more base pairs introduce a higher energy barrier against the structure-switching during aptamer ligand interaction. However, results from ACE-scan indicated that ACEs as long as 12 nt-long retained the ability to undergo structure-switching since the extra bases extend into the two aptamer binding pocket domains of the adenosine aptamer allowing for the ACE to dehybridize in a series of intermediate steps, therefore reducing the overall energy barrier of the induced fit mechanism.

Similarly, introducing a start-site domain between τ' and β_1' (Figure 1C) shifts the τ' domain along the aptamer sequence, which could cause structure-switching to occur more favorably due to better alignment of the ACE's sequence with the sequences in the two binding pockets of the adenosine aptamer. According to the ACE-scan study, shifting the ACE closer to the binding pocket increased the k^*_{off} , which implies that adding a start-site domain could also lead to improving the sensitivity of the AT. Figure 1C illustrates how the introduction of a 2 nt start-site domain pushes the 6 nt-long toehold further into the aptamer binding pocket region, while Figure 1E lists detailed information

on ACEs 6-9, 11, and 12 that contain a start-site domain between 1-3 nts in length. While an increase in sensitivity could be expected by adding a start-site domain between τ' and β_1' , longer start-site domains may also introduce extraneous leakage since it could allow a fuel strand to invade the start-site domain. Therefore, we have selected ACEs that have a maximum of three mismatched nucleotides in the start-site domain to suppress potential leakage reactions. Conversely, we expect additional leakage by adding a short start-site domain to be minimal, since the start-site domain remains sequestered in a small internal bulge loop within the AT complex, making it harder for the invading fuel to initiate strand displacement due to steric hindrance.

In their ACE-scan study, Munzar et al. also demonstrated that the introduction of a single mismatch into the 12 nt ACEs were effective in further increasing the k_{off}^* . The increase was explained by a net reduction of free-energy of the ACE bound to the aptamer, hence reducing the energy barrier for structure-switching step, which in turn leads to favorable ligand binding through intermediate ligand binding steps. Introduction of single nucleotide mismatches into the τ' of the 12 nt-long ATs (Figure 1D) is also expected to weaken the τ' toehold-aptamer complex and lower the energy barrier associated with structure-switching with minimal increase in leakage rate. Therefore, we have selected three 12 nt-long ACEs (ACEs 10-12 in Figure 1E) that incorporate a single nucleotide mismatch within the τ' domain which we expect will improve the overall AT sensitivity.

Finally, all ATs were designed for both 5' to 3' and 3' to 5' directions with mirroring the nucleotide lengths, start-sites, and single-mismatch locations since ACE-scan also showed a direction-dependent kinetic behavior. This kinetic difference is

explained by the adenosine aptamer binding domain's asymmetric placement within the aptamer sequence as evidenced by different asymmetric k_{off}^* rates in the ACE-scan study. To incorporate the ACEs possessing opposite directions to our original adenosine AT, the τ' and α domains were translated to either side of the β_1 and β_2 domains to incorporate both 5' to 3' directions. Each of the 12 ACEs shown in Figure 1E were tested in either the 5' or 3' configuration leading to a total of 24 ATs tested.

3.4.2 Modified AT Performances

Our kinetic model was used to fit each reaction trace for the ATs 1-12 in the 5' direction to determine both the k_l and $K_{d,eff}$ for each reaction (Figure 2), [See Supporting Information S2 for AT Reaction Traces]. The strand displacement reaction rate constant k_l with different adenosine concentrations did not produce large variances as $K_{d,eff}$ values did since the strand-displacement step is the rate limiting step, thus the reaction kinetic traces reflected the strand-displacement process more closely allowing for a more accurate measurement of k_l . The values of k_l for the 12 ATs tested in the 5' direction ranged roughly within an order of magnitude between 10^{-3} and 10^{-4} (nM·min)⁻¹. ATs with 11 or 12 nt-long ACEs (4-5 and 7-11, Figure 1E) showed smaller k_l with the lowest

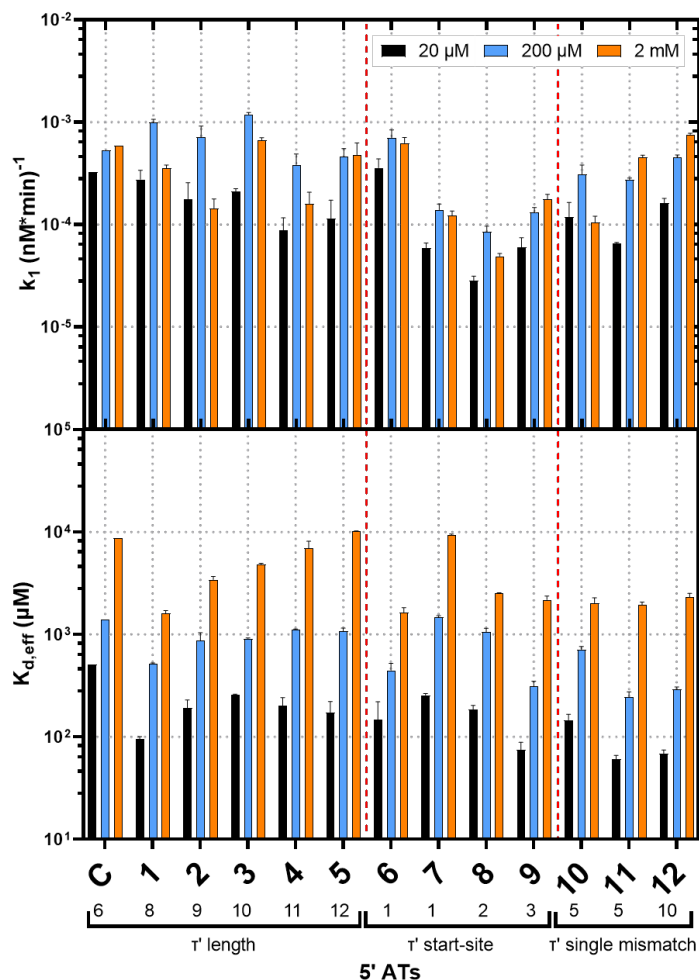


Figure 3.2: Both k_1 and $K_{d,\text{eff}}$ are shown for Selected 5' ATs 1-12 in the 5' direction, which were estimated by fitting the 20 μM , 200 μM and 2 mM reaction traces. The selected ACEs are grouped by τ' length, τ' start-site domain, and τ' single mismatch shown as the for comparison of reaction rate and equilibrium constants. The values below the AT sample numbers represent the length of τ' , position of start-site mismatch for τ' start-site domain, and the position of the single mismatch from the τ' - β_1' interface. (Note: AT 6 has 8 nt long while ATs 7-12 are 12 nt long. Also, ATs 11 and 12 have 2 and 3 nt long start-site mismatch, respectively)

values corresponding to ACEs 7-9, which had both 12 nt-long τ' domains and a start-site domain. Comparing the ATs 1-5 to the control (C) possessing a 6 nt-long τ' , we find that there is a general decrease in the k_1 of the strand displacement between the AT and fuel. As expected, the overall decrease in k_1 with the addition of bases to the τ' domain can be attributed to an increase in the number of branch migration steps required for the release

of the aptamer output strand (O1). Moreover, the increased τ' length increases the likelihood of reverse strand-displacement reaction since the adenosine aptamer domain remains in proximity of the τ' domain longer prior to its complete separation. It was previously shown that the rate of strand displacement reactions plateaus when the toehold is longer than 6 nts.³¹ In our case, the rate not only plateaued for increasing toehold length but also declined as the length of the toehold increased since the longer toehold reversed the structure-switching mechanism of the AT.

For ATs 10-12 possessing 12 nt-long ACE with a single mismatch, we observed an increase in k_f compared to the 12 nt-long ACE without a mismatch, likely due to reduction of reverse structure-switching, which can be attributed to the decrease in the energy barrier associated with adenosine binding due to the presence of mismatched base. With the addition of a single mismatch between the two binding pockets of the adenosine aptamer, the binding process can occur in two distinct intermediate steps that involve smaller total binding free energies than that required to bind in a single step. Such positive cooperativity between the two binding sites has been studied before.^{25,27,32} Consequently, it is also less likely that the aptamer ligand binding will spontaneously dissociate since two binding steps are required for rehybridization between the τ' domain and the O1 strand.

The effective dissociation constant $K_{d,eff}$ was also determined for the 12 ATs in the 5' direction for 20 μ M, 200 μ M, and 2 mM adenosine. $K_{d,eff}$ measured at three adenosine concentrations are separated by an order of magnitude for each of the different AT samples. Such significant concentration dependence is likely due to the approach used for fitting $K_{d,eff}$ directly from reaction traces near the extremes of AT operation,

where the strand displacement reaction causes maximum fluorescence to be reached too quickly or the reaction occurs too slowly causing a slight rise in fluorescence intensity after 100 minutes. Such extremes changes in the overall reaction rate cause the exponential in the fit function to reach an asymptotical limit reducing the accuracy of the measured fitting parameters. Another source of deviation could be the assumption that the equilibrium between adenosine and the aptamer is fast, which allowed us to use the equilibrium concentration to estimate the concentration of activated probes $[P_c^{*o}]$, since the overall fit function would change. It is possible that the concentration of activated probes $[P_c^{*o}]$ is concentration dependent and would require a more complex kinetic model to fully estimate. Regardless of the variation seen in $K_{d,eff}$, the 200 μM trace contains the most reasonable estimation of $K_{d,eff}$ for the ATs because the signal produced with 200 μM adenosine does not quickly reach a maximum, making the $K_{d,eff}$ easily distinguishable from the strand displacement reaction rate dictated by k_I . High adenosine concentrations yield very little distinction between reaction traces, and low adenosine concentrations result in low fluorescence responses, which are difficult to differentiate from the leakage signals. Regardless of the over- or underestimation of the $K_{d,eff}$ in 2 mM and 20 μM adenosine concentrations, the $K_{d,eff}$ measured at those concentrations still show similar trends between different ATs and are still useful for comparison of relative performance metrics, where normalization of $K_{d,eff}$ removes the magnitude difference seen between the three concentrations measured.

$K_{d,eff}$ of the 12 different ATs exhibited a range of sensitivities that span nearly an order of magnitude showing that the ATs become more sensitive with decreasing τ' length. In comparison to the control AT with 6 nt-long τ' domain, AT 1 that did not

contain a start-site domain or mismatch had the best sensitivity indicating that 8 nt is an optimal length for sensing in the 5' direction. Each additional nucleotide past 8 increased the $K_{d,eff}$, which can be explained by the reduction in the structure-switching rate caused by an increase in the number of dehybridization steps required for dissociation of τ' domain from the O1 strand. With the inclusion of a start-site domain to the 12 nt-long τ' (ATs 7-9), there was a significant decrease in $K_{d,eff}$, which implies that τ' domains extending further into the aptamer domain undergo structure-switching more readily resulting in a net increase in sensitivity. Similar decreases in $K_{d,eff}$ were also observed for ATs 10-12 possessing both a single-mismatch within the τ' domain and a start-site domain. ATs 11 and 12 possessed the lowest $K_{d,eff}$ values, but they also contained a start-site domain and single-mismatch nt within the τ' domain. In agreement with the ACE-scan study, the shift of the ACE start-site within the aptamer domain and the addition of a single-mismatch within the τ' domain increased the aptamer sensitivity due to a net reduction of binding energy and the destabilization of the ACE-aptamer complex, allowing for the formation of intermediate products during the two adenosine binding steps due to reduced overall energy barrier associated with structure-switching.²⁵

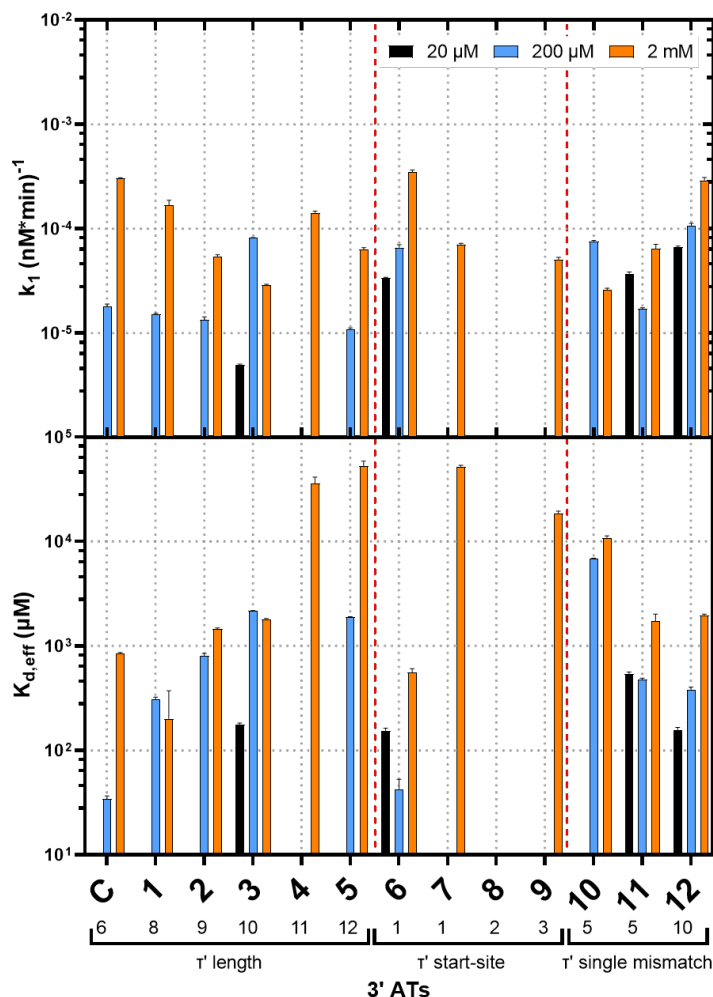


Figure 3.3: Both k_1 and $K_{d,\text{eff}}$ are shown for Selected 3' ATs 1-12 in the 5' direction which were estimated by fitting the 20 μM , 200 μM and 2 mM reaction traces. The selected ACEs are grouped by τ' length, τ' start-site domain, and τ' single mismatch for comparison of reaction rate and equilibrium constants. Note that missing data points for specific concentrations did not produce any distinguishable signal above system noise. The values below the AT sample numbers represent the length of τ' , position of start-site mismatch for τ' start-site domain, and the position of the single mismatch from the $\tau'-\beta_1'$ interface. (Note: AT 6 has 8 nt long while ATs 7-12 are 12 nt long. Also, ATs 11 and 12 have 2 and 3 nt long start-site mismatch, respectively)

The kinetic behaviors of ATs in the 3' direction, whose sequences mirror those in the 5' direction, were also measured using the same reporter complex (Figure 3) in 20 μM , 200 μM , and 2 mM adenosine. Many aptamers in 3' direction in 20 μM and 200 μM adenosine did not produce measurable signals. Also, AT 8 did not produce any detectable signal for any concentration of adenosine. The inability of some ATs with 3' direction

ACE to detect adenosine is in stark contrast to the 5' ATs, which were able to reliably detect adenosine at concentrations as low as 20 μM . Such results were most likely due to the misalignment of the τ' domain with the binding pockets of the aptamer, which were extend further into the aptamer sequence in the 3' direction than in the 5' direction.^{17,25} Therefore, the induced-fit, which typically causes structure-switching of the AT, was ineffective at freeing the τ' domain from the aptamer domain, necessitating a much higher concentration of adenosine to overcome the energy barrier and induce structure-switching. Kinetic data obtained at 2 mM adenosine concentration provided the most reliable information since they were easily distinguishable from the leakage signal. AT 12 was the only sample that produced a similar k_I and $K_{d,eff}$ to those of 5' ATs, which can be attributed to AT 12 possessing longest start-site domain and a single mismatch that allowed easier dehybridization of the τ' domain during the structure-switching step.

We found that k_I for 3'-direction ATs 1-5 decreased as the τ' domain length increased, which is in agreement with the ATs in the 5' direction, with the exception of ATs 4 and 5. Higher k_I for ATs 4 and 5 could be due to their τ' domains extending far enough into the aptamer binding pocket at the 11th and 12th nucleotides that would facilitate the dehybridization by opening a shorter toehold. Adding a single nucleotide start site domain to 8 nt-long AT6 significantly lowered the detection limit of this AT and improved the k_I compared to the other ATs because it had the best balance between τ' domain extending further into the binding pocket and a shorter τ' domain compared to other 12 nt-long ATs. For ATs 7-9, extending the 12 nt-long τ' domains further along the aptamer sequence produced mixed results. Specifically, AT 8 did not respond to any adenosine concentration and it is unclear why such deterrence to structure-switching may

have occurred. However, the result of ATs 7-9 clearly highlights the sensitivity of aptamer ligand binding process to different configurations of the ACE for duplexed aptamer biosensors. Finally for ATs 10-12, there was a marked increase in k_I , where ATs 11 and 12 were able to sense all three concentrations down to 20 μM . The increase in k_I for ATs 10-12 can be explained by the further extension of the τ' domain into the binding pocket domain of the aptamer, and by the reduction of free energy for structure-switching caused by splitting the aptamer binding into two intermediate steps, which we explained previously for the 5' ATs.

The domain length dependence of $K_{d,eff}$ for the 3' ATs 1-5 and the control AT was similar to that of their 5' AT counterparts at 2 mM adenosine concentration. AT 1 containing 8 nt-long τ' domain displayed the greatest sensitivity with the lowest $K_{d,eff}$. Increasing the τ' domain length from 8 to 12 nts also showed a general decrease in sensitivity as evidenced by an increase in $K_{d,eff}$, which agrees well with the trend shown by 5' ATs. A key difference in the behavior of the 3' ATs compared to those of 5' ATs is that the values of $K_{d,eff}$ for the 3' ATs were an order of magnitude larger with the exception of AT 12. The higher $K_{d,eff}$ for 3' ATs 1-11 might have been caused by notably lower signal output, caused by reduced structure-switching of the 3' ATs, which made reliable extraction $K_{d,eff}$ and k_I difficult due to lower signal-to-noise ratio and smaller difference between the signal and the leakage kinetic traces. The signal-to-noise ratio was sufficiently large for the 3' AT12 as compared to the other 3' ATs and therefore had comparable k_I and $K_{d,eff}$ with the 5' ATs.

3.4.3 ATs versus ACE-Scan

A total of 21 ATs were selected based on the results from ACE-scan data, namely $k_{off,diff}$ defined as the difference between k_{off} and k_{off}^* . For comparison, we developed a relative performance metric, $k_I/K_{d,eff}$, where larger k_I increases the relative performance and smaller $K_{d,eff}$, indicates biosensor sensitivity. Therefore, the most optimal biosensor maximizes k_I while also minimizing $K_{d,eff}$. The relative performances of the 5' and 3' ATs normalized by the AT with the highest relative performance, AT 12 for the 5' ATs and AT 6 for the 3', were compared to the highest $k_{off,diff}$ from the ACE-Scan results. Both a Pearson Correlation and p-values (Figure 4A) were computed comparing the data for each adenosine concentration against the ACE-Scan $k_{off,diff}$ values. Figure 4B directly compares the relative performance of the ATs with the ACE-Scan data and the performances were ordered in the order of increasing predicted response from left to right. The highest Pearson correlation value of 0.71 was observed for the comparison between the performances at 2 mM adenosine concentration and ACE-scan $k_{off,diff}$, while the lowest correlation of 0.58 was observed for the 200 μ M adenosine concentration and ACE-scan $k_{off,diff}$, where correlation values between 0.5 and 0.7 are considered a moderate correlation between data trends.³³ This result indicates that roughly 34-50% of the AT exhibited performances predicted by ACE-scan, showing that ACE-scan was moderately effective in predicting optimized AT performance. One of potential reason why ACE-scan may have fallen short in predicting the kinetic behavior of ATs is the major difference in the experimental setup of our study compared to ACE-scan. In the case of ACE-scan, many different ACEs were functionalized on a microarray surface and duplexed to the single dye labeled aptamer strand that were allowed to react until the

aptamer fully dissociated from the ACE to cause a response. Our AT biosensors differ from this ACE-scan method since the structure-switching event itself does not cause our aptamer domain to immediately separate from the complex. Instead, the aptamer domain is held in proximity to the ACE, the τ' domain in our case, for some time before the strand displacement reaction is allowed to separate O1 strand completely from the AT complex. Another source of deviation between the AT and ACE-scan data could be the fact that ATs are diffusing freely in solution, whereas the ACE-aptamer duplexes are functionalized to a surface before structure-switching is carried out. It is unclear how the presence of a surface may affect the aptamer structure-switching mechanism as compared to aptamers, which are free in solution.

A direct comparison of AT performances ($k_1/K_{d,eff}$) to ACE-scan performance metric ($k_{off,diff}$) (Figure 4B) reveals many outliers responsible for reducing the correlation between data sets. Outperformance of 5' AT1 and 5' AT6, both possessing 8 nt-long τ' domain, over their ACE-scan predictions suggests that the optimal toehold length for ATs is different from that of the ACE-scan prediction. According to ACE-scan results, the 5'-2 AT with a 9 nt-long τ' domain possesses the optimal length without any alterations to the start-site domain or with a single-mismatch. This single nucleotide difference between the optimal lengths is evidence that the difference in structural designs, where the adenosine aptamer is part of the complex in the AT design, makes a difference in the functionality of the biosensors. 5' AT 10, possessing a 12 nt-long τ' domain with a single-mismatch in the 5th base from the τ' - β_1' junction, underperformed compared to the ACE-scan prediction. Similarly, 5' AT 7 and 5' AT 8, each possessing 12 nt-long τ'

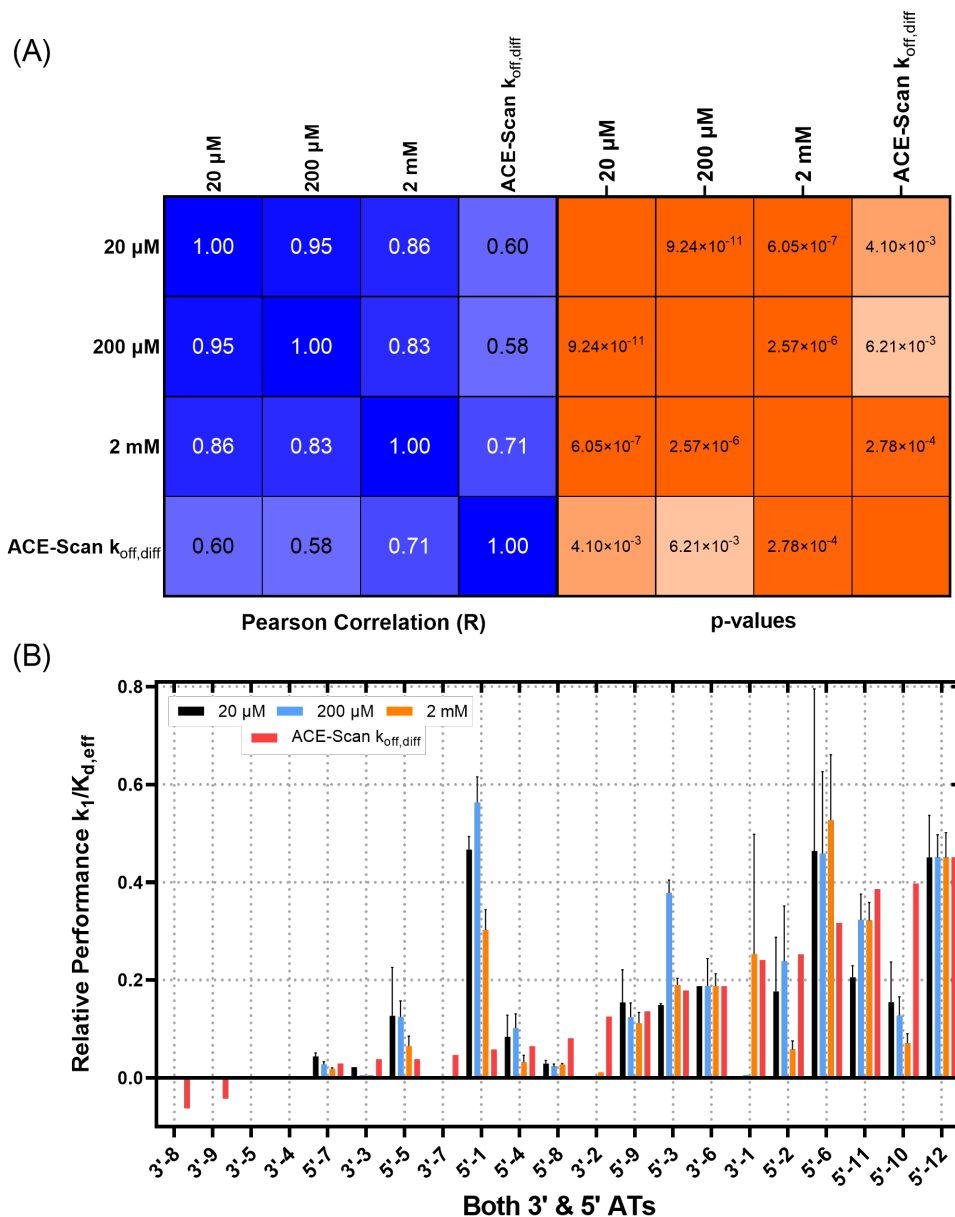


Figure 3.4: (A) A Pearson Correlation (R) (blue) between the ACE-Scan data results and the AT relative performance $k_1/K_{d,eff}$ for each tested adenosine concentration showing a strong correlation between different adenosine concentrations and a moderate correlation between ACE-scan and AT data. Roughly 34-50% ACE-Scan prediction corresponded to relative performance. P-values (orange) are also shown which indicate statistical significance for the data population analyzed. (B) Direct comparison of relative performance $k_1/K_{d,eff}$ for ATs tested versus ACE-scan $k_{off,diff}$ where ACE-scan predicted response increases from left to right (red). 5' ATs were normalized to AT 12 while 3' ATs were normalized to AT 6. ACE-scan $k_{off,diff}$ with low or negative data corresponded well with 3' ATs that had low signal. 8 nt length ATs overperformed compared to $k_{off,diff}$.

domains, underperformed compared to the ACE-scan, suggesting that the longer τ' domains lowered the availability of the toehold. However, addition of both a start-site domain and single mismatch to the 12 nt-long τ' domains in 5' AT 9, 5' AT 11, and 5' AT 12 resulted in improved matches with the ACE-scan data. Such improvements show that proper positioning of the ACE along the aptamer domain, including a start-site domain and mismatched bases, lowers the free-energy associated with structure-switching, which is essential in duplexed aptamer biosensor operation.

Results from the modified 24 ATs agree with the findings of the ACE-scan study with statistical significance, shown by our correlation between $k_{off,diff}$ and $k_1/K_{d,eff}$. Several outliers were caused by a clear difference in our experimental setup, where the ATs do not release the aptamer strand immediately after structure-switching. However, our study did show that the performance of adenosine ATs improve when the ACE domain is aligned with the adenosine aptamer binding domain, which is in direct agreement with the ACE-scan study. The result also supports the conclusion of induced fit mechanism for the adenosine aptamer. To improve upon the efficacy of using ACE-scan to select relevant ATs toward development of a high-throughput approach, we suggest that future work be done to develop an ACE-scan technique that more closely parallels the operation of ATs by developing a modality where the aptamer strand is not released from the ACE immediately after structure-switching.

3.5 Conclusions

Overall, the comparison of the ACE-scan data to the relative performances of the ATs demonstrates that the optimal ACE design parameters can vary between biosensor designs because the balancing the rates of two processes – structure-switching and strand displacement – is necessary for the optimization of AT performances. The optimal placement of the ACE along the aptamer sequence, with and without the inclusion of a single-mismatch, depended on the specific aptamer-ligand binding domain for induced fit aptamers. Reaction rates increased when the ACE was aligned with the bases responsible for binding with the ligand during structure-switching, while the inclusion of a single mismatch in the correct location along the duplexed aptamer improved the structure-switching by separating the two adenosine-aptamer binding steps.

In conclusion, we successfully showed that a selection of adenosine ATs based on insights derived from ACE-scan is a promising avenue in determining more well optimized ATs with higher performance, without the need to test a much larger set of ACEs, suggesting that ATs developed using other aptamers may also benefit from such a selection process. ACE-scan results for other aptamers may help to drastically reduce the number ATs that require testing to hone in on optimal AT performance. To improve the AT further, future work should aim to replace the adenosine aptamer with other known induce-fit binding aptamers and test their correlation with results derived from an ACE-scan selection. More work is required to conclusively show that ATs can flexibly accommodate other aptamers or aptamer mutations. Future studies should use various ACE lengths, start-site, and single-mismatches with other induced-fit aptamers to balance the reaction rates due to both structure-switching and strand displacement. Assuming

such a balance between reaction rates can be found reliably, it may be possible to create a generalized set of rules for the development of future ATs to further streamline the development of aptamer biosensors to sense many different analytes at lowered concentration, improving their sensitivity.

Acknowledgments

We thank members of the Boise State Nanoscale Materials and Device group for valuable assistance with this work. We also thank Boise State University Micron School of Materials Science & Engineering Department for supporting this work. This work was supported in part by grant no.1706065 from the National Science Foundation.

Supporting Information

The Supporting information is available free of charge on the ACS Publications website at DOI: 10.1021/acs.jpcc.3c01411

Strand sequences, NUPACK secondary structures results, optimization of AT-Fuel concentrations, optimization of buffer salt concentrations, and selectivity of the AT targeting adenosine are provided.

Author Information

Tim Hachigian: timhachigian@u.boisestate.edu (ORCID: 0000-0003-2499-4962)

Drew Lysne: drewlysne@u.boisestate.edu (ORCID: 0000-0001-6007-6478)

Elton Graugnard: eltongraugnard@boisestate.edu (ORCID: 0000-0002-0497-9821)

Jeunghoon Lee: jeunghoonlee@boisestate.edu (ORCID: 0000-0002-1909-4591)

3.6 References

- (1) Wang, K.; He, M. Q.; Zhai, F. H.; He, R. H.; Yu, Y. L. A Label-Free and Enzyme-Free Ratiometric Fluorescence Biosensor for Sensitive Detection of Carcinoembryonic Antigen Based on Target-Aptamer Complex Recycling Amplification. *Sens. Actuators, B* **2017**, *253*, 893–899.
- (2) Meng, H. M.; Liu, H.; Kuai, H.; Peng, R.; Mo, L.; Zhang, X. B. Aptamer-Integrated DNA Nanostructures for Biosensing, Bioimaging and Cancer Therapy. *Chem. Soc. Rev.* **2016**, *45*, 2583–2602.
- (3) Han, B.; Fang, C.; Sha, L.; Jalalah, M.; Al-Assiri, M. S.; Harraz, F. A.; Cao, Y. Cascade Strand Displacement Reaction-Assisted Aptamer-Based Highly Sensitive Detection of Ochratoxin A. *Food Chem.* **2021**, *338*, 127827.
- (4) Lee, J.; Jeon C H; Ahn S J; Ha T H. Highly Stable Colorimetric Aptamer Sensors for Detection of Ochratoxin A through Optimizing the Sequence with the Covalent Conjugation of Hemin. *Analyst* **2014**, *139*, 1622–1627.
- (5) Zhang, F.; Liu, J. Label-Free Colorimetric Biosensors Based on Aptamers and Gold Nanoparticles: A Critical Review. *Analysis Sensing* **2021**, *1*, 30–43.
- (6) Ravan, H. Implementing a Two-Layer Feed-Forward Catalytic DNA Circuit for Enzyme-Free and Colorimetric Detection of Nucleic Acids. *Anal. Chim. Acta* **2016**, *910*, 68–74.
- (7) Xu, J.; Xiang, J.; Chen, J.; Wan, T.; Deng, H.; Li, D. High Sensitivity Detection of Tumor Cells in Biological Samples Using a Multivalent Aptamer Strand Displacement Strategy. *Analyst* **2022**, *147*, 634–644.
- (8) Shlyahovsky, B.; Li, D.; Weizmann, Y.; Nowarski, R.; Kotler, M.; Willner, I. Spotlighting of Cocaine by an Autonomous Aptamer-Based Machine. *J. Am. Chem. Soc.* **2007**, *129*, 3814–3815.
- (9) Huizenga, D. E.; Szostak, J. W. A DNA Aptamer That Binds Adenosine and ATP. *Biochemistry* **1995**, *34*, 656–665.

- (10) Tuerk, C.; Gold, L. Systematic Evolution of Ligands by Exponential Enrichment: RNA Ligands to Bacteriophage T4 DNA Polymerase. *Science* **1990**, *249*, 505–510.
- (11) Jung, C.; Ellington A. D. Diagnostic Applications of Nucleic Acid Circuits. *Acc. Chem. Res.* **2014**, *47*, 1825–1835.
- (12) Fu B; Cao J; Wang L; Jiang W. A Novel Enzyme-Free and Label-Free Fluorescence Aptasensor for Amplified Detection of Adenosine. *Biosens. Bioelectron.* **2013**, *44*, 52–56.
- (13) Xiao, Y.; Piorek B. D.; Plaxco K. W.; Heeger A. J. A Reagentless Signal-on Architecture for Electronic, Aptamer-Based Sensors via Target-Induced Strand Displacement. *J. Am. Chem. Soc.* **2005**, *127*, 17990–17991.
- (14) Zheng, D.; Seferos D. S.; Giljohann D. A.; Patel P. C.; Mirkin C. A. Aptamer Nano-Flares for Molecular Detection in Living Cells. *Nano Lett.* **2009**, *9*, 3258–3261.
- (15) Dalirirad, S.; Steckl, A. J. Aptamer-Based Lateral Flow Assay for Point of Care Cortisol Detection in Sweat. *Sens. Actuators, B* **2019**, *283*, 79–86.
- (16) Xue, J.; Chen, F.; Bai, M.; Cao, X.; Fu, W.; Zhang, J.; Zhao, Y. Aptamer-Functionalized Microdevices for Bioanalysis. *ACS Appl. Mater. Interfaces* **2021**, *13*, 9402–9411.
- (17) Munzar J. D.; Ng, A.; Juncker, D. Duplexed Aptamers: History, Design, Theory, and Application to Biosensing. *Chem. Soc. Rev.* **2019**, *48*, 1390–1419.
- (18) Khan, N. I.; Song, E. Lab-on-a-Chip Systems for Aptamer-Based Biosensing. *Micromachines* **2020**, *11*, 220.
- (19) Kasoju, A.; Sagar Shrikrishna, N.; Shahdeo, D.; Azmat Ali Khan; Amer M. Alanazi; Gandhi, S. Microfluidic Paper Device for Rapid Detection of Aflatoxin B1 Using an Aptamer Based Colorimetric Assay. *RSC Adv.* **2020**, *10*, 11843–11850.

- (20) Cho E J; Yang, L.; Levy, M.; Ellington A D. Using a Deoxyribozyme Ligase and Rolling Circle Amplification to Detect a Non-Nucleic Acid Analyte, ATP. *J. Am. Chem. Soc.* **2005**, *127*, 2022–2023.
- (21) Yoo, H.; Jo, H.; Soo Oh, S. Detection and beyond: Challenges and Advances in Aptamer-Based Biosensors. *Mater. Adv.* **2020**, *1*, 2663–2687.
- (22) Li, B.; Ellington A D; Chen, X. Rational, Modular Adaptation of Enzyme-Free DNA Circuits to Multiple Detection Methods. *Nucleic Acids Res.* **2011**, *39*, e110.
- (23) Hachigian, T.; Lysne, D.; Graugnard, E.; Lee, J. Customizable Aptamer Transducer Network Designed for Feed-Forward Coupling. *ACS Omega* **2021**, *6*, 26888–26896.
- (24) Zhu, J.; Zhang, L.; Zhou, Z.; Dong, S.; Wang, E. Aptamer-Based Sensing Platform Using Three-Way DNA Junction-Driven Strand Displacement and Its Application in DNA Logic Circuit. *Anal. Chem.* **2014**, *86*, 312–316.
- (25) Munzar J. D.; Ng, A.; Juncker, D. Comprehensive Profiling of the Ligand Binding Landscapes of Duplexed Aptamer Families Reveals Widespread Induced Fit. *Nat. Commun.* **2018**, *9*, 343.
- (26) Dillen, A.; Vandezande, W.; Daems, D.; Lammertyn, J. Unraveling the Effect of the Aptamer Complementary Element on the Performance of Duplexed Aptamers: A Thermodynamic Study. *Anal. Bioanal. Chem.* **2021**, *413*, 4739–4750.
- (27) Armstrong R E; Strouse G F. Rationally Manipulating Aptamer Binding Affinities in a Stem-Loop Molecular Beacon. *Bioconjugate Chem.* **2014**, *25*, 1769–1776.
- (28) Zhang, Z.; Oni, O.; Liu, J. New Insights into a Classic Aptamer: Binding Sites, Cooperativity and More Sensitive Adenosine Detection. *Nucleic Acids Res.* **2017**, *45*, 7593–7601.
- (29) Kotani, S.; Hughes W L. Multi-Arm Junctions for Dynamic DNA Nanotechnology. *J. Am. Chem. Soc.* **2017**, *139*, 6363–6368.

- (30) Zhang, D. Y.; Turberfield, A. J.; Yurke, B.; Winfree, E. Engineering Entropy-Driven Reactions and Networks Catalyzed by DNA. *Science* **2007**, *318*, 1121–1125.
- (31) Srinivas, N.; Ouldrige T E; Sulc, P.; Schaeffer J M; Yurke, B.; Louis A A; Doye J P; Winfree, E. On the Biophysics and Kinetics of Toehold-Mediated DNA Strand Displacement. *Nucleic Acids Res.* **2013**, *44*, 10641–10658.
- (32) Slavkovic, S.; Zhu, Y.; Churcher, Z. R.; Shoara, A. A.; Johnson, A. E.; Johnson, P. E. Thermodynamic Analysis of Cooperative Ligand Binding by the ATP-Binding DNA Aptamer Indicates a Population-Shift Binding Mechanism. *Sci. Rep.* **2020**, *10*, 18944.
- (33) Mukaka, M. M. Statistics Corner: A Guide to Appropriate Use of Correlation Coefficient in Medical Research. *Malawi Med. J.* **2012**, *24*, 69–71.
- (34) Zadeh, J. N.; Steenberg, C. D.; Bois, J. S.; Wolfe, B. R.; Pierce, M. B.; Khan, A. R.; Dirks, R. M.; Pierce, N. A. NUPACK: Analysis and design of nucleic acid systems. *J. Comput. Chem.* **2011**, *32*, 170-173.

CHAPTER 4: FUTURE WORK AND FINAL REMARKS FOR THE APTAMER TRANSDUCER PLATFORM

4.1 Introduction

While our previous studies have established the utility of the customizable aptamer transducer using the adenosine binding DNA aptamer, the capacity of the AT framework to integrate other aptamer sequences into its structure-switching design still remains largely unexplored.¹ Demonstration of the ability to incorporate other aptamers into the structure-switching design used by the aptamer transducer framework is crucial for broader applicability of this approach.¹ Thus, it is imperative that future investigations explore the extent to which the AT can incorporate other aptamer sequences without significant modifications to its framework. In addition to the potential impact on biosensor development, further exploration of the AT could expand our understanding of aptamer-ligand interactions leading to further understanding of the kinetic mechanisms and biophysics of aptamers. Moreover, such studies could facilitate the development of multiplexed biosensors capable of detecting multiple targets simultaneously. This could have significant implications in medical diagnostics, enabling the rapid and accurate detection of multiple diseases in a single test.

Overall, further investigation into the AT framework is essential for advancing the AT framework into a more robust and well-defined system for real world application. In this chapter, we suggest routes toward further development of the AT framework, including the incorporation of other aptamer sequences into the structure-switching design, the development of multiplexed biosensors, and the further investigation of aptamer-ligand interactions.

In our previous work, we have developed a novel AT platform that has been capable of customizing the output domains targeting downstream strand displacement networks. Being able to show that this platform could target arbitrary DNA inputs was essential for creating a modular system and allows simple integration of the AT into many other strand displacement systems for signal processing and detection. On top of this, we have shown an effective selection process for determining well suited ACEs and have explored the kinetics of the structure-switching mechanism, which will provide a means to develop new sensors rapidly that target high sensitivity. Here, we would like to discuss the next steps in developing this framework and some challenges in the field.

4.2 Future Work

4.2.1 Discussion of Biomolecular Insights for Adenosine Binding AT

The adenosine binding DNA aptamer, specifically the 25-nucleotide Huizenga and Szostak aptamer, serves as a fundamental component of the aptamer-based biosensor system we have investigated in this work. This biosensor employs the cooperative action of the adenosine binding aptamer and an aptamer complementary element to initiate a strand displacement reaction, leading to a detectable signal. To delve deeper into the biomolecular insights of this process, it is crucial to examine the binding mechanisms between adenosine and the aptamer, as well as their implications on the kinetics of the system.

Upon introduction of adenosine, the adenosine binding DNA aptamer undergoes a significant conformational change, resulting in the formation of a stable complex with the ligand. This conformational alteration is essential for the aptamer's specific recognition and capture of adenosine. As described in Chapter 3, the $K_{d,eff}$ we found for multiple ATs

correlated with studies that favored the induced fit kinetic pathway. The induced fit pathway occurs when the aptamer fully conforms with the required structure to accept both ligands when the ligands are in proximity, within mere nanometers. The adenosine aptamer contains a well-defined binding pocket precisely tailored to accommodate the adenosine moiety through specific hydrogen bonding and stacking interactions. Most notably, binding of the adenosine occurs when the aromatic rings of the adenosine molecule establish critical contacts with the aptamer, further stabilizing the complex and enhancing its affinity for the ligand. For the induced fit to occur, the interactions between the adenosine and the aptamer in the AT would have to be strong enough to not only cause the conformational changes necessary to produce adequate binding pockets but would also have to disrupt the Watson-Crick base pairing between the aptamer and complementary element for the conformational change to occur.

Our work and those by others show that this disruption of base pairs does occur even with half the aptamer bases hybridized to the complementary element. This might be surprising since the conformation necessary to induce aptamer-ligand binding would be far from ideal with half the aptamer bases occupied, which was shown in Chapter 3. However, it is possible that breathing between the aptamer and the nucleobases of aptamer complementary element bases causes enough disruption to allow the AT to continuously undergo conformational changes. It is not yet fully understood what causes induced fit and the conformational selection pathway is not totally ruled out either. A deeper study of the AT binding process and mechanism will be needed in the future to fully answer the question of bimolecular mechanism.

Another aspect of the binding mechanism that is not currently explored in our study is the cooperativity of the adenosine aptamer binding sites. Since the adenosine aptamer contains two binding sites, it is possible that aptamer-ligand binding occurs in two conformational steps, and it is even more probable that one step will affect the favorability of the second step. Hence, cooperativity between binding sites might play a key role in the overall function of the AT. Future studies should aim to explore the influence of cooperativity of aptamer-ligand binding within the AT and attempt to elucidate the exact intermediate steps necessary to fully understand the binding process.

4.2.2 AT Kinetics Model Refinement

We suggest further work be done on improving the AT kinetics model we derived in Chapter 3 and Appendix B for the time-dependence of the kinetic reaction rate for ATs. The current kinetics model was useful in extracting a strand displacement rate constant, k_1 , and an effective dissociation constant K_d for ATs by fitting to sample data. However, there were many assumptions that were used in order to simplify the model, which may have led to under predictions or over predictions of the reaction network kinetics.

One major assumption that is made in the current model is that the concentration of several of the network components, i.e., the fuel strands and adenosine concentration, are held constant throughout the experiment. This was assumed since the fuel and adenosine concentrations are much greater than the AT complex at 10 nM, 300 nM and $\geq 2\mu\text{M}$, respectively. It might be possible that even small changes in the excess concentration of fuel and adenosine could contribute to noticeable changes in the model

since the adenosine aptamer is sensitive to the even minute changes in the concentration at its upper and lower bounds of the response curve.

Another assumption that was made was that the aptamer could be modeled with mutually exclusive binding sites that had no cooperativity. For simplicity, the initial model used only a single binding site, while it is known that the adenosine aptamer has two binding sites. In order to fully model the behavior of the AT, it will be imperative to study how cooperativity could contribute to the biosensor's activation. Including a Hill coefficient in the final model may yield a better result from the data extraction and may reveal that a difference in cooperativity between the two binding sites exists. If these models were explored in depth, it may yield better insight into the overall operation of the AT.

The AT is also thought to equilibrate quickly enough to assume that it had reached an equilibrium between the activated ATs and inactivated AT complexes before the strand displacement reaction occurs. However, this assumption about the basic functioning of the AT could be flawed, and the AT may be reacting in parallel to the aptamer-ligand binding process. This would require further exploration of the kinetics model and could include deriving a more generalized model that makes no assumptions about the overall speed of the reactions steps and instead assumes each reaction step occurs on a very similar time scale.

4.2.3 Market Analysis of AT Sensors

An in-depth market analysis of the ATs in industry would also make a good topic for future studies. Specifically, one where the ATs are shown to be incorporated into a paper-based biosensor that could be mass produced and provided to consumers at a low-

cost would be ideal for improving the world health outlook in the area of disease diagnosis. A quick “back of the bar napkin” approach to cost analysis reveals that the current ATs could be manufactured for a cost as little as \$0.60 per biosensing paper test. This estimate assumes that the sensor could be manufactured with a sample at 10 μL containing a roughly 10 μM ATs. This was calculated based on it costing about \$300 to order all the necessary components to manufacture a single AT system from IDT to produce roughly 5 mL of stock solution after the necessary purification steps. This cost could be further reduced by potentially synthesizing the DNA in house or functionalizing the DNA with a different Dye/Quencher setup, which accounts for most of the IDT cost of manufacturing. Overall, the AT biosensor could be a cost-effective solution in developing functional biosensor for use in everyday diagnostics.

4.2.4 AT Redesign: Incorporating other Aptamers

Exploration of the AT framework's potential in accommodating other aptamer sequences can have far-reaching implications in biomedical applications, especially the development of biosensors. A comprehensive understanding of the AT α domain's customizability can provide critical insights into the generalizability of aptamer-based structure-switching designs, thereby paving the way for future research. Thus, it is imperative that researchers thoroughly evaluate the potential of the AT framework in accommodating diverse aptamer sequences and investigate this avenue in future studies.

While we have shown the utility of customizable AT output domains, λ and μ , to initiate downstream reactions and have explored the underlying kinetics and biophysics of modifying the aptamer complementary element domain involved in structure switching, we have not shown that the AT framework can accommodate other aptamer

sequences into its structure-switching design.¹ Therefore, the next logical step in the future of this research involves demonstrating that the AT can incorporate other aptamers without significant design modifications to the AT framework.

One of the aptamer sequences that has exhibited considerable promise in the context of a structure-switching design is the thrombin-binding DNA aptamer (TBA).²⁻¹⁷ TBA binds to Exosite I on the surface of Human Alpha Thrombin, a protein that is crucial for the coagulation cascade in the human body during injury.²⁻¹⁹ TBA undergoes a conformational change to form a stacked G-quadruplex structure, which subsequently accommodates protein binding. The structure-switching of the TBA can produce the necessary conformational change needed to dehybridize an ACE via an induced fit mechanism, which could be easily incorporated into the AT framework, as has also been previously reported for the adenosine binding aptamer from our studies.¹⁻¹⁹ TBA is an ideal candidate for studying the customizability of the AT aptamer domain due to its high sensitivity and specificity in detecting thrombin. This is also why TBA has been widely used in previous biosensor studies.²⁻¹⁷

Future studies should consider replacing the adenosine aptamer with the thrombin aptamer in the AT network and evaluating its effectiveness as a biosensor. The researchers should also select several ACEs from the ACE-scan results in previous studies and optimize the structure-switching domain for a thrombin binding AT network.^{1,20,21} Using ACE-scan results from literature for both the adenosine and thrombin aptamer will further validate the efficacy of using ACE-scan as rapid ACE selection method for the development of ATs and for exploring the kinetic behavior of aptamer biosensors.^{20,20-23} This research will also provide a means of discovering the

effect of different τ' domains on the overall AT network performance in each case.¹ Results from such studies would validate that the AT is capable of being used as a more generalized framework for nucleic acid circuits, having the capacity to be customizable in both its input and output domains.^{10,13,21} Furthermore, developing an AT that targets thrombin will demonstrate that the AT can be useful for detecting both small molecules and macromolecules.

In addition to the TBA, future studies should aim to incorporate other aptamers into the AT framework. Other aptamers that undergo structure-switching have the greatest likelihood of successful AT integration. One promising candidate is the DNA aptamer that binds to immunoglobulin E (IgE), a protein involved in allergic reactions.^{24–32} This aptamer has demonstrated high affinity and specificity for IgE and has potential applications in the development of diagnostic tools and therapies for allergies.^{24–32} Other aptamers that could be considered for AT integration include the DNA aptamer that binds to the HIV-1 reverse transcriptase (HIV-1RT), and the DNA aptamer that binds to cocaine.^{20,21,33–50} The HIV-1RT aptamer binds to the reverse transcriptase enzyme of the HIV-1 virus, which plays an essential role in the replication of the viral genome, making it a potential candidate for the development of therapeutic agents.^{33–39} The cocaine aptamer, on the other hand, has potential applications in drug screening and detection, as it binds to cocaine with high specificity and affinity.^{40–50} These aptamers have been previously incorporated into structure-switching designs and have demonstrated the ability to initiate downstream reactions. Thus, future studies should focus on incorporating aptamers such as these into the AT framework without significant modifications to the AT design.

4.2.5 Multiplexing ATs

In future studies, the optimization of adenosine and thrombin aptamers can be explored to design a biosensing reaction network that can detect multiple analytes simultaneously.^{1,5,7,9,10,13,16,21,51,52} The most optimal ATs selected from previous studies can be used to guide the experimental conditions for multiplexing, which will involve stoichiometrically mixing the ATs in a single solution and testing their kinetic response. Here, we provide suggested multiplexing formats for two aptamers, namely the adenosine and thrombin, which could be multiplexed into a single solution sensor after first optimizing their respective ATs individually. Additionally, the ATs we show in a suggested multiplexing study are designed to target FRET reporters in both concurrent and consecutive formats.

To test DNA signals concurrently, the adenosine and thrombin ATs are shown to target two separate reporters in solution as illustrated in Figure 4.1. Each of the two reporters would be dye and quencher labeled with different fluorophores that possess different emission wavelengths. The separate fluorescence signals will be detected by fluorescence spectrophotometry in scanning mode with multiple measurements taken throughout the reaction time to obtain kinetic data. We expect that the simultaneous reaction of adenosine and thrombin ATs would produce a spectrum with two overlapping peaks that are proportional to the response of the individual ATs with a maximum peak height corresponding to both the reaction time and the amount of ligand added.

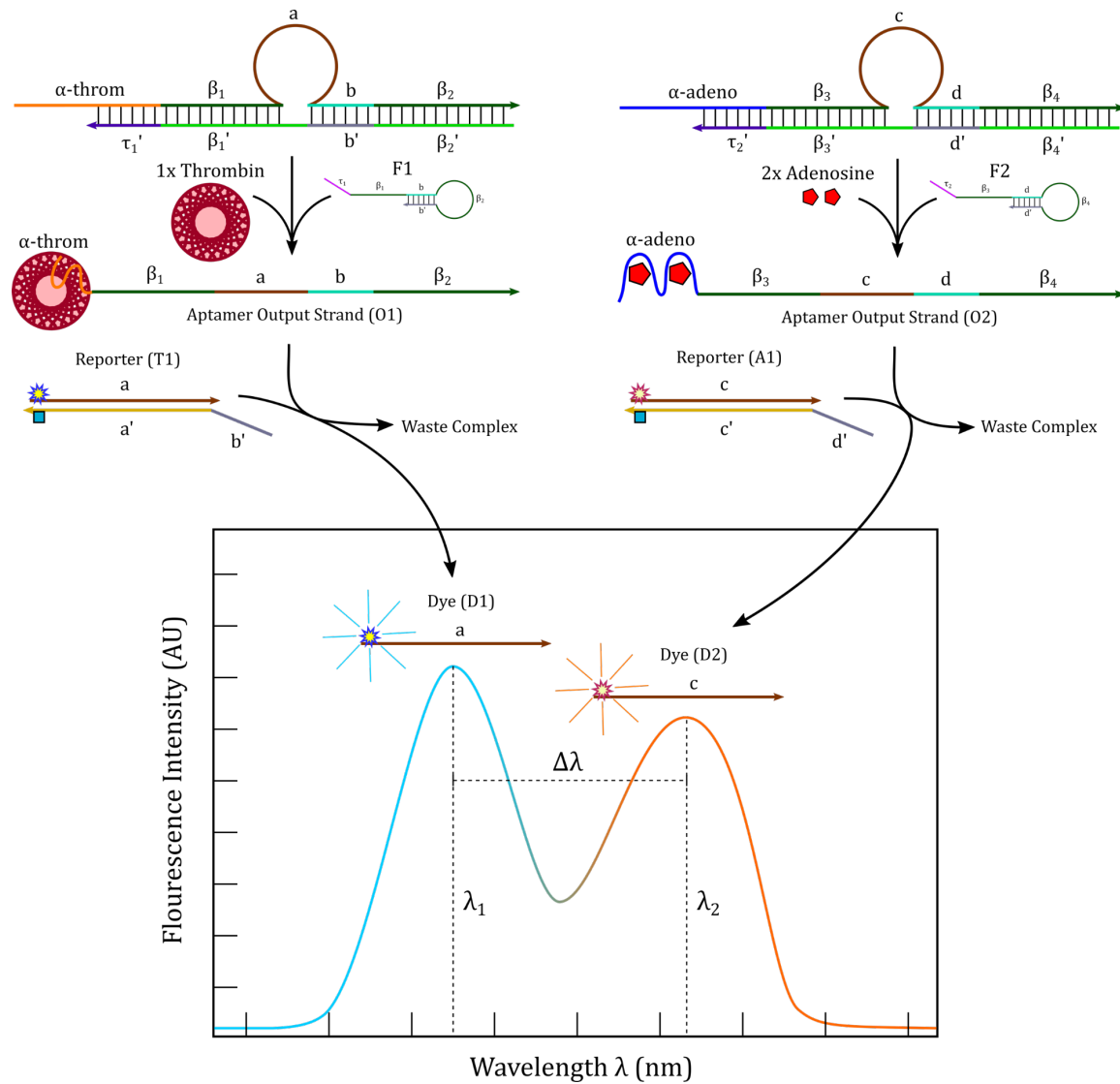


Figure 4.1: A concurrent mode for two multiplexed ATs designed to simultaneously sense adenosine and thrombin in a single solution each utilizing their own unique output domains to trigger two separate FRET reporters with different fluorescence emission wavelengths. Fluorescence measurements in scan mode are predicted to reveal two emission peaks separated by the fluorophores' maximum emission intensities, $\Delta\lambda$.

After testing the simultaneous detection of analytes, a consecutive method for detection should be investigated as shown in Figure 4.2. Both adenosine and thrombin ATs would be developed to target the same reporter sequence using a single FRET pair. In order to test a stepwise reaction, all network components would be added to a single solution except for the two distinct AT fuels, one for the adenosine AT complex and the other for thrombin AT complex. Fuels should be added to the solution one at a time with a time-delay, Δt , optimally waiting until the initial AT reaction has gone to completion. In this way, the response of each ligand could be measured individually from the same solution using only a single reporter. An advantage of this approach is that by withholding the fuel strands until the reaction start time, leakage signal should not occur in the AT network prior to sensing, making this approach the more stable of the two.

Incorporating multiple ATs in solution may pose significant challenges for the aforementioned research, including introducing additional network leakage pathways and a greater likelihood of crosstalk interactions between complexes. The aptamer structure-switching mechanisms in each case may also be hindered, and the ATs may not be selective enough to be multiplexed, leading to potential cross-reactivity issues. If selectivity issues arise, an in-depth analysis of the selectivity of each AT may be required, and additional study of the AT complexes' role in this behavior may be necessary. If crosstalk interactions are present, it could significantly slow down the overall reaction rate, requiring a redesign of the AT network to reduce crosstalk. Another challenge that may arise is the leakage of one or the other networks due to the incorporation of two different fuels and two AT complexes that may cross-react. To reduce this likelihood, domain sequences could be randomized on the AT backbone to

ensure specificity. In addition, it will be necessary to optimize the delay between reaction start times to distinguish AT output signals between adenosine and thrombin in the consecutive multiplexing format. Finally, finding two FRET reporters with adequate separation in emission wavelength will be necessary to distinguish separate AT signals by the multiplexed sensor in the concurrent format.

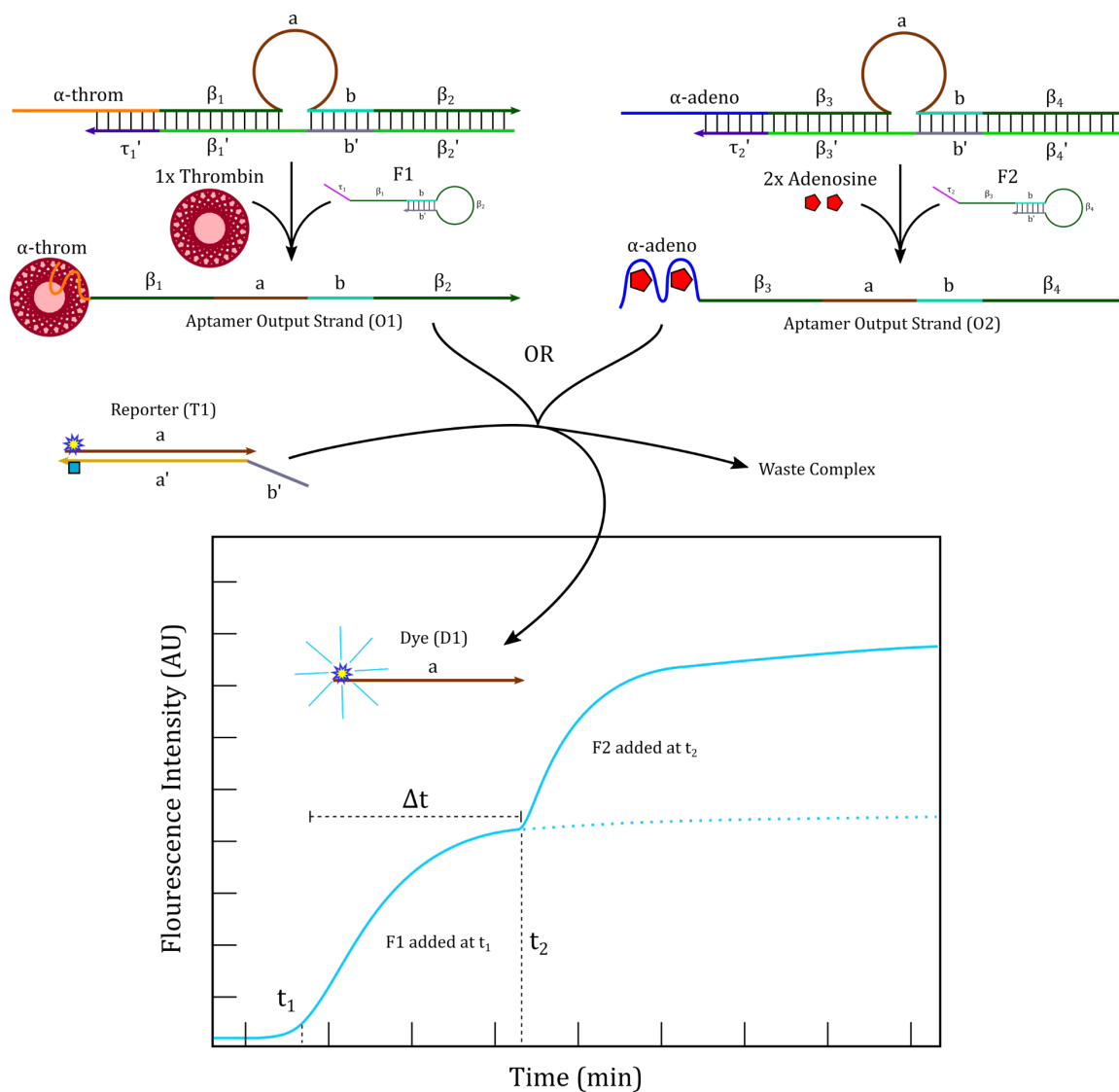


Figure 4.2: A consecutive mode for two multiplexed ATs designed to sense adenosine and thrombin in a single solution reacting at a set time interval Δt . At time t_1 fuel F1 is added to solution, reacting until near completion, providing a response due to the presence of thrombin. At time t_2 fuel F2 is added causing the reaction to continue, with a response due to the presence of adenosine, until output strands are O1 and O2 are depleted. The fluorescence intensity plot is predicted to be a single stair-stepped kinetics trace with a response for each step consistent with the aptamer sensing and strand displacement of each individual AT.

4.2.6 Signal Processing with Multiplexed ATs

It was shown previously that ATs can be used to initiate feed-forward catalytic amplification networks.¹ However, multiplexed ATs initiating feed-forward networks have not been shown. Here, we suggest that future research aim to add further complexity to our multiplexed biosensor by adding intermediate networks prior to FRET signal detection for the detection of adenosine and thrombin. Both catalytic amplification networks designed by Zhang et al. and Kotani et al. could be used to amplify AT signals prior to reporting (Figure 4.3A) in a time-delayed consecutive format, discussed previously in section 4.2.2.⁵³⁻⁵⁵ The multiplexed ATs would then be shown to react in a concurrent format with the addition of an AND gate shown in Figure 4.3B, which is based on the gate published by Zhang and Seelig seen in Figure 4.4C, which requires both adenosine and thrombin ATs to produce an output strand before the gate complex releases a strand triggering a FRET reporter.⁵⁶ In the same concurrent format, the multiplexed ATs would be reacted with an OR gate. Finally, a combination of gates will be tested along with an amplification network to show the use of ATs in a multilayered strand displacement cascade.

The benefits of adding complexity to the multiplexed biosensor by incorporating intermediate networks and gates prior to FRET signal detection are numerous. First, this research could provide a more sensitive and specific detection of adenosine and thrombin by amplifying the AT signals prior to reporting, using catalytic amplification networks. Additionally, the use of an AND gate would ensure that both adenosine and thrombin ATs are present before releasing a strand that triggers a FRET reporter, improving the selectivity of the final multiplexed biosensor. Using DNA logic gates in this way would

show that multiplexed AT systems could undergo multiple levels of signal processing allowing for “smart” biosensing functionality developed within a single-solution. Finally, by testing a combination of gates along with an amplification network, this research could demonstrate the use of ATs in a multilayered strand displacement cascade, paving the way for the development of more complex biosensors.

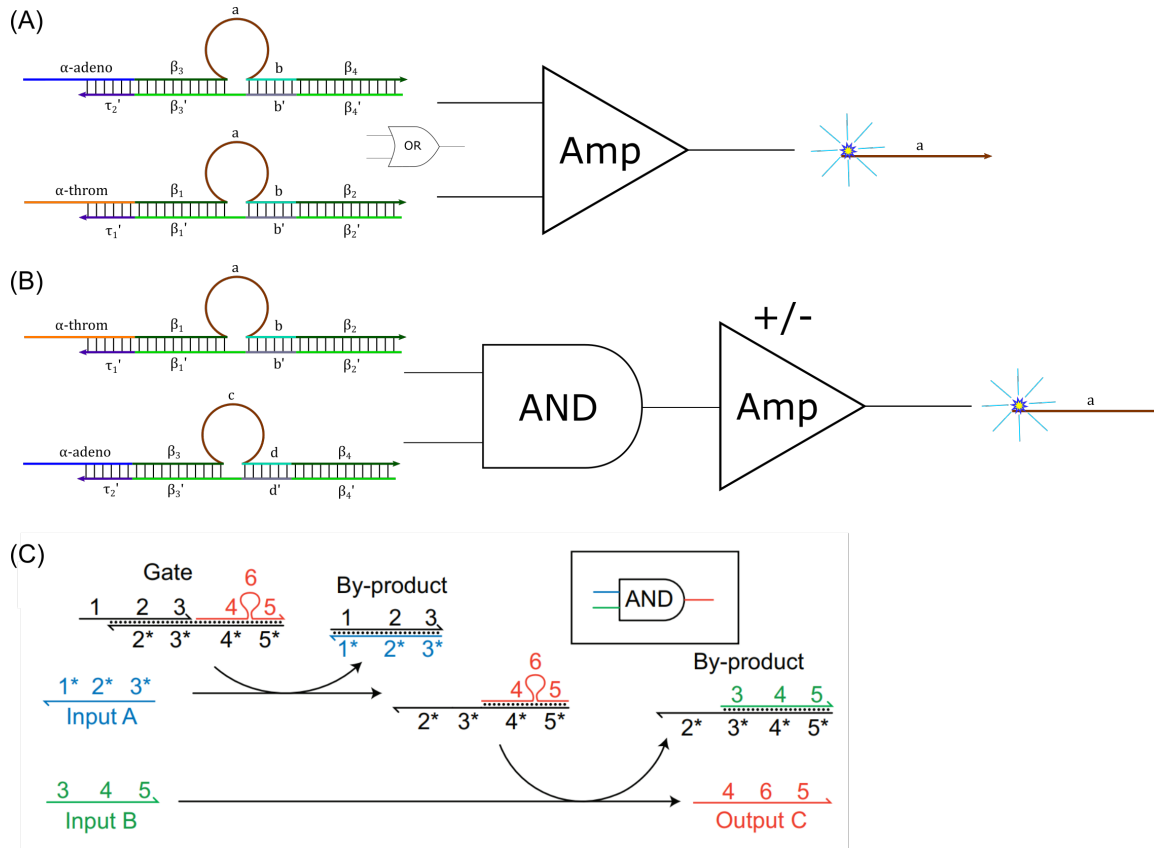


Figure 4.3: (A) Multiplexed ATs reacted in a consecutive format where the a and b domains from each AT are fed-forward into an amplification reaction network. The transduction step in this format can be represented by a logical OR operation since either AT reaction will produce an output signal prior to amplification. (B) Multiplexed ATs reacted in a concurrent format where output domains are unique fed into a logical AND gate displacement network with or without (+/-) the presence of an Amplification reaction network. (C) Logical AND gate operation based on work by Zhang and Seelig.⁵⁶

4.3 Final Remarks

Our aim in these studies has been to provide a generalizable DNA biosensor design wherein both the input and output of the device are customizable to be easily incorporated into applicable technologies for sensing within the medical, environmental, food-safety, and hazard detection fields. By providing an AT framework, we have anticipated to provide the means for researchers to rapidly develop new sensors by intuitive incorporation of ATs with other reaction network functionality or with the use of other aptamers. By developing such an AT framework, industries may one day be able to manufacture a sensor that utilizes our network designs and/or use our design to inspire new dynamic DNA nanotechnology to construct improved sensor functionality. Devices made from such AT designs may improve the standard of living of many societies by providing more rapid or accessible tests, which would typically require more expensive equipment or expertise and are therefore a worthwhile research pursuit. We hope that future research will explore and optimize the performance of our AT framework and adapt it to specific applications within various fields. This can involve modifying the input aptamers to detect different target molecules, incorporating new signal amplification strategies to enhance the sensitivity and specificity of the biosensors, or integrate the biosensor with other technologies to enable multiplexed detection.

Additionally, further research could focus on characterizing the stability and robustness of our AT-based biosensors in different environments and under various conditions, such as in the presence of interfering substances or at different temperatures and pH levels. This can help to identify potential limitations and challenges in the

practical application of these biosensors and inform the development of improved designs.

Finally, it would be valuable to explore the scalability and cost-effectiveness of our biosensor designs, with the aim of making them more accessible and affordable for widespread use. This could involve optimizing the manufacturing process or exploring alternative materials and fabrication methods to reduce the cost and increase production efficiency.

Overall, we believe that the development and optimization of our AT-based biosensor designs have significant potential to contribute to the advancement of various fields and benefit society as a whole.

4.4 References

- (1) Hachigian, T.; Lysne, D.; Graugnard, E.; Lee, J. Customizable Aptamer Transducer Network Designed for Feed-Forward Coupling. *ACS Omega* **2021**, *6* (41), 26888–26896. <https://doi.org/10.1021/acsomega.1c03146>.
- (2) Wang, K. Y.; McCurdy, S.; Shea, R. G.; Swaminathan, S.; Bolton, P. H. A DNA Aptamer Which Binds to and Inhibits Thrombin Exhibits a New Structural Motif for DNA. *Biochemistry* **1993**, *32* (8), 1899–1904. <https://doi.org/10.1021/bi00059a003>.
- (3) Wang, K.; Liao, J.; Yang, X.; Zhao, M.; Chen, M.; Yao, W.; Tan, W.; Lan, X. A Label-Free Aptasensor for Highly Sensitive Detection of ATP and Thrombin Based on Metal-Enhanced PicoGreen Fluorescence. *Biosensors and Bioelectronics* **2015**, *63*, 172–177. <https://doi.org/10.1016/j.bios.2014.07.022>.
- (4) Rong, X.; Zhang, H.; Cai, W.; Luo, F.; Lin, C.; Qiu, B.; Lin, Z.; Wang, J.; Jiang, Z.; Huang, H. A Label-Free Thrombin Photoelectrochemical Aptasensor Based on Structure-Switching in G-Quadruplexes. *Biosensors and Bioelectronics: X* **2022**, *11*, 100159. <https://doi.org/10.1016/j.biosx.2022.100159>.
- (5) Yang, H.; Ji, J.; Liu, Y.; Kong, J.; Liu, B. An Aptamer-Based Biosensor for Sensitive Thrombin Detection. *Electrochemistry Communications* **2009**, *11* (1), 38–40. <https://doi.org/10.1016/j.elecom.2008.10.024>.
- (6) Zhang, Z.; Mei, M.; Yao, J.; Ye, T.; Quan, J.; Liu, J. An off/on Thrombin Activated Energy Driven Molecular Machine for Sensitive Detection of Human Thrombin via Non-Enzymatic Catalyst Recycling Amplification. *Analyst* **2020**, *145* (21), 6868–6874. <https://doi.org/10.1039/D0AN01054E>.
- (7) Seok Kim, Y.; Ahmad Raston, N. H.; Bock Gu, M. Aptamer-Based Nanobiosensors. *Biosensors and Bioelectronics* **2016**, *76*, 2–19. <https://doi.org/10.1016/j.bios.2015.06.040>.

- (8) Mao, Y.; Liu, J.; He, D.; He, X.; Wang, K.; Shi, H.; Wen, L. Aptamer/Target Binding-Induced Triple Helix Forming for Signal-on Electrochemical Biosensing. *Talanta* **2015**, *143*, 381–387. <https://doi.org/10.1016/j.talanta.2015.05.009>.
- (9) Fortunati, S.; Pedrini, F.; Del Grosso, E.; Baranda Pellejero, L.; Bertucci, A. Design of Specific Nucleic Acid-Based Biosensors for Protein Binding Activity. *Analysis & Sensing* **2022**, *2* (6), e202200037. <https://doi.org/10.1002/anse.202200037>.
- (10) Yoo, H.; Jo, H.; Soo Oh, S. Detection and beyond: Challenges and Advances in Aptamer-Based Biosensors. *Materials Advances* **2020**, *1* (8), 2663–2687. <https://doi.org/10.1039/D0MA00639D>.
- (11) Na, W.; Liu, X.; Wang, L.; Su, X. Label-Free Aptamer Biosensor for Selective Detection of Thrombin. *Analytica Chimica Acta* **2015**, *899*, 85–90. <https://doi.org/10.1016/j.aca.2015.09.051>.
- (12) Yun, W.; Li, N.; Wang, R.; Yang, L.; Chen, L.; Tang, Y. Proximity Ligation Assay Induced Hairpin to DNzyme Structure Switching for Entropy-Driven Amplified Detection of Thrombin. *Analytica Chimica Acta* **2019**, *1064*, 104–111. <https://doi.org/10.1016/j.aca.2019.03.007>.
- (13) Feagin, T. A.; Maganzini, N.; Soh, H. T. Strategies for Creating Structure-Switching Aptamers. *ACS Sens.* **2018**, *3* (9), 1611–1615. <https://doi.org/10.1021/acssensors.8b00516>.
- (14) Li, J.; Wang, S.; Jiang, B.; Xiang, Y.; Yuan, R. Target-Induced Structure Switching of Aptamers Facilitates Strand Displacement for DNzyme Recycling Amplification Detection of Thrombin in Human Serum. *Analyst* **2019**, *144* (7), 2430–2435. <https://doi.org/10.1039/C9AN00030E>.
- (15) Yang, J.; Wu, Y.; Gan, C.; Yuan, R.; Xiang, Y. Target-Programmed and Autonomous Proximity Binding Aptasensor for Amplified Electronic Detection of Thrombin. *Biosensors and Bioelectronics* **2018**, *117*, 743–747. <https://doi.org/10.1016/j.bios.2018.06.069>.

- (16) Griffin, L. C.; Toole, J. J.; Leung, L. L. K. The Discovery and Characterization of a Novel Nucleotide-Based Thrombin Inhibitor. *Gene* **1993**, *137* (1), 25–31. [https://doi.org/10.1016/0378-1119\(93\)90247-Z](https://doi.org/10.1016/0378-1119(93)90247-Z).
- (17) Xu, Y.; Zhou, W.; Zhou, M.; Xiang, Y.; Yuan, R.; Chai, Y. Toehold Strand Displacement-Driven Assembly of G-Quadruplex DNA for Enzyme-Free and Non-Label Sensitive Fluorescent Detection of Thrombin. *Biosensors and Bioelectronics* **2015**, *64*, 306–310. <https://doi.org/10.1016/j.bios.2014.09.018>.
- (18) Paborsky, L. R.; McCurdy, S. N.; Griffin, L. C.; Toole, J. J.; Leung, L. L. The Single-Stranded DNA Aptamer-Binding Site of Human Thrombin. *Journal of Biological Chemistry* **1993**, *268* (28), 20808–20811. [https://doi.org/10.1016/S0021-9258\(19\)36856-5](https://doi.org/10.1016/S0021-9258(19)36856-5).
- (19) Russo Krauss, I.; Merlino, A.; Giancola, C.; Randazzo, A.; Mazzarella, L.; Sica, F. Thrombin–Aptamer Recognition: A Revealed Ambiguity. *Nucleic Acids Research* **2011**, *39* (17), 7858–7867. <https://doi.org/10.1093/nar/gkr522>.
- (20) Munzar J. D.; Ng, A.; Juncker, D. Comprehensive Profiling of the Ligand Binding Landscapes of Duplexed Aptamer Families Reveals Widespread Induced Fit. *Nature Communications* **2018**, *9* (1), 343. <https://doi.org/10.1038/s41467-017-02556-3>.
- (21) Munzar J. D.; Ng, A.; Juncker, D. Duplexed Aptamers: History, Design, Theory, and Application to Biosensing. *Chemical Society reviews* **2019**, *48* (5), 1390–1419. <https://doi.org/10.1039/c8cs00880a>.
- (22) Zhao, Y.; Yavari, K.; Liu, J. Critical Evaluation of Aptamer Binding for Biosensor Designs. *TrAC Trends in Analytical Chemistry* **2022**, *146*, 116480. <https://doi.org/10.1016/j.trac.2021.116480>.
- (23) Zhang, Z.; Oni, O.; Liu, J. New Insights into a Classic Aptamer: Binding Sites, Cooperativity and More Sensitive Adenosine Detection. *Nucleic Acids Research* **2017**, *45* (13), 7593–7601. <https://doi.org/10.1093/nar/gkx517>.
- (24) Han, K.; Liang, Z.; Zhou, N. Design Strategies for Aptamer-Based Biosensors. *Sensors* **2010**, *10* (5), 4541–4557. <https://doi.org/10.3390/s100504541>.

- (25) He, J.-L.; Wu, Z.-S.; Zhang, S.-B.; Shen, G.-L.; Yu, R.-Q. Novel Fluorescence Enhancement IgE Assay Using a DNA Aptamer. *Analyst* **2009**, *134* (5), 1003–1007. <https://doi.org/10.1039/B812450G>.
- (26) He, M.; Shang, N.; Zhu, Q.; Xu, J. Paper-Based Upconversion Fluorescence Aptasensor for the Quantitative Detection of Immunoglobulin E in Human Serum. *Analytica Chimica Acta* **2021**, *1143*, 93–100. <https://doi.org/10.1016/j.aca.2020.11.036>.
- (27) Jiang, Y.; Fang, X.; Bai, C. Signaling Aptamer/Protein Binding by a Molecular Light Switch Complex. *Anal. Chem.* **2004**, *76* (17), 5230–5235. <https://doi.org/10.1021/ac049565u>.
- (28) Jiang, Y.; Zhu, C.; Ling, L.; Wan, L.; Fang, X.; Bai, C. Specific Aptamer–Protein Interaction Studied by Atomic Force Microscopy. *Anal. Chem.* **2003**, *75* (9), 2112–2116. <https://doi.org/10.1021/ac026182s>.
- (29) Strehlitz, B.; Nikolaus, N.; Stoltenburg, R. Protein Detection with Aptamer Biosensors. *Sensors* **2008**, *8* (7), 4296–4307. <https://doi.org/10.3390/s8074296>.
- (30) Tombelli, S.; Minunni, M.; Mascini, M. Analytical Applications of Aptamers. *Biosensors and Bioelectronics* **2005**, *20* (12), 2424–2434. <https://doi.org/10.1016/j.bios.2004.11.006>.
- (31) Wu, Z.-S.; Zheng, F.; Shen, G.-L.; Yu, R.-Q. A Hairpin Aptamer-Based Electrochemical Biosensing Platform for the Sensitive Detection of Proteins. *Biomaterials* **2009**, *30* (15), 2950–2955. <https://doi.org/10.1016/j.biomaterials.2009.02.017>.
- (32) Zhang, H.; Li, F.; Dever, B.; Li, X.-F.; Le, X. C. DNA-Mediated Homogeneous Binding Assays for Nucleic Acids and Proteins. *Chem. Rev.* **2013**, *113* (4), 2812–2841. <https://doi.org/10.1021/cr300340p>.
- (33) Wang, Y.-X.; Ye, Z.-Z.; Si, C.-Y.; Ying, Y.-B. Application of Aptamer Based Biosensors for Detection of Pathogenic Microorganisms. *Chinese Journal of Analytical Chemistry* **2012**, *40* (4), 634–642. [https://doi.org/10.1016/S1872-2040\(11\)60542-2](https://doi.org/10.1016/S1872-2040(11)60542-2).

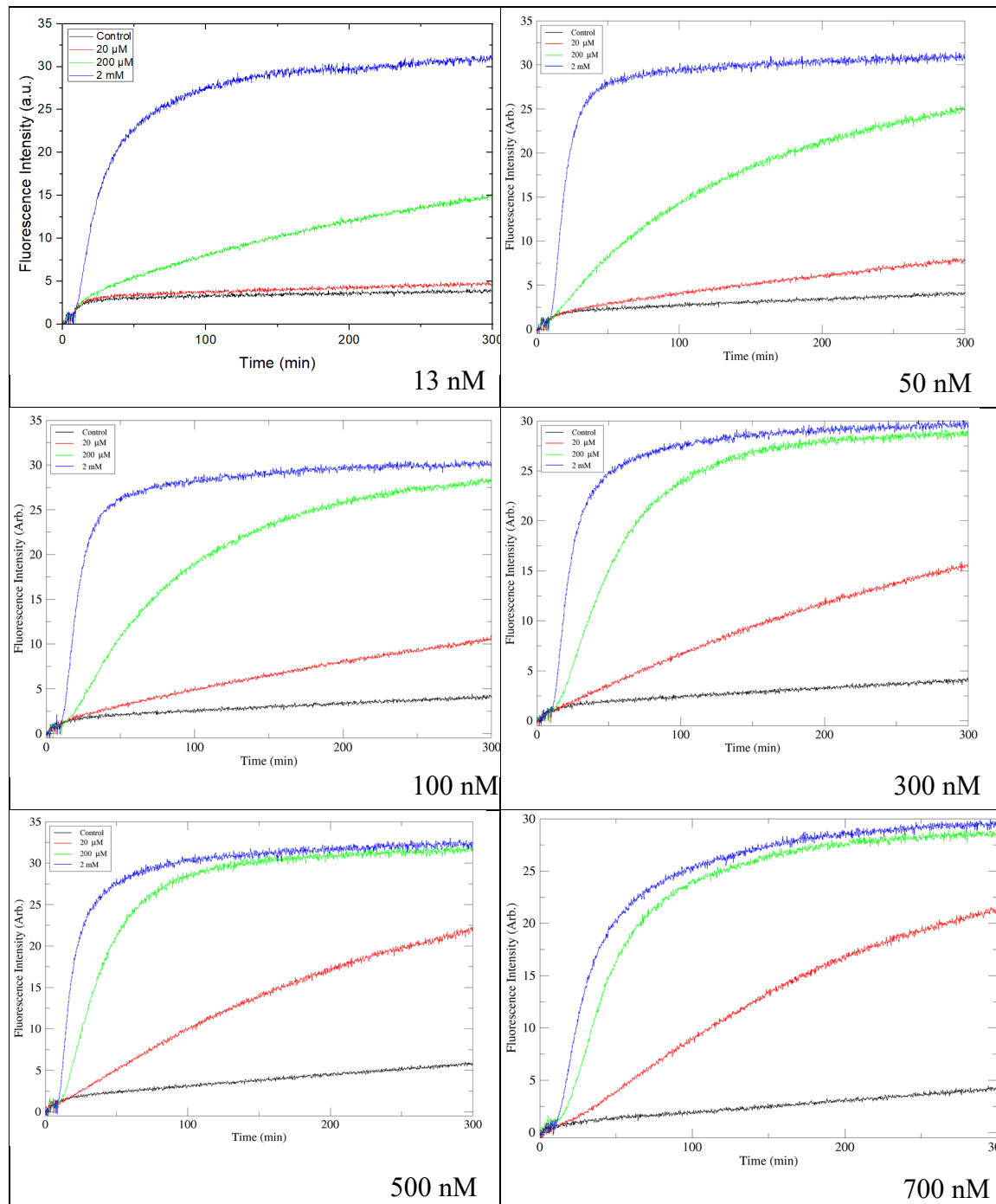
- (34) Tuske, S.; Zheng, J.; Olson, E. D.; Ruiz, F. X.; Pascal, B. D.; Hoang, A.; Bauman, J. D.; Das, K.; DeStefano, J. J.; Musier-Forsyth, K.; Griffin, P. R.; Arnold, E. Integrative Structural Biology Studies of HIV-1 Reverse Transcriptase Binding to a High-Affinity DNA Aptamer. *Current Research in Structural Biology* **2020**, *2*, 116–129. <https://doi.org/10.1016/j.crstbi.2020.06.002>.
- (35) Ning, Y.; Hu, J.; Lu, F. Aptamers Used for Biosensors and Targeted Therapy. *Biomedicine & Pharmacotherapy* **2020**, *132*, 110902. <https://doi.org/10.1016/j.biopha.2020.110902>.
- (36) Lou, B.; Liu, Y.; Shi, M.; Chen, J.; Li, K.; Tan, Y.; Chen, L.; Wu, Y.; Wang, T.; Liu, X.; Jiang, T.; Peng, D.; Liu, Z. Aptamer-Based Biosensors for Virus Protein Detection. *TrAC Trends in Analytical Chemistry* **2022**, *157*, 116738. <https://doi.org/10.1016/j.trac.2022.116738>.
- (37) Liang, Y.; Zhang, Z.; Wei, H.; Hu, Q.; Deng, J.; Guo, D.; Cui, Z.; Zhang, X.-E. Aptamer Beacons for Visualization of Endogenous Protein HIV-1 Reverse Transcriptase in Living Cells. *Biosensors and Bioelectronics* **2011**, *28* (1), 270–276. <https://doi.org/10.1016/j.bios.2011.07.031>.
- (38) DeStefano, J. J.; Nair, G. R. Novel Aptamer Inhibitors of Human Immunodeficiency Virus Reverse Transcriptase. *Oligonucleotides* **2008**, *18* (2), 133–144. <https://doi.org/10.1089/oli.2008.0103>.
- (39) Bala, J.; Chinnapaiyan, S.; Dutta, R. K.; Unwalla, H. Aptamers in HIV Research Diagnosis and Therapy. *RNA Biology* **2018**, *15* (3), 327–337. <https://doi.org/10.1080/15476286.2017.1414131>.
- (40) Zhang, S.; Wang, L.; Liu, M.; Qiu, Y.; Wang, M.; Liu, X.; Shen, G.; Yu, R. A Novel, Label-Free Fluorescent Aptasensor for Cocaine Detection Based on a G-Quadruplex and Ruthenium Polypyridyl Complex Molecular Light Switch. *Anal. Methods* **2016**, *8* (18), 3740–3746. <https://doi.org/10.1039/C6AY00231E>.
- (41) Vallée-Bélisle, A.; Plaxco, K. W. Structure-Switching Biosensors: Inspired by Nature. *Current Opinion in Structural Biology* **2010**, *20* (4), 518–526. <https://doi.org/10.1016/j.sbi.2010.05.001>.

- (42) Soni, S.; Jain, U.; Burke, D. H.; Chauhan, N. Recent Trends and Emerging Strategies for Aptasensing Technologies for Illicit Drugs Detection. *Journal of Electroanalytical Chemistry* **2022**, *910*, 116128. <https://doi.org/10.1016/j.jelechem.2022.116128>.
- (43) Simmel, F. C.; Yurke, B.; Singh, H. R. Principles and Applications of Nucleic Acid Strand Displacement Reactions. *Chem. Rev.* **2019**, *119* (10), 6326–6369. <https://doi.org/10.1021/acs.chemrev.8b00580>.
- (44) Shoara, A. A.; Reinstein, O.; Borhani, O. A.; Martin, T. R.; Slavkovic, S.; Churcher, Z. R.; Johnson, P. E. Development of a Thermal-Stable Structure-Switching Cocaine-Binding Aptamer. *Biochimie* **2018**, *145*, 137–144. <https://doi.org/10.1016/j.biochi.2017.08.010>.
- (45) Shi, Y.; Dai, H.; Sun, Y.; Hu, J.; Ni, P.; Li, Z. Fluorescent Sensing of Cocaine Based on a Structure Switching Aptamer, Gold Nanoparticles and Graphene Oxide. *Analyst* **2013**, *138* (23), 7152–7156. <https://doi.org/10.1039/C3AN00897E>.
- (46) Rauf, S.; Zhang, L.; Ali, A.; Liu, Y.; Li, J. Label-Free Nanopore Biosensor for Rapid and Highly Sensitive Cocaine Detection in Complex Biological Fluids. *ACS Sens.* **2017**, *2* (2), 227–234. <https://doi.org/10.1021/acssensors.6b00627>.
- (47) Neves, M. A. D.; Shoara, A. A.; Reinstein, O.; Abbasi Borhani, O.; Martin, T. R.; Johnson, P. E. Optimizing Stem Length To Improve Ligand Selectivity in a Structure-Switching Cocaine-Binding Aptamer. *ACS Sens.* **2017**, *2* (10), 1539–1545. <https://doi.org/10.1021/acssensors.7b00619>.
- (48) Mao, K.; Ma, J.; Li, X.; Yang, Z. Rapid Duplexed Detection of Illicit Drugs in Wastewater Using Gold Nanoparticle Conjugated Aptamer Sensors. *Science of The Total Environment* **2019**, *688*, 771–779. <https://doi.org/10.1016/j.scitotenv.2019.06.325>.
- (49) Debiais, M.; Lelievre, A.; Smietana, M.; Müller, S. Splitting Aptamers and Nucleic Acid Enzymes for the Development of Advanced Biosensors. *Nucleic Acids Research* **2020**, *48* (7), 3400–3422. <https://doi.org/10.1093/nar/gkaa132>.

- (50) Alkhamis, O.; Canoura, J.; Yu, H.; Liu, Y.; Xiao, Y. Innovative Engineering and Sensing Strategies for Aptamer-Based Small-Molecule Detection. *TrAC Trends in Analytical Chemistry* **2019**, *121*, 115699. <https://doi.org/10.1016/j.trac.2019.115699>.
- (51) Huizenga, D. E.; Szostak, J. W. A DNA Aptamer That Binds Adenosine and ATP. *Biochemistry* **1995**, *34* (2), 656–665. <https://doi.org/10.1021/bi00002a033>.
- (52) Nakamura, I.; Shi A C; Nutiu, R.; Yu J M; Li, Y. Kinetics of Signaling-DNA-Aptamer-ATP Binding. *Physical review. E, Statistical, nonlinear, and soft matter physics* **2009**, *79* (3 Pt 1), 31906. <https://doi.org/10.1103/PhysRevE.79.031906>.
- (53) Kotani, S.; Hughes W L. Multi-Arm Junctions for Dynamic DNA Nanotechnology. *Journal of the American Chemical Society* **2017**, *139* (18), 6363–6368. <https://doi.org/10.1021/jacs.7b00530>.
- (54) Zhang, D. Y.; Turberfield, A. J.; Yurke, B.; Winfree, E. Engineering Entropy-Driven Reactions and Networks Catalyzed by DNA. *Science* **2007**, *318* (5853), 1121–1125. <https://doi.org/10.1126/science.1148532>.
- (55) Srinivas, N.; Ouldridge T E; Sulc, P.; Schaeffer J M; Yurke, B.; Louis A A; Doye J P; Winfree, E. On the Biophysics and Kinetics of Toehold-Mediated DNA Strand Displacement. *Nucleic acids research* **2013**, *41* (22), 10641–10658. <https://doi.org/10.1093/nar/gkt801>.
- (56) Zhang D. Y.; Seelig, G. Dynamic DNA Nanotechnology Using Strand-Displacement Reactions. *Nature chemistry* **2011**, *3* (2), 103–113. <https://doi.org/10.1038/nchem>.

APPENDIX A

**Supporting Information for “A Customizable Aptamer Transducer Network
Designed for Feed-Forward Coupling”**

S1. Optimization of AT-Fuel Concentration**Table A1: Kinetics traces for each fuel concentration in excess of the AT concentration of 10 nM used for optimization of the AT-fuel reaction, reported with KR.**

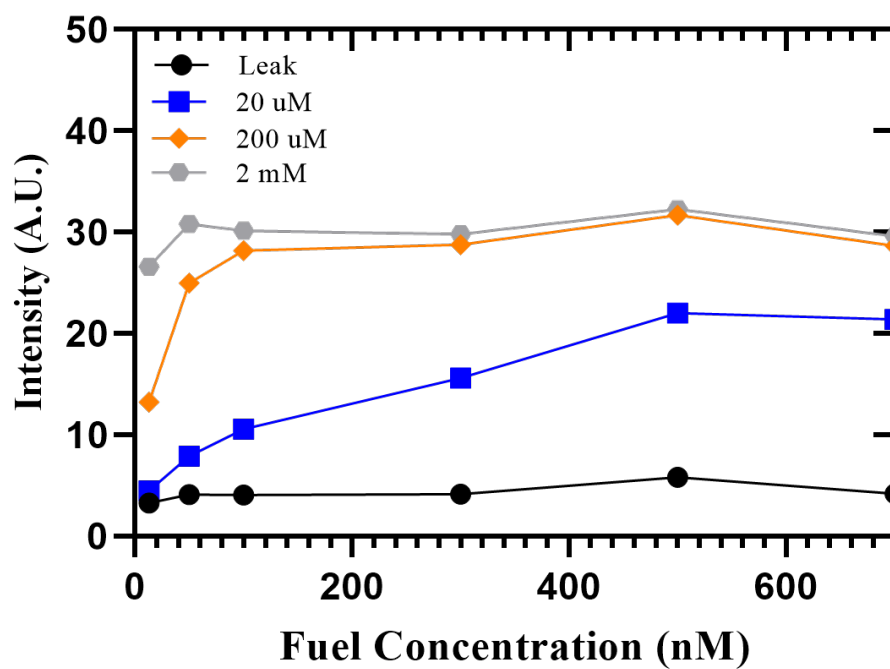
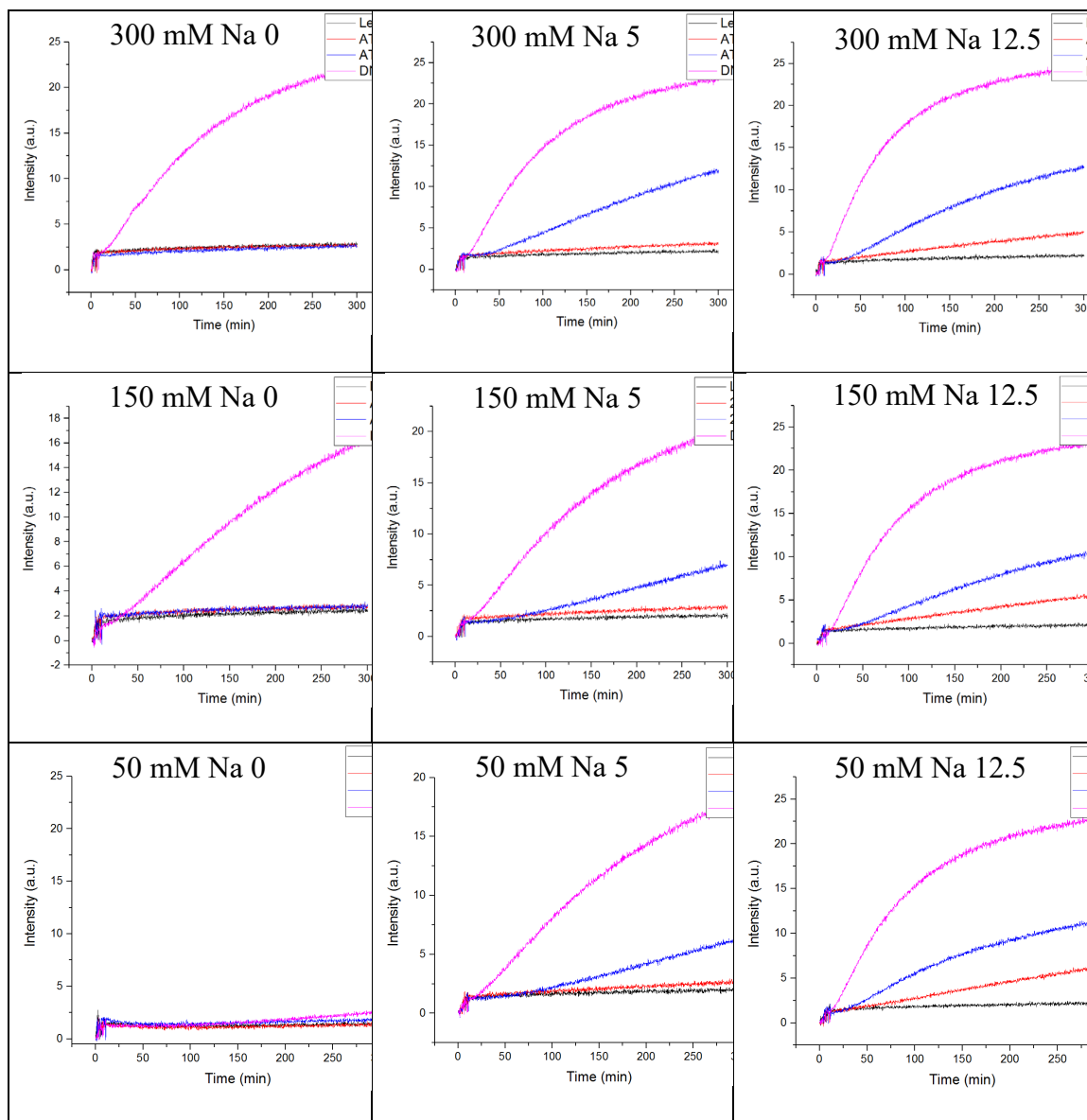


Figure A1: AT reacted with 13 nM to 700 nM AT-fuel using 20, 200, and 2000 μ M adenosine. Fluorescence intensities were measured after 300 minutes. 300 nM fuel was selected for excess fuel experiments since it had much greater intensity for 20 μ M adenosine and lower leak compared to 500 nM. Data is shown here without error bars intentionally as it was not triplicated and only used as a rapid approximation for the optimal AT fuel concentration.

S2. Optimization of AT Buffer Salt Concentration

Table A2: Kinetics traces for each Na and Mg buffer salt concentration using 13 nM AT-fuel for 200 μ M 2 mM adenosine and a DNA initiated AT using ZR. The signal of the AT was especially sensitive to Mg concentration and therefore a high Mg buffer (25 mM Mg 0 mM Na 1xTE) concentration was used for all further experiments.



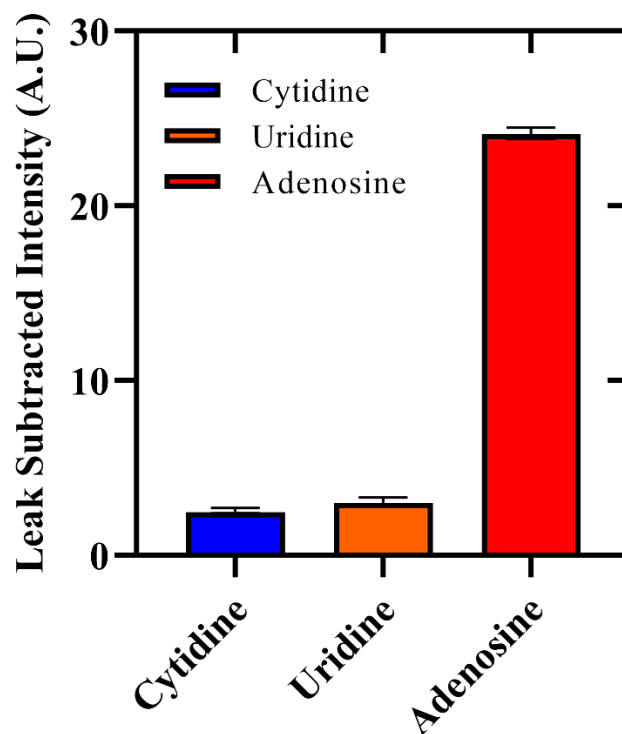
S3. Selectivity of AT targeting Adenosine

Figure A2. AT-ZR reacted with 2 mM Cytidine, Uridine, and Adenosine using 300 nM AT-fuel. Fluorescence intensities were measured after 24 hrs and subtracted by the AT network leakage measured at 24 hrs. The Adenosine intensity was 9.56x and 7.93x greater than the Cytidine and Uridine intensities respectively showing that the AT is selective to Adenosine.

S4. Strand Sequences for Aptamer Transducer and Catalytic Amplification networks

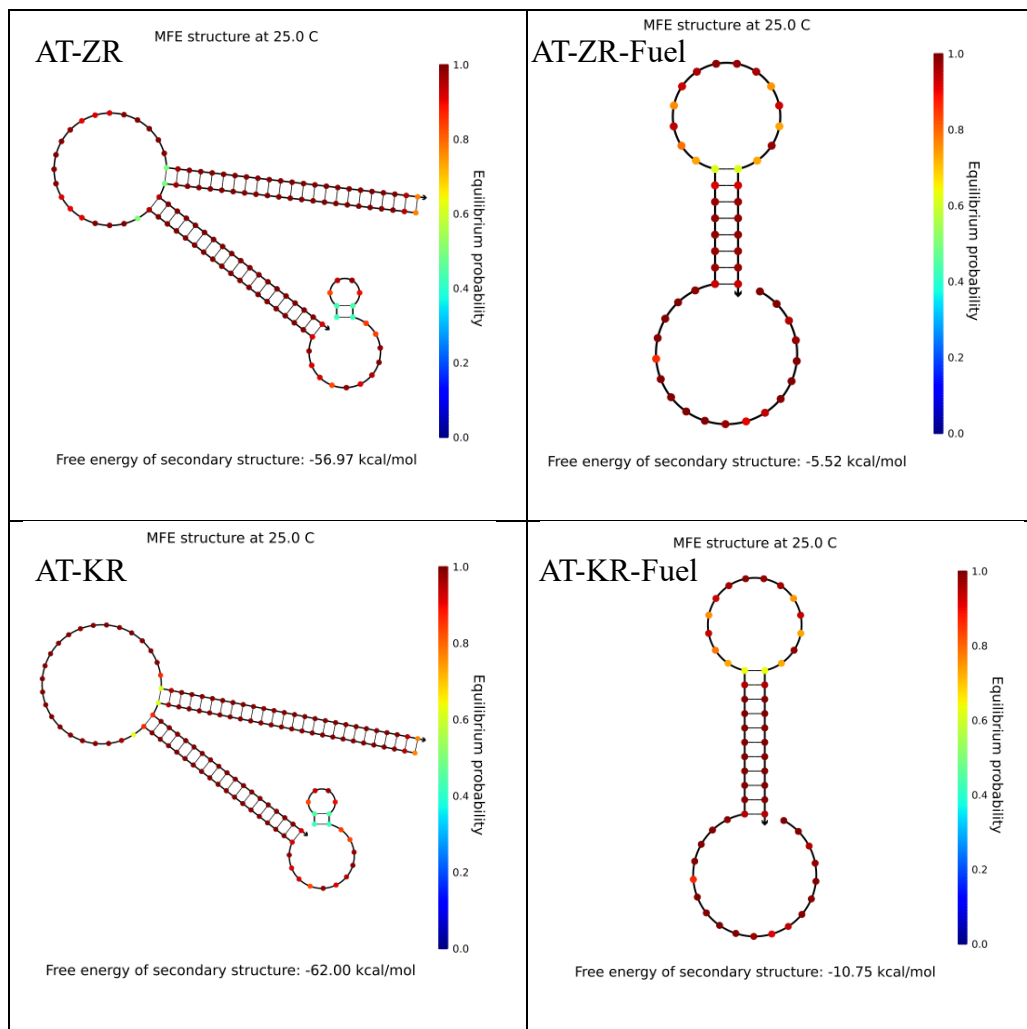
Table A3. Strand sequences for the four AT reaction networks including the AT strands (Output and Backbone), Fuel and the corresponding direct reporters for each AT. The substrates used for catalytic amplification for ZN and KN are also shown.

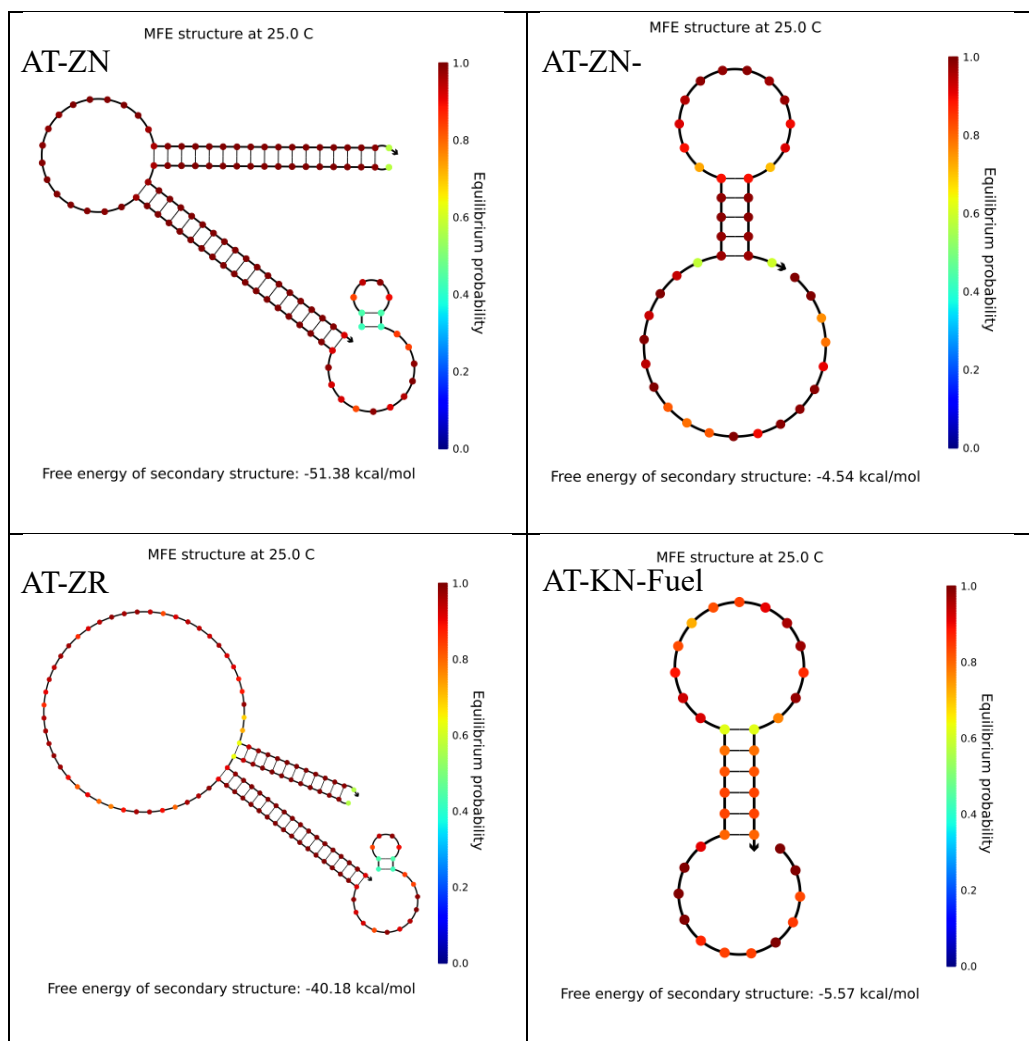
System	Complex	Name	Domains	Sequence (5' to 3')
AT-ZR	AT-ZR	AT-ZR-Output	α - β 1-6-3-4a- β 2	CCTGGGGGAGTATTGCGGAGGAAGG GTAAGAAGTGGGA CCACATACATCATATT CCCT CATTCAA TAAGTTTGTGAGTGTG
		AT-ZR-Backbone	β 2'-4a'- β 1'- τ '	CACACTCACAACTTA TTGAATG TCCCACTTCTTAC CCTTCC
		AT-ZR-Fuel	τ - β 1-4a- β 2-4a'	GGAAGG GTAAGAAGTGGGA CATTCAA TAAGTTTGTGAGTGTG TTGAATG
	ZR	ZR-D	D-6-3	/5TET/ CCACATACATCATATT CCCT
		ZR-Q	4a'-3'-6'-Q	TTGAATG AGGG AATATGATGTATGTGG /3IABkFQ/
AT-KR	AT-KR	AT-KR-Output	α - β 1-d1-d2-3- β 2	CCTGGGGGAGTATTGCGGAGGAAGG GTAAGAAGTGGGA CTCCAAACCTTCATCTTC TACTCG CCTCTACTCA TAAGTTTGTGAGTGTG
		AT-KR-Backbone	β 2'-3'- β 1'- τ '	CACACTCACAACTTA TGAGTAGAGG TCCCACTTCTTAC CCTTCC
		AT-KR-Fuel	τ - β 1-3- β 2-3'	GGAAGG GTAAGAAGTGGGA CCTCTACTCA TAAGTTTGTGAGTGTG TGAGTAGAGG
	KR	KR-D	D-d1-d2	/5TET/CTCCAAACCTTCATCTTC TACTCG
		KR-Q	3'-d2'-d1'-Q	TGAGTAGAGG CGAGTA GAAGATGAAGTTTGGAG /3IABkFQ/
AT-ZN	AT-Z	AT-ZN-Output	α - β 1m1-4-5- β 2m1	CCTGGGGGAGTATTGCGGAGGAAGG TGAGTTTGTGAGT CATTCAATACCCTACG TCTCCA GTAAGAGTGTGT
		AT-ZN-Backbone	β 2'-5'- β 1'- τ '	ACACACTCTTAC TGGAGA ACTCACAACTCA CCTTCC
		AT-ZN-Fuel	τ - β 1-5- β 2-5'	GGAAGG TGAGTTTGTGAGT TCTCCA GTAAGAGTGTGT TGGAGA
	ZRm	ZRm-D	D-4	/5TET/ CATTCAATACCCTACG
		ZRm-Q	5'-4'-Q	TGGAGA CGTAGGTATTGAATG /3IABkFQ/
AT-KN	AT-K	AT-KN-Output	α - β 1m2-1-c-a- β 2m2	CCTGGGGGAGTATTGCGGAGGAAGG GTAAGA CCGTTT CCAGATCAGCAGCCATTCGTTT CAGTCCCAAGTCACCACCTAGC TAAGTTTGTGAGT
		AT-KN-Backbone	β 2'-1'- β 1'- τ '	ACTCACAACTTA AAACGG TCTTAC CCTTCC
		AT-KN-Fuel	τ - β 1-1- β 2-1'	GGAAGG GTAAGA CCGTTT TAAGTTTGTGAGT AAACGG
	KRm	KRm-D	D-c-a	/5TET/ CCAGATCAGCAGCCATTCGTTT CAGTCCCAAGTCACCACCTAGC

		KRm-Q	a'-c'-1'-Q	GCTAGGTGGTGACTTGGGACTG GAACGAATGGCTGCTGATCTGG AAACGG /3IABkFQ/
ZN	zS1	Sig 1	6-3-4	CCACATACATCATATT CCCT CATTCAATACCCTACG
		O1	1-2	CTACTTTCAC CCTACGTCTCCAACCTAECTTACGG
		B1	5'-4'-3'-2'	TGGAGA CGTAGGGTATTGAATG AGGG CCGTAAGTTAGTTGGAGACGTAGG
	zF	2-3-4-5	CCTACGTCTCCAACCTAECTTACGG CCCT CATTCAATACCCTACG TCTCCA	
KN	S1	A1	2'-a'-c'-1'	GGATGT GCTAGGTGGTGACTTGGGACTG GAACGAATGGCTGCTGATCTGG AAACGG
		A2	d1-b-a-2	CCAAACCTTCATCTTCTT GCACTCGGATACGAGGCCTGG CAGTCCCAAGTCACCACCTAGC ACATCC
		A3	c-b'	CCAGATCAGCAGCCATTCGTTC CCAGGCCTCGTATCGCGAGTGC
	S2	B1	1-c-a	CCGTTT CCAGATCAGCAGCCATTC GTTCCAGTCCCAAGTCACCACCTAGC
		B2	2'-a'-b'-d2'-3	GGATGT GCTAGGTGGTGACTTGGGACTG CCAGGCCTCGTATCGCGAGTGC TACTCG CCTCTACTCA
		B3	b-c'-1'	GCACTCGGATACGAGGCCTGG GAACGAATGGCTGCTGATCTGG AAACGG

S5. NUPACK Secondary Structures of ATs

Table A4. NUPACK was used to verify most probable secondary structures for ATs at 25 °C for both ATs and AT-Fuels. Equilibrium bonding probability remained constant for AT aptamer regions on each AT variant.

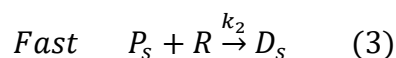
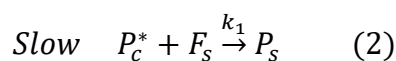
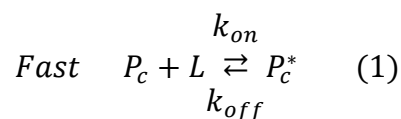




APPENDIX B**Supporting Information for “Targeted Selection of Aptamer Complementary
Elements Toward Rapid Screening of Aptamer Transducers”**

S1. Aptamer Transducer Kinetics Model

In order to evaluate and quantify the relationship between the behavior of our modified ATs and the ACE-scan data, it was essential to develop a quantitative kinetic model that included both the effective dissociation constant $K_{d,eff}$ and the strand displacement rate constant, k_l . A simple kinetic rate equation, including several key assumptions, was derived to fit our fluorescence response based on the following set of reaction steps:



First, the probe complex P_c undergoes an equilibrium reaction with the ligand L yielding an activated probe complex P_c^* with k_{off} and k_{on} rates, which differ from those rates defined by ACE-scan, where $K_{d,eff} = k_{off}/k_{on}$. The P_c - L binding equilibration was assumed to be fast since $[L^0] \gg [P_c^0]$, indicating that the equilibration occurs near $t=0$, and therefore $[P_c^{*0}]$ can be determined as:

$$\frac{d[P_c]}{dt} = -k_{on}[P_c][L] + k_{off}[P_c^*] \quad (4)$$

$$0 = -k_{on}[P_c]_{eq}[L]_{eq} + k_{off}[P_c^*]_{eq} \quad (5)$$

$$[P_c^*]_{eq} = \frac{k_{on}}{k_{off}} [P_c]_{eq}[L]_{eq} \quad (6)$$

Note: $[L^0] \gg [P_c^0]$ therefore $[L^0] \approx [L]_{eq}$ also, $[P_c]_{eq} = [P_c^0] - [P_c^*]_{eq}$ which can be substituted into (6) to obtain:

$$[P_c^{*o}] = [P_c^*]_{eq} = \frac{[P_c^o]}{\frac{k_{off}}{k_{on}[L^o]} + 1} = \frac{[P_c^o]}{\frac{K_{d,eff}}{[L^o]} + 1} \quad (7)$$

Next, P_c^* reacts with a fuel strand F_s (2) leading to the strand displacement rate constant k_l where we assume that $[F_s(t)] = [F_s^o]$ since $[F_s^o] \gg [P_c]$ providing that a pseudo-first order differential rate law can be written in terms of dP_c^*/dt :

$$\frac{dP_c^*}{dt} = -k_1[P_c^*]F_s^o \quad (8)$$

Solving for $[P_c^*(t)]$ from (5) yields:

$$[P_c^*(t)] = [P_c^{*o}]e^{-k_1F_s^ot} \quad (9)$$

In terms of the released probe strand P_s , while also incorporating $[P_c^{*o}]$ from (7), this becomes:

$$\begin{aligned} [P_s(t)] &= [P_c^{*o}] - [P_c^*(t)] = [P_c^{*o}] - [P_c^{*o}]e^{-k_1F_s^ot} \\ &= \frac{[P_c^o]}{\frac{K_{d,eff}}{[L^o]} + 1} - \frac{[P_c^o]}{\frac{K_{d,eff}}{[L^o]} + 1} e^{-k_1F_s^ot} \end{aligned} \quad (10)$$

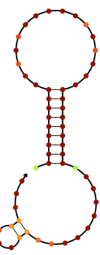
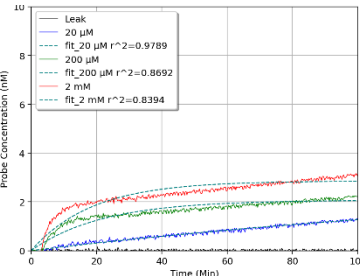
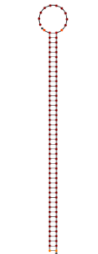
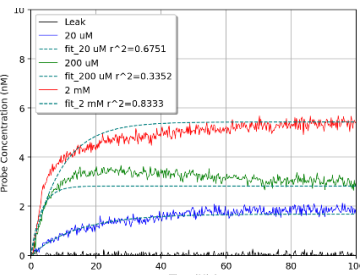
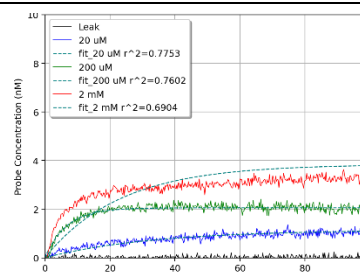
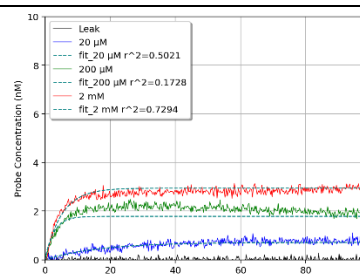
Since the final reaction (3) is fast compared to (2) provided that $k_2 \gg k_l$, $[D_s(t)]$ will be equal to the released probe strands $[P_s(t)]$ at time t :

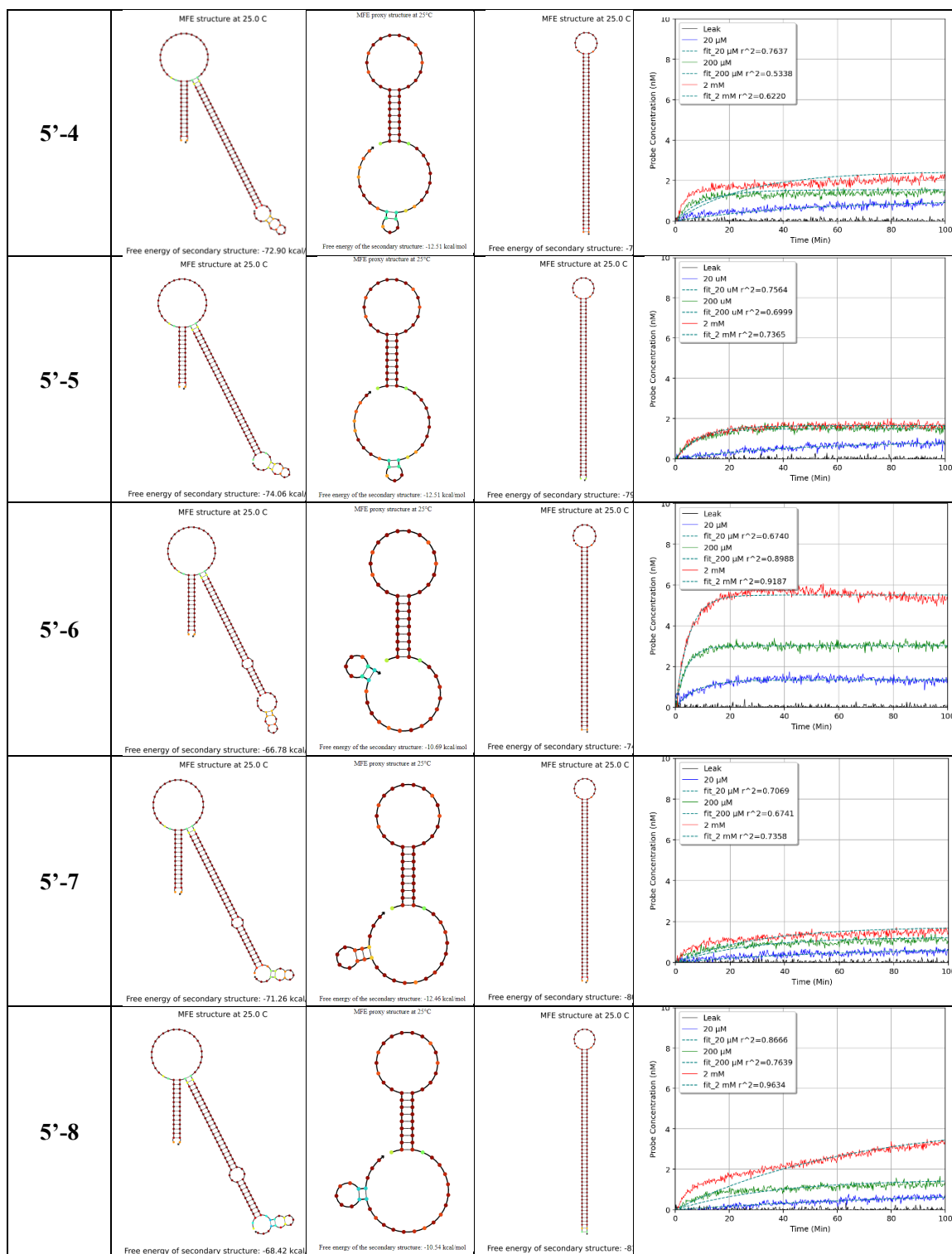
$$[D_s(t)] \approx [P_s(t)] \quad (11)$$

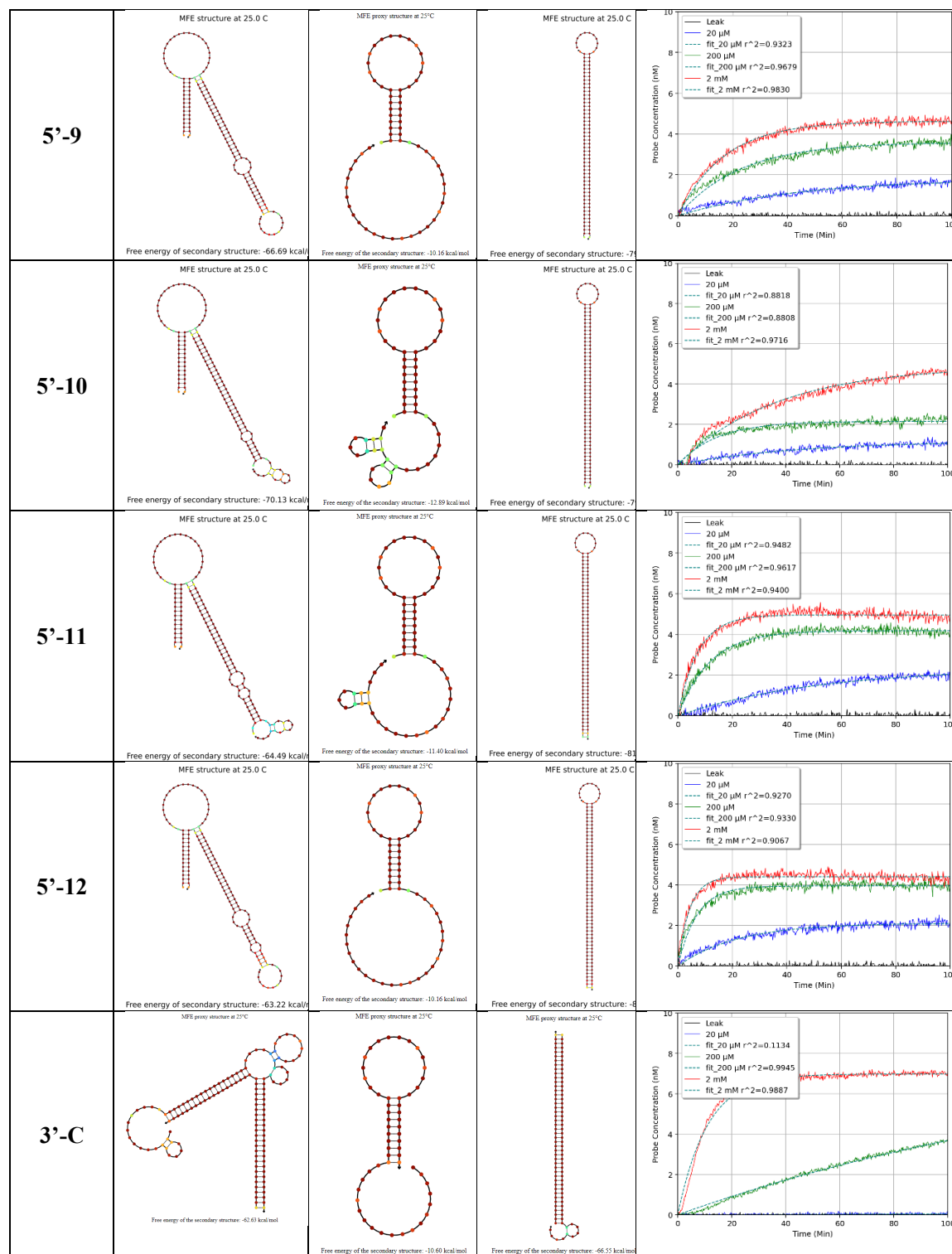
Therefore, simply fitting $[P_s]$ as a function of time to equation (10), both k_l and $K_{d,eff}$ can be measured. To fit our experimental data, the leakage reaction trace was subtracted from each AT reaction trace for 20 μ M, 200 μ M and 2 mM adenosine and normalized by the maximum response for each AT to the initial probe concentration $[P_c^o]$.

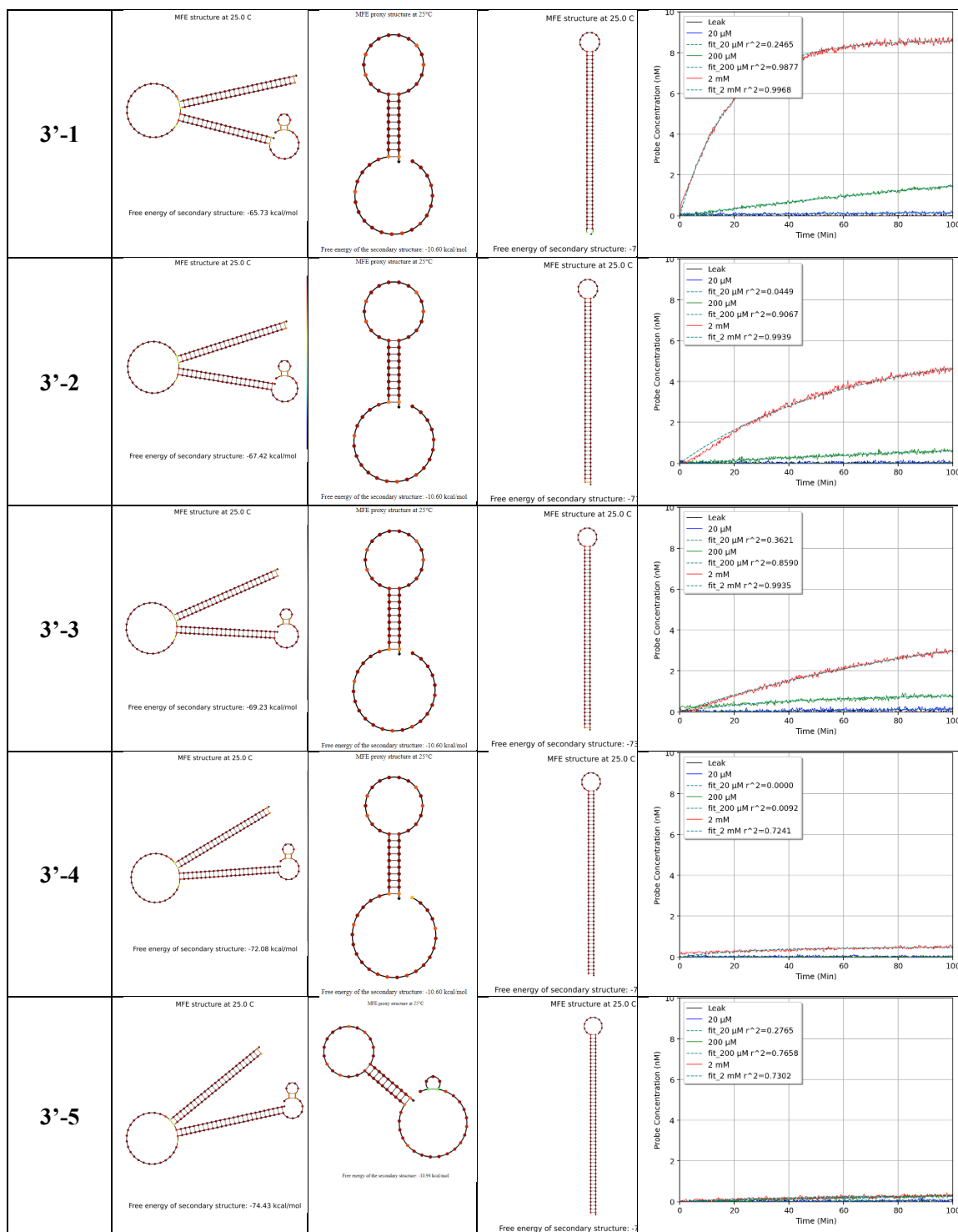
S2. Aptamer Transducer Secondary Structures and Raw Kinetics Traces

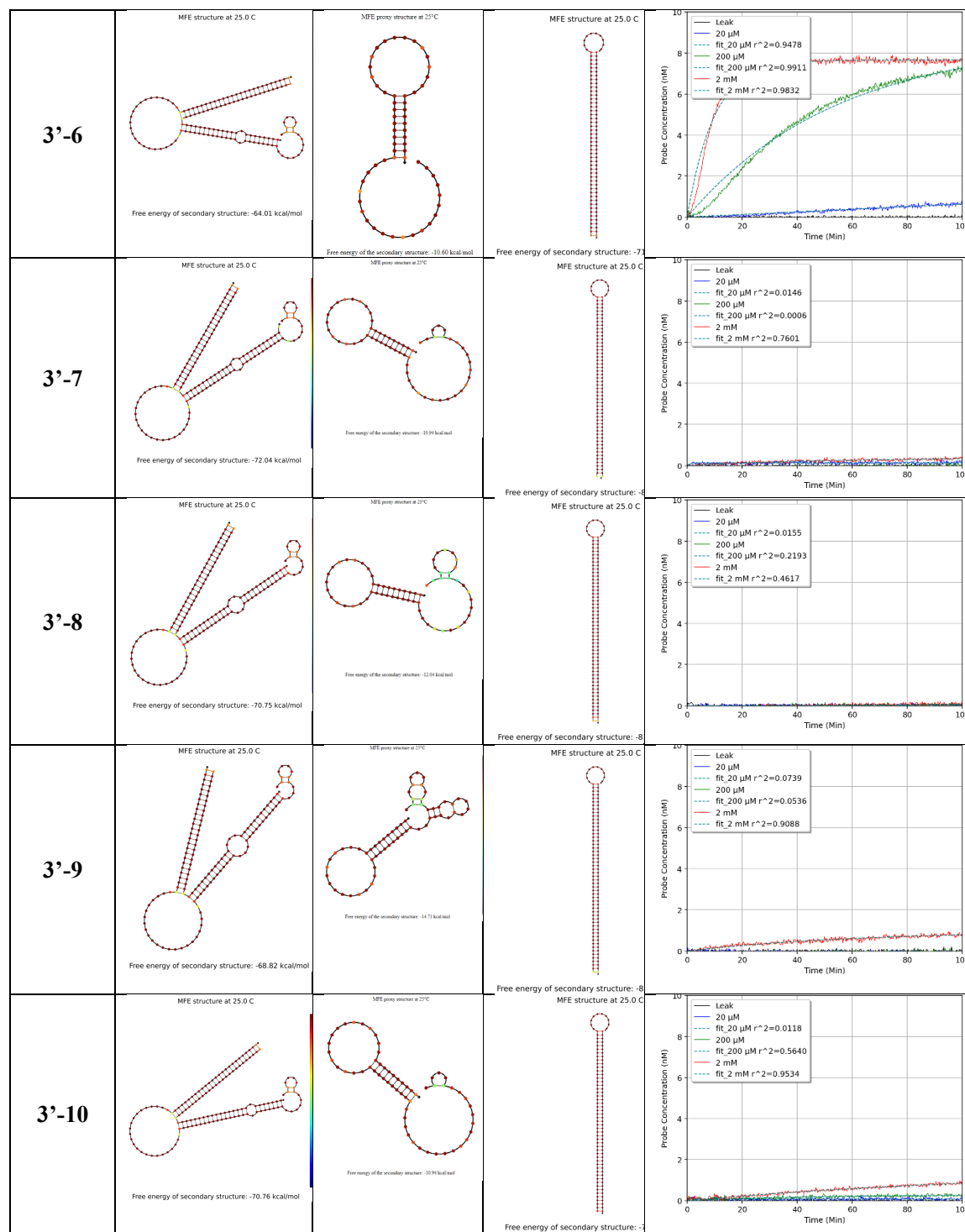
Table S1. Nupack predicted secondary structures for the AT Complex, AT Fuel, and resulting Waste 1 Complex. Raw kinetics traces for each AT system used fit with our kinetics model.

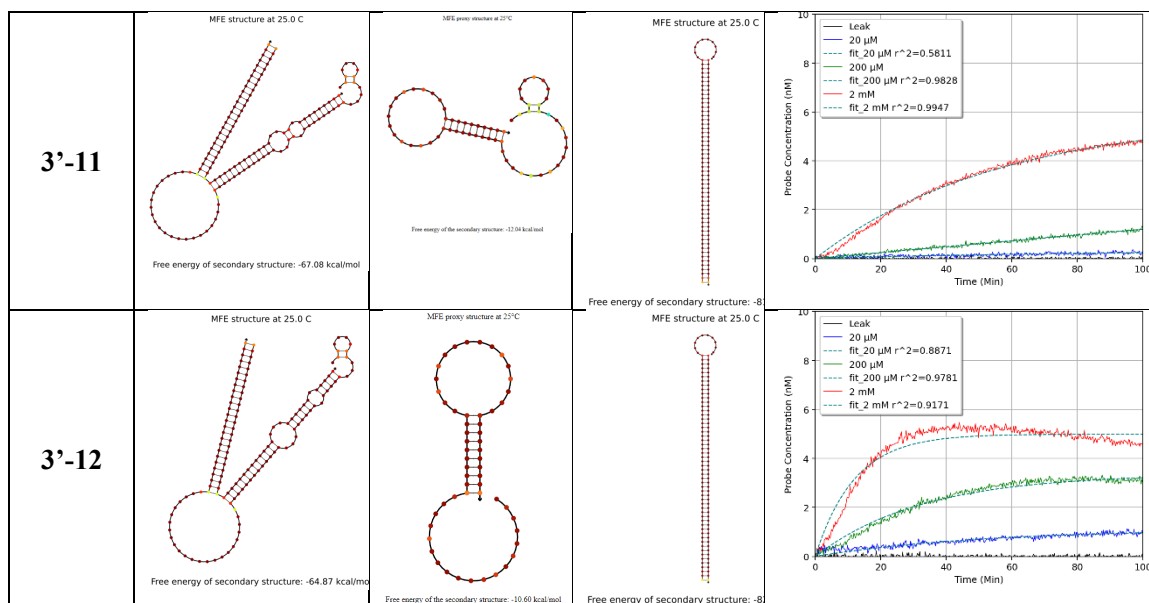
Name	AT Complex	AT Fuel	Waste 1 Complex	Raw Kinetics Trace
5'-C	<p>MFE proxy structure at 25°C</p>  <p>Free energy of the secondary structure: -64.43 kcal/mol</p>	<p>MFE proxy structure at 25°C</p>  <p>Free energy of the secondary structure: -12.51 kcal/mol</p>	<p>MFE proxy structure at 25°C</p>  <p>Free energy of the secondary structure: -68.49 kcal/mol</p>	 <p>Legend: Leak, 20 μM, fit_20 μM $r^2=0.9789$, 200 μM, fit_200 μM $r^2=0.8692$, 2 mM, fit_2 mM $r^2=0.8394$</p>
5'-1	<p>MFE structure at 25.0 C</p>  <p>Free energy of secondary structure: -67.97 kcal/mol</p>	<p>MFE proxy structure at 25°C</p>  <p>Free energy of the secondary structure: -12.51 kcal/mol</p>	<p>MFE structure at 25.0 C</p>  <p>Free energy of secondary structure: -72.6</p>	 <p>Legend: Leak, 20 μM, fit_20 μM $r^2=0.6751$, 200 μM, fit_200 μM $r^2=0.3352$, 2 mM, fit_2 mM $r^2=0.8333$</p>
5'-2	<p>MFE structure at 25.0 C</p>  <p>Free energy of secondary structure: -70.38 kcal/mol</p>	<p>MFE proxy structure at 25°C</p>  <p>Free energy of the secondary structure: -12.51 kcal/mol</p>	<p>MFE structure at 25.0 C</p>  <p>Free energy of secondary structure: -7</p>	 <p>Legend: Leak, 20 μM, fit_20 μM $r^2=0.7753$, 200 μM, fit_200 μM $r^2=0.7602$, 2 mM, fit_2 mM $r^2=0.6904$</p>
5'-3	<p>MFE structure at 25.0 C</p>  <p>Free energy of secondary structure: -71.09 kcal/mol</p>	<p>MFE proxy structure at 25°C</p>  <p>Free energy of the secondary structure: -12.51 kcal/mol</p>	<p>MFE structure at 25.0 C</p>  <p>Free energy of secondary structure: -7</p>	 <p>Legend: Leak, 20 μM, fit_20 μM $r^2=0.5021$, 200 μM, fit_200 μM $r^2=0.1728$, 2 mM, fit_2 mM $r^2=0.7294$</p>











S3. Strand Sequences for Aptamer Transducers

Table S2. Strand sequences for AT reaction networks including the AT strands (Output and Backbone), Fuel and the reporter used to test all networks are shown. Note: Common Output strands in both 5' and 3' directions were bound to backbone single strands to develop each AT while modifications to each Backbone and Fuel strand were used to change the ACEs tested.

Strand Name	Domains	Sequence (5' to 3')
5'-AT-Output (5'-O1)	$\beta_2\text{-}\mu\text{-}\lambda\text{-}\beta_1\text{-}\alpha$	TAAGTTTGTGAGTGTG CTCCAAACCTTCATCTTCTACTCG CCTCTACTCA GTAAGAAGTGGGA ACCTGGGGGAGTATTGCGGAGGAAGGT
3'-AT-Output (3'-O1)	$\alpha\text{-}\beta_1\text{-}\lambda\text{-}\mu\text{-}\beta_2$	ACCTGGGGGAGTATTGCGGAGGAAGGT GTAAGAAGTGGGA CTCCAAACCTTCATCTTCTACTCG CCTCTACTCA TAAGTTTGTGAGTGTG
Reporter Dye (D1)	D- λ	/5TET/ CTCCAAACCTTCATCTTCTACTCG
Reporter Quencher (Q1)	$\mu'\text{-}\lambda'\text{-}Q$	TGAGTAGAGG CGAGTAGAAGATGAAGGTTTGGAG /3IABkFQ/
5'-Control-Backbone (5'-C-B)	$C\tau'_5\text{-}\beta_1\text{-}\mu'\text{-}\beta_2'$	CCAGGT TCCCACTTCTTAC TGAGTAGAGG CACACTCACAAACTTA
5'-Control Fuel (5'-C-F)	$\mu'\text{-}\beta_2\text{-}\mu\text{-}\beta_1\text{-}C\tau_5$	TGAGTAGAGG TAAGTTTGTGAGTGTG CCTCTACTCA GTAAGAAGTGGGA ACCTGG
5'-1-Backbone (5'-1-B)	$1\tau'_5\text{-}\beta_1\text{-}\mu'\text{-}\beta_2'$	CCCCAGGT TCCCACTTCTTAC TGAGTAGAGG CACACTCACAAACTTA
5'-1-Fuel (5'-1-F)	$\mu'\text{-}\beta_2\text{-}\mu\text{-}\beta_1\text{-}1\tau_5$	TGAGTAGAGG TAAGTTTGTGAGTGTG CCTCTACTCA GTAAGAAGTGGGA ACCTGGGG
5'-2-Backbone (5'-2-B)	$2\tau'_5\text{-}\beta_1\text{-}\mu'\text{-}\beta_2'$	CCCCAGGT TCCCACTTCTTAC TGAGTAGAGG CACACTCACAAACTTA
5'-2-Fuel (5'-2-F)	$\mu'\text{-}\beta_2\text{-}\mu\text{-}\beta_1\text{-}2\tau_5$	TGAGTAGAGG TAAGTTTGTGAGTGTG CCTCTACTCA GTAAGAAGTGGGA ACCTGGGGG
5'-3-Backbone (5'-3-B)	$3\tau'_5\text{-}\beta_1\text{-}\mu'\text{-}\beta_2'$	TCCCCAGGT TCCCACTTCTTAC TGAGTAGAGG CACACTCACAAACTTA
5'-3-Fuel (5'-3-F)	$\mu'\text{-}\beta_2\text{-}\mu\text{-}\beta_1\text{-}3\tau_5$	TGAGTAGAGG TAAGTTTGTGAGTGTG CCTCTACTCA GTAAGAAGTGGGA ACCTGGGGGA
5'-4-Backbone (5'-4-B)	$4\tau'_5\text{-}\beta_1\text{-}\mu'\text{-}\beta_2'$	CTCCCCAGGT TCCCACTTCTTAC TGAGTAGAGG CACACTCACAAACTTA
5'-4-Fuel (5'-4-F)	$\mu'\text{-}\beta_2\text{-}\mu\text{-}\beta_1\text{-}4\tau_5$	TGAGTAGAGG TAAGTTTGTGAGTGTG CCTCTACTCA GTAAGAAGTGGGA ACCTGGGGGAG
5'-5-Backbone (5'-5-B)	$5\tau'_5\text{-}\beta_1\text{-}\mu'\text{-}\beta_2'$	ACTCCCCAGGT TCCCACTTCTTAC TGAGTAGAGG CACACTCACAAACTTA
5'-5-Fuel (5'-5-F)	$\mu'\text{-}\beta_2\text{-}\mu\text{-}\beta_1\text{-}5\tau_5$	TGAGTAGAGG TAAGTTTGTGAGTGTG CCTCTACTCA GTAAGAAGTGGGA ACCTGGGGGAGT
5'-6-Backbone (5'-6-B)	$6\tau'_5\text{-}\beta_1\text{-}\mu'\text{-}\beta_2'$	CCCCAGGA TCCCACTTCTTAC TGAGTAGAGG CACACTCACAAACTTA
5'-6-Fuel (5'-6-F)	$\mu'\text{-}\beta_2\text{-}\mu\text{-}\beta_1\text{-}6\tau_5$	TGAGTAGAGG TAAGTTTGTGAGTGTG CCTCTACTCA GTAAGAAGTGGGA TCCTGGGGG
5'-7-Backbone (5'-7-B)	$7\tau'_5\text{-}\beta_1\text{-}\mu'\text{-}\beta_2'$	TACTCCCCAGGA TCCCACTTCTTAC TGAGTAGAGG CACACTCACAAACTTA
5'-7-Fuel (5'-7-F)	$\mu'\text{-}\beta_2\text{-}\mu\text{-}\beta_1\text{-}7\tau_5$	TGAGTAGAGG TAAGTTTGTGAGTGTG CCTCTACTCA GTAAGAAGTGGGA TCCTGGGGGAGTA
5'-8-Backbone (5'-8-B)	$8\tau'_5\text{-}\beta_1\text{-}\mu'\text{-}\beta_2'$	ATACTCCCCAGCA TCCCACTTCTTAC TGAGTAGAGG CACACTCACAAACTTA
5'-8-Fuel (5'-8-F)	$\mu'\text{-}\beta_2\text{-}\mu\text{-}\beta_1\text{-}8\tau_5$	TGAGTAGAGG TAAGTTTGTGAGTGTG CCTCTACTCA GTAAGAAGTGGGA TGCTGGGGGAGTAT
5'-9-Backbone (5'-9-B)	$9\tau'_5\text{-}\beta_1\text{-}\mu'\text{-}\beta_2'$	AATACTCCCCACCA TCCCACTTCTTAC TGAGTAGAGG CACACTCACAAACTTA
5'-9-Fuel (5'-9-F)	$\mu'\text{-}\beta_2\text{-}\mu\text{-}\beta_1\text{-}9\tau_5$	TGAGTAGAGG TAAGTTTGTGAGTGTG CCTCTACTCA GTAAGAAGTGGGA TGGTGGGGGAGTATT

5'-10-Backbone (5'-10-B)	$10\tau'_5-\beta'_1-\mu'-\beta'_2$	ACTCCCCGAGGT TCCCACCTTCTTAC TGAGTAGAGG CACACTCACAAACTTA
5'-10-Fuel (5'-10-F)	$\mu'-\beta_2-\mu-\beta_1-10\tau_5$	TGAGTAGAGG TAAGTTTGTGAGTGTG CCTCTACTCA GTAAGAAGTGGGA ACCTCGGGGAGT
5'-11-Backbone (5'-11-B)	$11\tau'_5-\beta'_1-\mu'-\beta'_2$	ATACTCCCCGAGCA TCCCACCTTCTTAC TGAGTAGAGG CACACTCACAAACTTA
5'-11-Fuel (5'-11-F)	$\mu'-\beta_2-\mu-\beta_1-11\tau_5$	TGAGTAGAGG TAAGTTTGTGAGTGTG CCTCTACTCA GTAAGAAGTGGGA TGCTCGGGGAGTAT
5'-12-Backbone (5'-12-B)	$12\tau'_5-\beta'_1-\mu'-\beta'_2$	AATACACCCCCACCA TCCCACCTTCTTAC TGAGTAGAGG CACACTCACAAACTTA
5'-12-Fuel (5'-12-F)	$\mu'-\beta_2-\mu-\beta_1-12\tau_5$	TGAGTAGAGG TAAGTTTGTGAGTGTG CCTCTACTCA GTAAGAAGTGGGA ACCTGG
3'-Control-Backbone (3'-C-B)	$\beta'_2-\mu'-\beta'_1-C\tau'_3$	CACACTCACAAACTTA TGAGTAGAGG TCCCACCTTCTTAC ACCTTC
5'-Control Fuel (3'-C-F)	$C\tau_3-\beta_1-\mu-\beta_2-\mu'$	GAAGGT GTAAGAAGTGGGA CCTCTACTCA TAAGTTTGTGAGTGTG TGAGTAGAGG
3'-1-Backbone (3'-1-B)	$\beta'_2-\mu'-\beta'_1-1\tau'_3$	CACACTCACAAACTTA TGAGTAGAGG TCCCACCTTCTTAC ACCTTCCT
3'-1-Fuel (3'-1-F)	$1\tau_3-\beta_1-\mu-\beta_2-\mu'$	AGGAAGGT GTAAGAAGTGGGA CCTCTACTCA TAAGTTTGTGAGTGTG TGAGTAGAGG
3'-2-Backbone (3'-2-B)	$\beta'_2-\mu'-\beta'_1-2\tau'_3$	CACACTCACAAACTTA TGAGTAGAGG TCCCACCTTCTTAC ACCTTCCTC
3'-2-Fuel (3'-2-F)	$2\tau_3-\beta_1-\mu-\beta_2-\mu'$	GAGGAAGGT GTAAGAAGTGGGA CCTCTACTCA TAAGTTTGTGAGTGTG TGAGTAGAGG
3'-3-Backbone (3'-3-B)	$\beta'_2-\mu'-\beta'_1-3\tau'_3$	CACACTCACAAACTTA TGAGTAGAGG TCCCACCTTCTTAC ACCTTCCTCC
3'-3-Fuel (3'-3-F)	$3\tau_3-\beta_1-\mu-\beta_2-\mu'$	GGAGGAAGGT GTAAGAAGTGGGA CCTCTACTCA TAAGTTTGTGAGTGTG TGAGTAGAGG
3'-4-Backbone (3'-4-B)	$\beta'_2-\mu'-\beta'_1-4\tau'_3$	CACACTCACAAACTTA TGAGTAGAGG TCCCACCTTCTTAC ACCTTCCTCCG
3'-4-Fuel (3'-4-F)	$4\tau_3-\beta_1-\mu-\beta_2-\mu'$	CGGAGGAAGGT GTAAGAAGTGGGA CCTCTACTCA TAAGTTTGTGAGTGTG TGAGTAGAGG
3'-5-Backbone (3'-5-B)	$\beta'_2-\mu'-\beta'_1-5\tau'_3$	CACACTCACAAACTTA TGAGTAGAGG TCCCACCTTCTTAC ACCTTCCTCCGC
3'-5-Fuel (3'-5-F)	$5\tau_3-\beta_1-\mu-\beta_2-\mu'$	GCGGAGGAAGGT GTAAGAAGTGGGA CCTCTACTCA TAAGTTTGTGAGTGTG TGAGTAGAGG
3'-6-Backbone (3'-6-B)	$\beta'_2-\mu'-\beta'_1-6\tau'_3$	CACACTCACAAACTTA TGAGTAGAGG TCCCACCTTCTTAC TCCTTCCTC
3'-6-Fuel (3'-6-F)	$6\tau_3-\beta_1-\mu-\beta_2-\mu'$	GAGGAAGGA GTAAGAAGTGGGA CCTCTACTCA TAAGTTTGTGAGTGTG TGAGTAGAGG
3'-7-Backbone (3'-7-B)	$\beta'_2-\mu'-\beta'_1-7\tau'_3$	CACACTCACAAACTTA TGAGTAGAGG TCCCACCTTCTTAC TCCTTCCTCCGCA
3'-7-Fuel (3'-7-F)	$7\tau_3-\beta_1-\mu-\beta_2-\mu'$	TGCGGAGGAAGGA GTAAGAAGTGGGA CCTCTACTCA TAAGTTTGTGAGTGTG TGAGTAGAGG
3'-8-Backbone (3'-8-B)	$\beta'_2-\mu'-\beta'_1-8\tau'_3$	CACACTCACAAACTTA TGAGTAGAGG TCCCACCTTCTTAC TGCTTCCTCCGCAA
3'-8-Fuel (3'-8-F)	$8\tau_3-\beta_1-\mu-\beta_2-\mu'$	TTGCGGAGGAAGCA GTAAGAAGTGGGA CCTCTACTCA TAAGTTTGTGAGTGTG TGAGTAGAGG
3'-9-Backbone (3'-9-B)	$\beta'_2-\mu'-\beta'_1-9\tau'_3$	CACACTCACAAACTTA TGAGTAGAGG TCCCACCTTCTTAC TGGTTCCTCCGCAAT
3'-9-Fuel (3'-9-F)	$9\tau_3-\beta_1-\mu-\beta_2-\mu'$	ATTGCGGAGGAACCA GTAAGAAGTGGGA CCTCTACTCA TAAGTTTGTGAGTGTG TGAGTAGAGG
3'-10-Backbone (3'-10-B)	$\beta'_2-\mu'-\beta'_1-10\tau'_3$	CACACTCACAAACTTA TGAGTAGAGG TCCCACCTTCTTAC ACCTACCTCCGC
3'-10-Fuel (3'-10-F)	$10\tau_3-\beta_1-\mu-\beta_2-\mu'$	GCGGAGGTAGGT GTAAGAAGTGGGA CCTCTACTCA TAAGTTTGTGAGTGTG TGAGTAGAGG
3'-11-Backbone (3'-11-B)	$\beta'_2-\mu'-\beta'_1-11\tau'_3$	CACACTCACAAACTTA TGAGTAGAGG TCCCACCTTCTTAC TGCTACCTCCGCAA
3'-11-Fuel (3'-11-F)	$11\tau_3-\beta_1-\mu-\beta_2-\mu'$	TTGCGGAGGTAGCA GTAAGAAGTGGGA CCTCTACTCA TAAGTTTGTGAGTGTG TGAGTAGAGG

3'-12-Backbone (3'-12-B)	$\beta_2'-\mu'-\beta_1'-12\tau_3'$	CACACTCACAACTTA TGAGTAGAGG TCCCACTTCTTAC TGGTTCCCTCGGCAAT
3'-12-Fuel (3'-12-F)	$12\tau_3-\beta_1-\mu-\beta_2-\mu'$	ATTGCCGAGGAACCA GTAAGAAGTGGGA CCTCTACTCA TAAGTTTGTGAGTGTG TGAGTAGAGG

S4. Python3 Code for AT Kinetics Fitting

```

import glob
import matplotlib.pyplot as plt
import numpy as np
import pandas as pd
from scipy.signal import savgol_filter
from scipy.optimize import curve_fit
from scipy.odr import ODR, Model, Data, RealData
from matplotlib.widgets import Slider, Button
import os

folderName = input("Name of Output Folder: ") #Determine the folder
name to create

"""Model Reaction Parameters"""
pc = 10          #Initial Probe Concentration (nM)
finit = 300     #Initial Fuel Concentration (nM)
kdinit = 100    #Aptamer dissociation constant (uM)
koffinit = 0.006 #Initial off rate
koninit = 0.0001 #Initial on rate
k1init = 0.0001362 #AT reaction rate Fuel with Substrate
([ps]/min)
ligConcs = [20,200,2000] #Ligand Concentration (uM)

while True:
    autoScale = input("Auto-Scale Plots? (y/n): ")
    if autoScale == 'y':
        break
    elif autoScale == 'n':
        break
    else:
        print("Please provide a valid y/n input...")

if autoScale == 'n':
    xMax = int(input("Experiment maximum time (min): "))
    yMax = int(input("Maximum Plot Intensity (AU): "))

while True:
    subtractLeak = input("Subtract Leak Control Trace? (y/n): ")
    if subtractLeak == 'y':
        break
    elif subtractLeak == 'n':

```

```

        break
    else:
        print("Please provide a valid y/n input...")

while True:
    shiftOrigin = input("Shift Origin to Experiment Start? (y/n): ")
    if shiftOrigin == 'y':
        break
    elif shiftOrigin == 'n':
        break
    else:
        print("Please provide a valid y/n input...")

while True:
    removeOutliers = input("Remove Outliers? (y/n): ")
    if removeOutliers == 'y':
        break
    elif removeOutliers == 'n':
        break
    else:
        print("Please provide a valid y/n input...")

if removeOutliers == 'y':
    while True:
        try:
            cutoff = input("Cutoff value (default 0.5): ")
            if cutoff == '':
                cutoff = 0.5
                break
            cutoff = float(cutoff)
            break
        except ValueError:
            print("Ooops! That was not a valid decimal between 0.01-1.0 Try again...")

while True:
    normalize_pc = input("Normalize to initial AT Probe Concentration (uses NormalizationValues.csv)? (y/n): ")
    if normalize_pc == 'y':
        break
    elif normalize_pc == 'n':
        break
    else:
        print("Please provide a valid y/n input...")

```

```

while True:
    curvefit = input("Fit Curve? (y/n): ")
    if curvefit == 'y':
        break
    elif curvefit == 'n':
        break
    else:
        print("Please provide a valid y/n input...")

    if not os.path.exists(os.getcwd()+"\\"+folderName): #If the folder
doesn't already exist create one
        os.makedirs(os.getcwd()+"\\"+folderName)

    for filename in glob.glob('*.*csv'):

        if filename == "NormalizationValues.csv": #Continues the loop if
it finds the NormalizationValues.csv file
            continue

        print(filename)
        #os.system('pause')
        name = filename[:-4]
        """Read and parse the data using the Pandas Dataframe object"""
        data = pd.read_csv(filename, encoding = "ISO-8859-
1",header=None)
        data = data.dropna(axis=1,how='all') #Drops NaN columns only if
every entry is NaN
        dataHead,data = np.split(data,[2]) #Splits the data labels from
the beginning of the file
        dataHead = dataHead.drop(1,axis=0) #Removes the axis titles and
leaves the plot line labels
        numHead = dataHead.values[0] #Creates a numpy array with plot
line labels
        cleanData = data.dropna() #Removes the tail of the file with NaN
values
        cleanData = cleanData.reset_index(drop=True) #Resets the row and
column indicies of the dataframe
        cleanData = cleanData.astype(float)
        originalData = cleanData.astype(float) #Original Data Containing
Outliers and no shift

        """Outlier Removal Routine in case of Instrument Errors"""
        if removeOutliers == 'y':
            odd_columns = []

```

```

    for col in range(0,len(cleanData.columns)):
        if col % 2 == 1:
            odd_columns.append(col)

    avgstart = len(cleanData.columns)
    for col in odd_columns:
        cleanData[len(cleanData.columns)] =
savgol_filter(cleanData[col],25,3) #Creates a 10 point moving average and
assigns the data to its own column

    for col in odd_columns:
        upper = cutoff*cleanData[col].std()+cleanData[avgstart]
#Using the standard deviation and the cutoff value applied to the 10 point
moving average create an upper limit trace
        lower = -cutoff*cleanData[col].std()+cleanData[avgstart]
#Using the standard deviation and the cutoff value applied to the 10 point
moving average create an lower limit trace
        cleanData =
cleanData[(cleanData[col]<upper)&(cleanData[col]>lower)] #Apply the upper
and lower limit traces as a boolean filter to remove outlier data points
        avgstart+=1

    if not
os.path.exists(os.getcwd()+"\\"+folderName+"\\OutliersRemoved"): #If
the folder doesn't already exist create one
        os.makedirs(os.getcwd()+"\\"+folderName+"\\OutliersRe
moved")

        cleanData.to_csv(os.getcwd()+"\\"+folderName+"\\OutliersR
emoved"+"\\name+'_OutliersRemoved.csv')

        cleanData = cleanData.reset_index(drop=True) #Resets the row
and column indicies of the dataframe
        #print(cleanData)

#print(cleanData.loc[0][0])

"""Origin Shifting to experimental start time and intensity"""
if shiftOrigin == 'y':
    odd_columns = []
    for col in range(0,len(cleanData.columns)):
        if col % 2 == 1:
            odd_columns.append(col)
    #print(odd_columns)
    negatives = []

```

```

        #print(odd_columns)
        for col in odd_columns:
            negativeData = cleanData[(cleanData[col]<=0.1)] #Boolean
            filter to determine negative or zero rows from the original dataset
            negatives.append(negativeData.last_valid_index())
#Creates a list of row index numbers for the last negative entry in the
filtered data
            negatives = list(filter(None,negatives)) #Removes any None
values from the negatives list
            cleanData = cleanData[max(negatives)-1:] #Removes any data
prior to the latest negative entry in the experiment
            cleanData = cleanData.reset_index(drop=True) #Resets the row
and column indicies of the dataframe
            #print(cleanData)

        for col in odd_columns:
            #print(cleanData.loc[0][0])
            #print(cleanData.loc[0][col])
            lowerbound = float(cleanData.loc[0][7])
            cleanData[col] = cleanData[col]-lowerbound
            timebound = float(cleanData.loc[0][6])
            cleanData[col-1]=cleanData[col-1]-timebound

        if not
os.path.exists(os.getcwd()+"\\"+folderName+"\\"+"OriginShifted"): #If the
folder doesn't already exist create one
            os.makedirs(os.getcwd()+"\\"+folderName+"\\"+"OriginShif
ted")

            cleanData.to_csv(os.getcwd()+"\\"+folderName+"\\"+"OriginShi
fted"+"\\"+name+'_OriginShifted.csv')

        """Normalize the Data to Max Probe Concentration for ATs"""
        if normalize_pc == 'y': #Normalizes the plot if and only if a
key is found in NormalizationValues.csv by the listed value.

            NormVals = pd.read_csv('NormalizationValues.csv',
header=None, index_col=0)
            NormVals = NormVals.squeeze()
            NormVals_dict = NormVals.to_dict()
            columns = [1,3,5,7]

            for key, value in NormVals_dict.items():
                if filename.find(key) == -1:
                    continue
                else:

```

```

        if value == 1: #Breaks the loop before normalization
if the NormalizationValue is equal to 1 (the default value)
            break

        print(f"Normalized {key} by {value}.")
        at_name=key #Provides the item key to be used later
during fitting
        for col in columns:
            cleanData[col] = (pc*cleanData[col])/value
#Normalizes by the normalization value listed in NormalizationValues.csv
            break

    """Subtract the Leakage Trace from the data"""
    if subtractLeak == 'y':
        odd_columns = []
        for col in range(0,len(cleanData.columns)):
            if col % 2 == 1:
                odd_columns.append(col)

        #print(odd_columns)
        cleanData[len(cleanData.columns)] =
savgol_filter(cleanData[1],25,3) #Creates a 25 point moving average of the
leak trace and assigns the data to its own column
        length = len(cleanData.columns)-1
        for col in odd_columns:
            cleanData[col] = cleanData[col] - cleanData[length]
#Apply the upper and lower limit traces as a boolean filter to remove
outlier data points
            cleanData = cleanData.dropna()
            cleanData = cleanData.reset_index(drop=True) #Resets the row
and column indicies of the dataframe
            if not
os.path.exists(os.getcwd()+"\\"+folderName+"\\"+"LeakSubtracted"): #If the
folder doesn't already exist create one
                os.makedirs(os.getcwd()+"\\"+folderName+"\\"+"LeakSubtra
cted")

            cleanData.to_csv(os.getcwd()+"\\"+folderName+"\\"+"LeakSubtr
acted"+"\\"+name+'_LeakSubtracted.csv')

    """Define a Class for our Fitting function for ATs"""

    class bindFxn:

        def __init__(self) -> None:
            pass

```

```

def single_binding(self,x,k,kd):

    #Model that assumes instantaneous equilibration
    #return ((finit-finit*np.exp(k*x*(finit-
((pc)/(kd/self.ligConc+1)))))/(1-
(finit/((pc)/(kd/self.ligConc+1)))*np.exp(k*x*(finit-
((pc)/(kd/self.ligConc+1))))))

    #Model that includes time dependent probe complex
activation
    #return (finit-
finit*np.exp(k*x*(finit+(pc)/((koff)/(kon*self.ligConc)+1)*(k-1+(1-
(k)/(kon*self.ligConc+koff+k))*np.exp(-
(kon*self.ligConc+koff+k)*x)))))/(1-(finit)/(-
(pc)/((koff)/(kon*self.ligConc+1)*(k-1+(1-
(k)/(kon*self.ligConc+koff+k))*np.exp(-
(kon*self.ligConc+koff+k)*x))*np.exp(k*x*(finit+(pc)/((koff)/(kon*self.li
gConc+1)*(k-1+(1-(k)/(kon*self.ligConc+koff+k))*np.exp(-
(kon*self.ligConc+koff+k)*x))))))

    #A new derivation of the time dependent probe complex
activation model
    #return
(((k*finit*pc)/((koff)/(kon*self.ligConc)+1))*((k*finit)/(kon*self.ligConc
+koff+k*finit)-1)*((1-np.exp(-
(kon*self.ligConc+koff+k*finit)*x))/(kon*self.ligConc+koff+k*finit)+x))
    #New Model Again
    #return
((k*finit*(kon*self.ligConc+koff)*((pc)/((koff)/(kon*self.ligConc)+1)))/(k
on*self.ligConc+koff+k*finit))*((np.exp(-
(kon*self.ligConc+koff+k*finit)*x)-1)/(kon*self.ligConc+koff+k*finit)+x)
    #Simple Model with fast equilibrium

    return ((pc)/((kd)/(self.ligConc+1))-
((pc)/((kd)/(self.ligConc+1))*np.exp(-k*finit*x)

    """Fitting the ATs with our fit function and returning the
results"""
    if curvefit == 'y':

        plt.gcf().clear() #Clears the current figure before each new
iteration
        #plt.style.use('seaborn-bright')

```

```

plt.title(name)
plt.xlabel("Time (Min)")
plt.ylabel("Probe Concentration (nM)")
plt.axis([0, xMax,0, yMax])

'''Plot the Leakage Trace'''
xdat=cleanData[0]
ydat=cleanData[1]
plt.plot(xdat,ydat,'k',linewidth=0.7,label=numHead[0])

'''Plot the Kinetics Traces'''
columns = [3,5,7]
colors = ['b','g','r']
i = 0
x = np.linspace(0,xMax,1000)
for col in columns:
    xdat=cleanData[col-1]
    ydat=cleanData[col]
    single_bind = bindFxn()
    single_bind.ligConc = ligConcs[i]
    print(single_bind.ligConc)
    print(ligConcs[i])
    popt, pcov = curve_fit(
        f=single_bind.single_binding,
        xdata=xdat,
        ydata=ydat,
        p0 = (k1init,kdinit)
    )
    print(popt)
    k1_opt, kd_opt = popt
    corr_matrix =
np.corrcoef(ydat,single_bind.single_binding(xdat,k1_opt,kd_opt)) #for
calculating the correlation matrix
    corr = corr_matrix[0,1] #get correlation from data
    R2 = corr**2 #determine r squared correlation
    print("r^2 = %10.6f" % R2)
    plt.plot(xdat,ydat,colors[i],linewidth=0.7,label=numHead
[col-1])
    i+=1
    plt.plot(x,
single_bind.single_binding(x,k1_opt,kd_opt),'teal',linestyle='--',
linewidth = 1,label=f'fit_{numHead[col-1]} r^2={R2:.4f}')

'''Change plot options and export'''
plt.grid(True)

```

```

        plt.legend(loc="upper left",shadow=True)
        plt.savefig(os.getcwd()+"\\"+folderName+"\\"+name+'.png',bbox_inches='tight',dpi=180)

    print(' ')

    """Data Transposition Before Plotting"""

    originalData = originalData.T #Transposes the
    cleandata set into rows for x and y.
    numData2 = originalData.values.astype(float) #Converts the
    data to a numpy array object as a float dtype

    cleanData = cleanData.T #Transposes the
    cleandata set into rows for x and y.
    numData = cleanData.values.astype(float) #Converts the
    data to a numpy array object as a float dtype

    """Plot the Data using Matplotlib"""
    if autoScale == 'n' and curvefit == 'n':

        plt.gcf().clear() #Clears the current figure before each new
iteration
        #plt.style.use('seaborn-bright')
        plt.title(name)
        plt.xlabel("Time (Min)")
        plt.ylabel("Intensity (A.U.)")
        plt.axis([0, xMax,0, yMax])
        l1 = plt.plot(numData[0],numData[1], 'k',linewidth=0.7)
        l2 = plt.plot(numData[2],numData[3], 'b',linewidth=0.7)
        l3 = plt.plot(numData[4],numData[5], 'g',linewidth=0.7)
        l4 = plt.plot(numData[6],numData[7], 'r',linewidth=0.7)
        plt.grid(True)
        plt.legend((numHead[0],numHead[2],numHead[4],numHead[6]),loc
="upper left",shadow=True)
        plt.savefig(os.getcwd()+"\\"+folderName+"\\"+name+'.png',bbox_inches='tight',dpi=180)
        #plt.show()

        if removeOutliers == 'y' or shiftOrigin == 'y' and curvefit
== 'n':

```

```

plt.gcf().clear() #Clears the current figure before each
new iteration
plt.style.use('seaborn-bright')
plt.title(name+' Original Data')
plt.xlabel("Time (Min)")
plt.ylabel("Intensity (A.U.)")
plt.axis([0, xMax,0,
round(np.max(numData2[[1,3,5,7],:]))*1.05])
l1 = plt.plot(numData2[0],numData2[1], 'k',linewidth=0.7)
l2 = plt.plot(numData2[2],numData2[3], 'b',linewidth=0.7)
l3 = plt.plot(numData2[4],numData2[5], 'g',linewidth=0.7)
l4 = plt.plot(numData2[6],numData2[7], 'r',linewidth=0.7)
plt.grid(True)
plt.legend((numHead[0],numHead[2],numHead[4],numHead[6])
,loc="upper left",shadow=True)
plt.savefig(os.getcwd()+"\\"+folderName+"\\"+name+'_Orig
inalData.png',bbox_inches='tight',dpi=180)
plt.show()

if autoScale == 'y' and curvefit == 'n':
    if not os.path.exists(os.getcwd()+"\\"+folderName): #If the
folder doesn't already exist create one
        os.makedirs(os.getcwd()+"\\"+folderName)

plt.gcf().clear() #Clears the current figure before each new
iteration
plt.style.use('seaborn-bright')
plt.title(name)
plt.xlabel("Time (Min)")
plt.ylabel("Intensity (A.U.)")
plt.axis([0, int(round(numData[0][ -
1])),np.min(numData[[1,3,5,7],:]),
round(np.max(numData[[1,3,5,7],:]))*1.05])
l1 = plt.plot(numData[0],numData[1], 'k',linewidth=0.7)
l2 = plt.plot(numData[2],numData[3], 'b',linewidth=0.7)
l3 = plt.plot(numData[4],numData[5], 'g',linewidth=0.7)
l4 = plt.plot(numData[6],numData[7], 'r',linewidth=0.7)
plt.grid(True)
plt.legend((numHead[0],numHead[2],numHead[4],numHead[6]),loc
="upper left",shadow=True)
plt.savefig(os.getcwd()+"\\"+folderName+"\\"+name+'.png',bbo
x_inches='tight',dpi=180)
plt.show()

```

```

        if removeOutliers == 'y' or shiftOrigin == 'y' and curvefit
        == 'n':
            plt.gcf().clear() #Clears the current figure before each
            new iteration
            #plt.style.use('seaborn-bright')
            plt.title(name+' Original Data')
            plt.xlabel("Time (Min)")
            plt.ylabel("Intensity (A.U.)")
            plt.axis([0, int(round(numData2[0][-
1])),np.min(numData2[[1,3,5,7],:]),
            round(np.max(numData2[[1,3,5,7],:]))*1.05])
            l1 = plt.plot(numData2[0],numData2[1], 'k',linewidth=0.7)
            l2 = plt.plot(numData2[2],numData2[3], 'b',linewidth=0.7)
            l3 = plt.plot(numData2[4],numData2[5], 'g',linewidth=0.7)
            l4 = plt.plot(numData2[6],numData2[7], 'r',linewidth=0.7)
            plt.grid(True)
            plt.legend((numHead[0],numHead[2],numHead[4],numHead[6])
            ,loc="upper left",shadow=True)
            plt.savefig(os.getcwd()+"\\"+folderName+"\\"+name+'_Orig
            inalData.png',bbox_inches='tight',dpi=180)
            #plt.show()

        #Testing with addint a new comment. Here we go a new line.

```